Live cell imaging, cell tracking and lineage analysis as a tool to investigate dynamic culture processes in heterogeneous cell systems

by

Duane R. Moogk

A thesis
presented to the University of Waterloo
in fulfillment of the
thesis requirement for the degree of
Doctor of Philosophy
in
Chemical Engineering

Waterloo, Ontario, Canada, 2009

Author's Declaration

I hereby declare that I am the sole author of this thesis. This is a true copy of the thesis, including any required final revisions, as accepted by my examiners.

I understand that my thesis may be made electronically available to the public.

Abstract

Live cell imaging can be used to study dynamic cellular systems at single cell resolution. In heterogeneous cell populations, analyzing cell properties at the single cell level reduces the generalization of results caused by population-based assays. This thesis details the implementation of live cell imaging and single cell tracking to characterize heterogeneous cell systems undergoing dynamic processes over multiple generations. This approach enables the consideration of both spatial and temporal variables as well as the mapping of cell phenotype trajectories along their generational lineages. Cell-, lineage-, and colony-level properties are used as descriptors of the underlying molecular mechanisms that they are produced by. These may be unexpected, emergent properties that can not be predicted or completely characterized at the molecular level. Analysis of these properties can reveal and characterize the properties and processes of dynamic, heterogeneous cell systems.

Live cell imaging culture strategies were developed to enable characterization of both two- and three-dimensional cell systems. Computational modeling was performed to evaluate the conditions imposed by a confined imaging chamber that enables single cell resolution imaging of monolayer and multilayer cell systems. Imaging chamber dimensions and cell colony/aggregate sizes were calculated that would prevent the introduction of metabolite transport limitations and allow for stable, long term imaging. Methods for single cell tracking and analysis were also developed, which produces a database detailing the tracked, observed and extracted properties of every cell and colony, while maintaining the lineage structure of the data. Visualizations such as lineages, histograms and scatter plots were implemented to enable interactive data analysis and querying.

These methods were used to characterize heterogeneity in two separate cell systems: human islet of Langerhans-derived progenitor cells, and human embryonic stem cells. Islet-derived progenitors are an expandable source of cells with potential for treatment of diabetes. Here, it was shown that there is an unequal contribution of islets to the progenitor derivation process. Islet-derived progenitors consist of two distinct sub-populations of cells that were distinguished by morphological identification during live cell image analysis. These sub-populations possess unique proliferation profiles and appear to exist in a dynamic state with each other. Three-dimensional tracking of islet progenitor derivation was implemented, but suffered from a lack of resolution to capture the dynamic nature of the transformation process. However, entire islets were imaged and

tracked successfully under maintenance conditions, suggesting that this system may be useful for other cell types. These results highlight that live cell imaging and cell tracking may not be suitable for all cell systems and that inclusion of other analytical information, such as immunocytochemistry, would improve the power of cell tracking analysis.

Human embryonic stem cell cultures were studied using live cell imaging to identify the mechanisms by which they differentiate to produce supportive niche cells. Cell tracking, morphology scoring and lineage analysis revealed a previously unappreciated level of heterogeneity within human embryonic stem cell colonies. The results show that a sub-population of human embryonic stem cells exist that are precursors to niche cell differentiation. However, these cells exist in a dynamic equilibrium with self-renewing stem cells, which is dependant on the presence of existing local niche cells. Sub-optimal niche conditions leads to the production of niche differentiation-competent cells and, significantly, considerable cell death. The effect of cell death is the clonal selection of self-renewing cells that contribute to colony expansion. Overall, these results highlight the importance of the co-transfer of existing niche cells and the dynamic balance that regulates human embryonic stem cell self-renewal and differentiation.

This thesis displays the utility of live cell imaging, cell tracking and cell, colony and lineage analysis for studying dynamic heterogeneous systems. Furthermore, it highlight the fact that cell-, lineage- and colony-level analysis can uncover previously unappreciated heterogeneity and unknown sub-populations of cells. The system does not rely on characterization at the molecular level, but uses higher order measures to generalize them. However, future incorporation of cell, lineage and colony information with molecular-level information may results in analytical power not possible from either level alone. Such systems will be valuable tools in the growing fields of stem cell biology and systems biology.

Acknowledgements

I would like to acknowledge, first and foremost, my supervisor, Dr. Eric Jervis, for his guidance and support in all aspects of my graduate studies, for intriguing and fruitful chats about music, movies, music, books, and music. I am grateful to have been mentored by someone with such a pure passion for scientific discovery.

I would also like to acknowledge three people without whom this thesis would not have been possible. Thank you to John Ramunas, my predecessor, trainer and guru of all things live cell imaging, for all of your help in the early days of my studies and for your endless effort and enthusiasm that contributed so much to the lab. To April Blaylock, for her friendship and her work on development of the image acquisition system that was so important to this research. And, finally, to Darik Gamble for his friendship and his immense contribution to the cell tracking and analysis program and for putting up with the constant feature creep involved in its development.

This work would also not have been possible without the countless hours of work put in by our team of data trackers – Monique, Allie, Steve, Ian, Nathan, Curtis Anne, Kiwi, Devin, Peter. Also, I'd like to thank Kevin for all of his tracking efforts, coffee runs, and drives to school.

I would like to thank the members of my examination committee – Dr. Ali Elkamel, Dr. Mario Ioannidis, Dr. Guy Guillemette, and Dr. Mungo Marsden from the University of Waterloo, and Dr. Alain Garnier from Laval University – for reading, commenting on, and hopefully enjoying my thesis.

And finally, I would like to acknowledge the entire cast of the Jervis lab that I have had the pleasure to work with over the years – Jeremy, Heather, Liam, Richard, Julien, Erika, Jonathan, and Genevieve. It's been fun!

Dedication

To my parents. For all of their support over my many years of education. You have instilled in me the values and qualities that have enabled me to come this far. I love you both very much.

To Katie. You have been there with me as we both pursued too many degrees to mention, and I know that I would not have been able to complete this one without you. You are the love of my life.

Table of Contents

List of Figures

List of Abbreviations

α	islet alpha cell
β	islet beta cell
δ	islet delta cell
AMCA	7-amino-4-methylcoumarin-3-acetic acid
bFGF	basic fibroblast growth factor
BSA	bovine serum albumin
cAMP	cyclic adenosine monophosphate
CCD	charge-coupled device
ck-19	cytokeratin-19
CO2	carbon dioxide
CSV	comma-separated value
DAPI	4',6-diamidino-2-phenylindole
DIC	differential interference contrast
DLS	duct-like structures
DNA	deoxyribonucleic acid
e	edge human embryonic stem cell
ECM	extracellular matrix
EMT	epithelial-to-mesenchymal transition
FACS	fluorescence-activated cell sorting
FBS	foetal bovine serum
FGFR	fibroblast growth factor receptor
FITC	fluorescein isothiocyanate
FOV	field of view
GLUT-2	glucose transporter-2
GLUT-4	glucose transporter-4
hdF	human embryonic stem cell-derived fibroblast-like cells
hESC	human embryonic stem cells
hIPC	human islet-derived progenitor
HSC	hematopoietic stem cell

i	internal human embryonic stem cell
IGF-II	insulin-like growth factor
IGFR	insulin-like growth factor receptor
ILS	islet-like structures
INGAP	islet neogenesis-associated protein
IPC	islet-derived progenitor
IRS1	insulin receptor substrate-1
LCI	live cell imaging
LED	light-emitting diode
MEF	mouse embryonic feeder
MEFCM	mouse embryonic fibroblast-conditioned media
mESC	mouse embryonic stem cell
MSC	mesenchymal stem cell
NaOH	sodium hydroxide
NDS	normal donkey serum
Oct-3/4	octamer-3/4
PBS	phosphate buffered saline
Pdx-1	pancreatic duodenal homeobox-1
PP	pancreatic polypeptide
RT	room temperature
Sox2	sex determining region Y-box2
SQL	structured query language
SSEA-3	stage-specific embryonic antigen-3
TGF-β	transforming growth factor-β
TRITC	tetramethyl rhodamine iso-thiocyanate

Chapter 1 Introduction

Biology has long been studied at many levels, from entire ecosystems to species, single cells to sub-cellular molecules. Indeed these scales, though vast, are intrinsically interconnected and it is the complexity of these interactions that enables the existence of life itself. The hierarchy of biological complexity dictates that multiple individual components at a given level interact to produce new, complex, and unpredicted emergent properties at the next level.

Areas of biomedical research rarely span more than one level of complexity (Kriete 2006), but it is often the description of the interaction across multiple scales that poses the most difficult challenges. For example, the behavior of an individual organism will no doubt have an effect on its population and community. This may be easily documented and correlated. However, when the actions and interactions of many organisms are considered, the understanding of their effect on both higher and lower order scales becomes much less clear. In the same respect, biologists and biochemists have studied and described the roles of individual intracellular molecules within cellular reaction pathways or specific cellular processes. Yet these results are often confounded by redundancies whereby a given molecule, or entire reaction, is sufficient to achieve a given outcome, yet is not necessary (Schrattenholz and Soskic 2008). New technologies, such as microarrays, may provide a description of the entire transcriptional level of a cell, but are also confounded by the fact that the data is a result of averages of a large number of cells, which may vary over a large range for any single data point. Furthermore, the presence or absence of a given molecule may not be a determining factor of its action, as concentration thresholds may exist. It is here where the emerging field of systems biology aims to describe and understand biological systems at a higher level, through characterization of the complex interaction networks that comprise cellular compartments and the cell as a whole.

Cell-level properties and phenomena, such as morphology, size, migration, division and death are the result of numerous complex genetic and molecular-level actions and interactions. In many cases, the complete set of molecules and reaction pathways that govern a given cell-level phenomenon are not completely known or measurable, yet the phenomenon itself is observable and/or measurable. Although this level of information amounts to a ‘black-box’ in terms of the sub-cellular components involved, it is still the true description of the manifestation of cell-level properties that

arise from them. Therefore, observation at the cellular level may enable the characterization of cellular events, properties and processes without the implicit knowledge of the molecular-level elements that govern them. Furthermore, the characterization of cells based on the combination of multiple cell-level properties may allow for the identification of unique cell phenotypes that are not discoverable based on the combination of molecular markers alone.

While cell-level observation can describe the combination of molecular-level events, in areas such as developmental and stem cell biology it is becoming increasingly important to put measurements and observations made on single cells into a context that relates them to a larger cell population. In this respect, another level of information arises resulting from the combination of individual cell measurements, describing the properties of cell colonies or aggregates *in vitro*, or tissues *in vivo*. Here, it is the combination of multiple cell types that exist in various locations spatially, and instances temporally to reveal colony properties and functions. In the case of molecular-level events, time scales range anywhere from nanoseconds to minutes, whereas cell-level events occur at times scales of seconds to hours, and colony and tissues can be describes in terms of hours to days.

Although consideration of a cell system (i.e. colony, tissue) as a whole may reveal emergent properties resulting from the interaction of the cells comprising the system, care must be take to consider the case of heterogeneous cell systems. The contribution to a specific event, behavior, or property of a cell system by sub-populations of cells may vary, and therefore population-based average measurement may mask underlying distributions of sub-population contributions (Schroeder 2005) and cannot capture the temporal evolution of the cell population heterogeneity (Glauche et al. 2009). Study of such systems therefore requires single cell-level resolution. Furthermore, in systems where dynamic events, such as differentiation and death, lead to temporal variability in the cell heterogeneity, generational relationships in the form of lineage can provide a further level of information.

1.1 Objectives

Live cell imaging (LCI) is an ideal method for obtaining cell-level properties such as size and morphology, dynamic cell measures such as migration and division, and generational relationships

provided by lineage. The objective of this research was to obtain cell-, lineage-, and colony-level information using LCI to characterize heterogeneity and describe specific dynamic processes in multicellular *in vitro* cell systems. To do this, LCI, cell tracking and analysis strategies had to be developed and tested on specific cell systems of biological significance.

The underlying hypothesis of this thesis is:

Heterogeneity within in vitro cellular systems, which may not be known or measurable at the molecular level, can be uncovered and described at the cell and lineage level to identify emergent properties and behavioral phenotypes resulting from dynamic spatiotemporal cell and colony interactions, and may lead to understanding complex, dynamic biological processes that have not been fully characterized at the molecular level.

To test this hypothesis, the following objectives were identified:

Objective 1: Develop LCI strategies that facilitate acquisition of high spatial and temporal resolution of multicellular two- and three-dimensional cell systems.

Objective 2: Develop cell, lineage, and colony tracking tools to obtain single cell and lineage histories of cell cultures including extractable qualitative and quantitative properties. Also, develop tools and strategies for analysis of tracked data to account for and include the unique structure of lineage and colony information.

Objective 3: Implement these tools to investigate specific cell systems and explore relevant biological questions pertaining to the dynamic heterogeneity of these systems.

Objective 3 required the identification of cellular systems with which to test the hypothesis. In particular, this required systems that had been identified as having some level of heterogeneity that was not fully characterized or understood. Furthermore, cell systems were sought in which the characterization of their heterogeneity would contribute significantly to the current knowledge of the field. Two cell systems were identified.

(1) Human islet of Langerhans

To supplement the significant need for donor islets for treatment of type 1 diabetes, a method for the *in vitro* expansion of cells suitable for transplantation or capable of induction to produce suitable cells is sought. Two protocols for the production of proliferative islet-derived cells have been described (Gallo et al. 2007; Jamal et al. 2003), yet the source of these cells from native islets is not fully understood. Furthermore, multiple cell types have been described in both systems, yet how these sub-populations of cells contribute to both the proliferation and differentiation potential of the overall cell population has not been described.

(2) Human embryonic stem cells

Human embryonic stem cells (hESC) have the potential to produce specialized cell types to treat a range of diseases and injuries. Although protocols for the differentiation of hESCs to desired cells types is a major field of interest, much remains unknown about the properties of hESCs and the conditions required to maintain their stem cell properties (Skottman et al. 2007). Recent studies suggest that differentiated hESC-derived cells are required to provide a supportive niche to maintain hESC pluripotency and differentiation potential (Bendall et al. 2008; Bendall et al. 2007). Given the documented heterogeneity with hESC cultures, based on differentiation potential (Stewart et al. 2006), it remained unclear if such a heterogeneity existed in terms of niche differentiation.

Chapter 2 Literature Review

2.1 Live cell imaging

In general, LCI refers to semi-continuous imaging of cells over intervals on the order of a few minutes and durations of hours to days (Schroeder 2008), and is employed to study a range interactions from single molecules to highly organized multicellular structures and even entire organisms (Abud et al. 2008; Keller et al. 2005; Keller et al. 2008; Kirchhausen et al. 2005; Mashanov et al. 2006) (a general discussion of the fundamentals of microscopy is presented in Appendix A). LCI is becoming a standard tool for many biology laboratories, as microscopes and imaging hardware and software become more accessible. Furthermore, advances in fluorescent probes and imaging techniques to observe and quantify sub-cellular compartments and single molecule dynamics now allow LCI to investigate a wide variety of biological questions (Haraguchi 2002).

Depending on its purpose, LCI systems are selected based on considerations of the speed of acquisition required, the time scale of cellular or molecular events being studied, the detection sensitivity required to acquire the desired information, and the effect of imaging on the viability of the cells (Stephens and Allan 2003). The main attraction of LCI to biologists is that it enables the observation and characterization of dynamic molecular, cell and tissue processes. The utility of LCI is generally limited by one of the following: 1) the resolution of the microscope, 2) the temporal resolution of image acquisition, or 3) the ability to observe and extract the desired information purely from imaging data (i.e. given molecular-level resolution of the microscope, the ability to identify and discriminate between the molecule of interest and other molecules).

The growing fields of stem cell biology and regenerative medicine involve processes such as differentiation and transdifferentiation that span numerous generations. The nature of these processes means that the types of cells and their population distributions change over time. Therefore, in the absence of experimental observation at a resolution that enables the tracking of individual cell fates and lineage relationships, confusion and uncertainty may arise regarding, for example, the lineage potential of stem cells, the proliferative activity of cells, or the contribution of specific cells to

regenerative processes (Schroeder 2008).

Single cell resolution LCI is therefore ideal for investigation of heterogeneous dynamic cell populations. Generation of data at the single cell level eliminates the need for population averaged-based assays and other approximations (Kriete 2005), which may fail to uncover cell and culture heterogeneity. Furthermore, LCI enables the creation of multi-parametric data sets. For example, bright field LCI can be used to obtain measures of cellular microenvironment, cell-cell orientations, lineage, and morphology all within a single experimental data set. The combination of these cell- and culture-level properties into a single data space can be used to uncover classifiable sub-populations of cells without the incorporation of specific molecular markers. In this respect, LCI enables the description of cell, lineage, and culture *behaviors*, representing the macroscopic display of the combination of many molecular reactions and interactions, which may not be fully known or understood.

Integration of other levels of information from existing analytical methods may enable the connection of LCI-level information to molecular-level information. For example, immunocytochemistry can be implemented immediately following LCI to relate the expression of specific molecules to an observed morphology or behaviour. LCI may also be incorporated downstream of existing methods, for example as an additional level of discrimination to complement fluorescence-activated cell sorting (FACS) (Dykstra et al. 2006). The ability to incorporate other analytical measures and methods will ultimately depend on whether the cells are recoverable and maintain viability following any given analytical method, and the utility of such combinations will only be appreciated if other methods retain the single cell- or lineage-level information that LCI provides.

2.1.1 Microscope configurations

LCI generally requires an inverted microscope, usually equipped with a charge-coupled device (CCD) camera. An inverted microscope allows the objective lens to be brought as close to the bottom surface of the culture vessel as needed. The objective lens and contrast method implemented will depend on the specific information to be obtained, and may range between 5x to 100x, utilizing DIC or phase contrast or fluorescent illumination (epifluorescence). A low magnification objective will

allow a larger culture area, and therefore more cells, to be imaged, at the expense of cellular and sub-cellular detail. However the use of a motorized microscope stage enables imaging of large areas with higher resolution air objectives through the creation of tiled mosaic arrays. Maintenance of focus over long term imaging experiments is of utmost importance and can be achieved with autofocus algorithms that automatically adjust the objective and microscope stage (Shen et al. 2006a).

A major consideration of LCI is cellular damage caused by exposure to light. Ultra-violet light can cause deoxyribonucleic acid (DNA) damage, infrared light can caused localized heating, and fluorescence can cause damage due to phototoxicity (Pattison and Davies 2006). Phototoxicity is mainly caused by oxygen-dependent reaction of free radicals, generated during fluorescence excitation (Sugden 2004), and therefore excitation intensity should be minimized as much as possible. In general, light source illumination should be minimized, but not beyond the point where the signal-to-noise ratio is too low to extract the desired image information. Unless using light-emitting diode (LED) light sources, which can be turned on and off quickly and without any penalty to their lifetime, a shutter is required between the light source and specimen that is open only as long as required for image acquisition. Transmitted light microscopy generally does not have an adverse affect on cells, but high intensity and highly focused white light can, as it contains near-ultra violet and near-infrared components (Frigault et al. 2009).

In the context of imaging live cells, methods to enhance image contrast are required as live cells are basically transparent. Vital dyes, which bind specifically to cell membrane or intracellular components, have long been used to enhance contrast. However, methods of optically enhancing contrast are preferred because vital dyes can affect normal cell operation or be altogether toxic. Standard bright field microscopy generates contrast as phase-shifted diffracted waves, which recombine with much higher intensity, and therefore dominant, non-diffracted (zero order) waves. In phase contrast, the intensity of the zero order waves are decreased, by roughly 90%, to a level comparable to the diffracted waves by passing them through the phase ring of a phase plate positioned after the objective. The resulting waves have similar intensities and therefore the effects of interference are increased. Contrast is also increased by further shifting the diffracted waves out of phase with the zero order waves. This is achieved when the diffracted waves travel through a thicker region of the quartz phase plate compared to the zero order waves traveling through the phase ring.

Differential interference contrast (DIC) microscopy takes advantage of the fact that two

waves traveling through parts of a specimen with different optical densities will have different optical path lengths. If the two waves are close together, when they are recombined the resulting phase differences lead to intensity differences. This produces a shadowing effect at all specimen interfaces, for example between a cellular organelle and the cytoplasm. Firstly, plane-polarized light is separated into wavelets traveling parallel and very close together by passing them through a Nomarski-modified Wollaston prism. After traveling through the specimen and objective lens, the wavelets are recombined in a second prism. Any wavelets that traveled through regions of differing optical density (i.e. refractive index or thickness) experience different optical path lengths and will be out of phase when recombined. Furthermore, the resulting wave will no longer be polarized in the original plane. When these waves travel through the analyzing filter they are rotated either towards or away from the analyzer axis, resulting in a higher or lower intensity wave, resulting in the appearance of a highlighted or shadowed region, respectively. DIC optics also have a relatively low depth of focus, such that specimen features just above or below the focal plane do not contribute significantly to the contrast enhancement in creating the final image. This allows specimens to be optically sectioned to produce three-dimensional reconstructions.

Fluorescence microscopy has gained wide use in biology because of recent developments enabling characterization of dynamic single protein interactions (Haraguchi 2002) (a review of the fundamentals of fluorescence is presented in appendix A). Fluorophores can be introduced to specimens as fusion proteins (Miyawaki et al. 2005), vital dyes and biosensors (Giuliano et al. 1995) or antibody-conjugated molecules for immunocytochemistry, all of which localize to specific sub-cellular structure or molecules. Ratiometric fluorescence imaging is also employed to quantify the concentration of cellular molecules (Rink 1988). In this application, quantification is not reliant on absolute intensity values, only the ratio between two excitation/emission pairs. All of these applications have advanced the field of biology significantly. Selection of appropriate fluorophores is an important aspect of live cell fluorescent imaging, compared to immunocytochemistry, as phototoxicity must be considered. A fluorophore with a large Stokes shift is desirable so that the emission spectra can be separated from the excitation spectra with the appropriate filters. This ensures that the resulting image contains intensity information from the emission spectra only. However, if multiple fluorophores are to be used in a single specimen, a balance must be struck between a large Stokes shift and the desire to minimize overlap of excitation and emission spectra of different fluorophores. Fluorophores are generally selected that have a high yield of fluorescent de-excitation versus all other de-excitation pathways (i.e. high quantum yield).

2.1.2 Live cell imaging hardware

While there are many possible LCI configurations, which will depend on the specific experiment and available equipment, all LCI experiments generally require specifically designed culture vessels, environment controls, and image acquisition software. The combination of these must ensure that conditions of both cell viability and image resolvability are met. To enable long term imaging, the cell culture must be maintained in an environment that does not induce a stress response. Cultures are imaged within an environment-controlled microscope stage, which must be maintained at 37˚C for most applications, and with sufficient humidity to prevent significant evaporation of culture media. Ideally, the entire microscope will be enclosed in the temperature-controlled environment, as fluctuations in temperature can affect both normal cellular function and microscope focus and alignment. However, such enclosures can take several hours for the temperature to stabilize, and therefore sample focus during this period can be an issue.

A bicarbonate-based culture medium and 5% carbon dioxide (CO_2) environment is generally required to buffer the culture medium. Furthermore, the presence of carbonate in the media is required for many cellular processes, and so although alternative buffers, such as HEPES or TRIS are also used, they are often only supplemental to the bicarbonate buffer system (Kanaan et al. 2007). Typically, the CO_2 gas is bubbled through a water reservoir to maintain humidity in the culture environment. This is done to avoid changes in osmolarity due to evaporation of culture media, which can cause osmotic shock through the rapid exit of water from cells and the inability of substrates and factors to enter the cell.

2.1.3 Culture chambers

An appropriate culture chamber is required that provides the conditions for cell survival and growth and good optical quality to attain high resolution images. The surface on which the specimen is imaged must be flat, and other surfaces should generally be parallel or perpendicular to the imaging surface, and all surfaces should be transparent (Christiansen et al. 1953). Cells can be imaged in Petri dishes or multi-well plastic plates, but these limit resolution due to their thickness. Instead, the

bottom surface of an LCI culture chamber is generally a cover slip or microscope slide so that the objective lens can be brought within its working distance required to enable high resolution imaging. For cell survival and growth, requirements include sterility, optimum temperature, and adequate nutrition and oxygenation (Christiansen et al. 1953). Short term LCI experiments, with maximum duration of 10-20 minutes, can be performed with simple chambers, which are basically two surfaces (microscope slide and cover slip) separated by cells, spacers and media and sealed along all edges. Here, conditions such as temperature and pH are not controlled for, but longer LCI experiments require controls to provide physiological conditions to ensure long term viability.

Experiments that require no intervention for the duration of imaging require only sterility, separating the culture from the microscope environment, while still allowing gas exchange. This is ideal, as the imaging process is not disrupted, but for long term experiments media changes are required to account for both nutrient depletion and media evaporation. If media changes can be performed by removal of the imaging chamber to a sterile flow hood, a simpler chamber design can be used and sterility can be ensured. Such media changes should only be performed if the chamber can easily be removed from the microscope, it can be returned precisely to its previous conditions for image registration, and the time required to do so does not significantly disrupt the image time course. Media should be equilibrated to the same temperature and atmospheric conditions as the imaging chamber before being added. Systems requiring microinjection, addition of reagents, or physical manipulation of cells mid-experiment must allow easy access while not compromising sterility (Terryn et al. 2009).

There are many examples of imaging chambers that incorporate perfusion for the purposes of continual media flow or the addition of reagents (Rieder and Cole 1998). In addition, perfusion chambers can also be used to sample the media for metabolic by-products. The advantage of perfusion chambers is that it they enable much tighter control of culture conditions, such as pH and osmolarity, compared to chambers that require periodic media changes. The effects of perfusion must be considered if experiments are designed to characterize cellular properties or processes that are affected by gradients, such as cell migration or polarization. In these cases, measurements must be corrected to compensate for convection caused by perfusion, or the cells should be shielded from the bulk convection through design of appropriate culture vessels. Conversely, perfusion systems can also be implemented to introduce and control desired flow and shear rates (Long et al. 2004), but consideration must be taken as to the affect of shear on cell stress responses and the overall health of

the culture.

Microfluidic devices are also becoming common in live cell imaging applications, as they offer the ability to control a number of parameters, creating an array of experimental conditions across a large number of microwells (Thompson et al. 2004). These devices are attractive because they have low reagent cost due to small volumes used, they can be controlled precisely, and multiple factors can be controlled temporally (Yu et al. 2009). However, the drawbacks of such devices include the fact that the cells are often unrecoverable, and devices may not be reusable. Furthermore, the provision of the appropriate conditions for cell viability, such as cell-cell contact and extracellular matrix become a significant issue. The biggest drawback of microfluidics for LCI is that they are not designed to allow exponential colony growth for periods of days or weeks, which in this time even a single cell-derived colony would grow to hundreds of cells. Cell viability would likely suffer as both the confined nature of the device and the very small volume of media would limit nutrient supply to all the cells in a colony.

2.1.4 Image acquisition

There are a number of software packages available for image acquisition and control of LCI experiments, including InVivo™ by Media Cybernetics, NIS-Elements™ by Nikon, and iQ™ by Andor. In general, these packages provide the ability to control image quality (gain, shutter speed, focus), environmental conditions (temperature, CO_2), acquisition dimensions and size (scanning, tiling, z-series), light channel (bright field, fluorescence) and other parameters. Most packages also include separate analysis tools as well. An important consideration is the trade off between imaging quality (spatial and temporal resolution) and physical hard drive requirements. A large amount of hard drive space is required to store the data obtained continuously over long term time courses. For example, imaging a 10x10 array at an interval of 3 minutes (i.e. 100 images every 3 minutes) produces over 60 gigabytes of image data per day (personal observation). Therefore, the amount of data obtained for each time point should be considered and weighed against the required length of the experiment.

2.1.5 Live cell imaging configurations

LCI of two-dimensional cultures (i.e. monolayers of cells on a culture surface) has been used for almost a century to study phagocytosis (Comandon 1917), lifespan (Froese 1964; Hsu 1960), growth (Elfwing et al. 2004; Killander and Zetterberg 1965b), death (Marin and Bender 1966), contact inhibition (Martz and Steinberg 1972), migration (DiMilla et al. 1993), clonal heterogeneity (Absher et al. 1975), and lineage (Qian et al. 1998) on large cell populations. Such experiments are often performed with cells plated on glass or plastic culture surfaces, which are often pre-coated with extracellular matrix components such as collagen, fibronectin, or laminin (DiMilla et al. 1993; Donaldson and Mahan 1984; Newgreen et al. 1982). Monolayer systems are ideal for imaging and analysis as identification and tracking of individual cells with high levels of confidence is generally possible, provided the images are acquired at a sufficient spatial and temporal resolution. Because of this, culture systems have been developed that force cells to maintain a monolayer configuration, making analysis easier (Ramunas et al. 2006).

Monolayer cultures are not always possible and forced monolayer cultures are not always appropriate, as disruption of three-dimensional multi-cellular systems for the purposes of imaging is not feasible when three-dimensional cell-cell and cell-extracellular matrix interactions are required, such as in embryo development. Therefore, systems for three-dimensional LCI have been developed. Incorporation of nucleus-specific fluorophores in combination with wide field epifluorescence is generally required for three-dimensional LCI to produce images in which individual cells can be identified and tracked (Stephens and Allan 2003). Three-dimensional image stacks are rendered through deconvolution of the raw fluorescent LCI images (Stephens and Allan 2003). Live cell fluorescent imaging is commonly used for a variety of purposes, including localization and quantification of cellular molecules, nuclear staining to aid in cell identification, and detection of molecular motions and interactions (Otto 1994; Paredes et al. 2008; Wu and Brand 1994). The introduction of green fluorescent protein and its variants for use as a reporter of gene expression has greatly advanced the field of biology (Chalfie et al. 1994; Gerdes and Kaether 1996; Prasher et al. 1992; Welsh and Kay 1997). The use of fluorescence in long term LCI requires careful consideration of excitation/emission peaks, imaging frequency and total experiment duration to ensure that phototoxicity does not compromise cell viability or the cellular processes being studied. Most imaging systems utilizing fluorescence, such as confocal or multi-photon microscopy, introduce phototoxicity that reaches unacceptable levels for long term imaging applications (Keller et al. 2008). However, use of less phototoxic fluorescent proteins (i.e. longer wavelengths) and new imaging

systems has enabled long term tracking of thousands of cells, but still only for periods of less than 24 hours (Keller et al. 2008).

Three-dimensional LCI methods that don't incorporate fluorescence are generally only suitable for small cells with low granularity, and generally cannot track cell aggregates greater than 30 cells (Hamahashi et al. 2005; Heid et al. 2002). Three-dimensional DIC imaging and reconstruction of single cells at very high temporal resolution has been used to elucidate the roles of cytoskeletal and regulatory elements in chemotaxis (Heid et al. 2002; Wessels et al. 1998), and further developed to image developing *Caenorhabditis elegans* embryos in three dimensions (Heid et al. 2002). This method required 75 optical sections per time point at 5 second intervals to image an embryo of up to 28 cells, which would produce close to 200 gigabytes of data per day of uncompressed images. Systems using three-dimensional DIC optical sectioning have been used mostly to study *C. elegans*, zebrafish, Drosophila and other cell types that are relatively transparent and small, over short time periods. Implementation of these systems to human cell systems has not been presented.

2.1.6 Image analysis

Depending on the LCI acquisition system and cell system being studied, extraction of quantifiable information from image data can be accomplished through automated, semi-automated, or manual data analysis (Fanti et al. 2008; Hand et al. 2009; Li et al. 2007; Ramunas et al. 2006). Fully automated procedures are often limited by errors in identification and tracking of cells or specific features, while fully manual methods can be extremely laborious and inconsistent. As a result, the majority of image analysis systems implement semi-automated methods, enabling high throughput of data with the support of human visual identification or confirmation of features that may not otherwise be identifiable through automated algorithms. The most important features of such analysis tools are that they create data sets in numerical forms that can be further analyzed and interpreted. Also, given the large amount of data that can be generated from LCI experiments, the data must be stored efficiently so that it is accessible for further analysis. Compression of image data has historically been required (Heid et al. 2002), but the availability of large, relatively inexpensive hard drives allows LCI image data to be stored and analyzed uncompressed, and therefore retain possibly useful image detail.

The first stage of LCI analysis is cell identification and tracking. Cell positions are tracked over time with a system that logs the x- and y- co-ordinates (and z- in the case of three-dimensional imaging) of each cell in each image. From these logged co-ordinates, parameters such as cell speed and migration paths can be extracted. Automated tracking of non-adherent cells (i.e. cell that do not grow in adherent colonies, but as individual cells) from DIC or phase contrast LCI experiments is common, provided the imaging data is obtained in high enough spatial and temporal resolution (Al-Kofahi et al. 2006; Shen et al. 2006b). However, adherent cells that grow in two- or three-dimensional colonies generally require modification, such as histone-fluorescent protein fusions, to facilitate tracking by enabling identification of individual cell nuclei (Kanda et al. 1998; Keller et al. 2008). Such modifications then require the implementation of live cell fluorescence, either alone or in combination with bright field. In the absence of such modifications, manual cell tracking is required.

Many software packages are available for tracking and extraction of cell properties (Bao et al. 2006; Boyle et al. 2006; Braun et al. 2003; Parvin et al. 2002; Tassy et al. 2006). The number and type of cell features that can be extracted and quantified depends on the microscope configuration. For example, using a 20X DIC air objective one can, for most cell types, score features including cell outline, area, volume, granularity, number of nucleoli, nuclear area, speed, position, lifespan (with minute-scale resolution), and projections (e.g. uropods). With a 5X objective, however, only cell position, speed, lineage, and overall cellular outline can be scored. Therefore, microscope and image acquisition settings should be configured with consideration for the specific information to be extracted from the experiment.

Cell lineage trees are a natural format in which to store, analyze, and present information associated with dividing cells. The ability to retain the generational relationships of dividing cell populations provides potential to study temporally dynamic cultures, such as differentiating stem cell populations. Without lineage information the pathway of differentiation and the differentiation potential of cells at each generation cannot be elucidated. Commonly, lineage trees that are known to be invariant, such as the developmental path of *C. elegans* (Bao et al. 2006), are studied through genetic or chemical perturbation to characterize the specific effects on the lineage (Bao et al. 2006). Characterizing and analyzing cell systems with unknown or variant lineages, which may vary due to minor changes in preparation, culture conditions or passage number, require the simultaneous

acquisition of control lineages to account for these possible variations.

The unique structure of the lineage provides a challenge for performing quantitative analysis. While structurally similar to phylogenetic trees, the information contained within cell lineages is inherently different (Glauche et al. 2009). Phylogenetic trees have been studied for decades, yet appropriate statistical analysis is not well established (Holmes 2003; Nei 1996). Statistical measures and analytical techniques for lineage trees have been even less established, and only recently has a set of measures been proposed for analyzing such data (Glauche et al. 2009). It is clear that further tools are required for analysis of lineage-structured data, specifically which enable inclusion of multiple cell-level properties. This is important, because discrimination between cell types based on cell-level properties may not be possible without the combination of a number of these properties, and the identification of trends in identified sub-populations of cells across multiple generations may not possible without the lineage structure.

2.2 Islet of Langerhans, diabetes, and islet regenerative potential

2.2.1 The pancreas

The human pancreas has two distinct functions; contributing to both the exocrine and endocrine systems. The majority of the pancreatic mass, roughly 98% in humans, is composed of exocrine cells, responsible for producing, secreting and transporting at least 22 different digestive enzymes such as proteases, amylases, lipases as well as electrolyte fluids to the duodenum through its branching ductal network (Slack 1995). The endocrine cells are scattered throughout the exocrine pancreas, mostly in clusters called islet of Langerhans. Islets consist of four main cell types, alpha (α), beta (β), delta (δ) and pancreatic polypeptide secreting cells (PP), which are responsible for production of the hormones glucagon, insulin, somatostatin and pancreatic polypeptide, respectively. Insulin, glucagon and somatostatin act together to maintain a state of normal physiological blood sugar levels, or euglycemia, while the biological role of pancreatic polypeptide remains unclear. Although the exocrine and endocrine functions of the pancreas are unrelated, there is evidence that these endocrine islet hormones may play a role in maintaining or enhancing exocrine function (Go 1993).

2.2.2 Islets of Langerhans

Islets of Langerhans are dispersed throughout the exocrine pancreas and range in size from dozens to thousands of cells (the fundamentals of islet development are presented in Appendix B). Those with a diameter greater than 250 µm represent only 15% of the islet population, yet account for 60% of the volume, whereas those 160 µm and smaller represent 75% of the islet population, yet only 15% of islet volume (Hazelwood 1989). Each islet is surrounded by a capsule, a single layer of fibroblasts and the collagen fibers they lay down, which defines a subcapsular interstitial space continuous with the precapillary interstitial space. Although islets represent only two percent of the cellular volume in the pancreas, 20% of pancreatic arterial blood flow is directed to the islets, conferring the importance of islet cell contact with arterial blood to sense and respond to blood glucose levels. Islet cell organization and vasculature is shown in Figure 2-1.

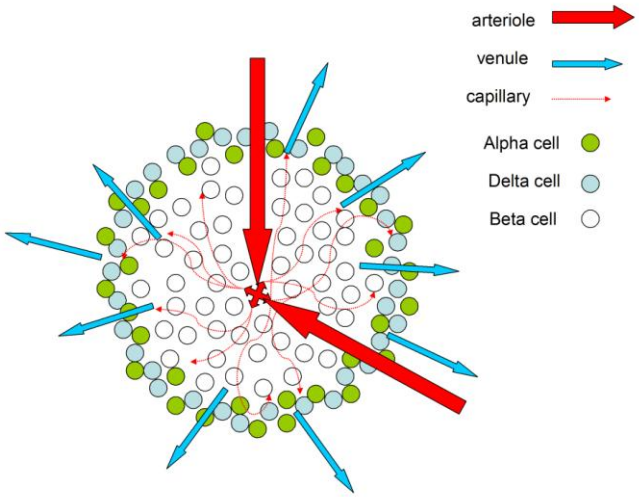

Figure 2-1. Schematic illustration of islet structure, specifically the occupation of the β-cells at the islet core, surrounded by a mantle of non-β cells. Also illustrating the vascularization of an islet, showing arteriole blood supply penetrating directly to the core.

The four main cells types, α-, β-, δ-, and PP-cells make up the majority of the islet, with several other less populous cell types also present. For example, so called 'small cells' have been

observed and isolated and express pancreatic duodenal homeobox-1 (Pdx-1), as well as insulin, glucagon, somatostatin and pancreatic polypeptide (Petropavlovskaia and Rosenberg 2002), however their specific function remains unclear. It also remains unclear whether a population of stem or progenitor cells exist within the islet, although studies have suggested this possibility (Guz et al. 2001; Seaberg et al. 2004; Zulewski et al. 2001).

In general, the core of the islet contains insulin-producing β-cells and is surrounded by a discontinuous mantle of non-β-cells, generally only one to three cells thick. As in islet development, it is apparent that the organization of cells in the islets is inherent and maintained through adulthood (Hazelwood 1989). Arterioles penetrate the islet mantle and form capillaries once they have reached the β-cell inner core, allowing arterial blood to contact the β-cells before moving outward to perfuse the peripheral non-β-cells. The importance of this directed blood flow is discussed below.

Islet cells produce hormones that regulate circulating blood glucose levels. Glucose in the blood can be taken up by hepatocytes, muscle and adipose cells. It is in these cells that glucose is converted to and stored as glycogen. When blood glucose levels are low, or hypoglycemic, these cells are stimulated to convert glycogen back to glucose or to metabolically useful substrates. Blood glucose levels must be stringently controlled, as departure from a small concentration range can affect many cellular functions. High glucose levels in the blood, or hyperglycemia, stimulates the release of insulin from β-cells in the core of the islet. This is the main pathway for insulin release, although others do occur including neural and other hormonal stimulation (Bolander 2004). Glucose is transported into the β-cell via facilitated diffusion by glucose transporter-2 (GLUT-2). Once inside the cell, products of glucose metabolism stimulate a number of events including insulin production, insulin release and increased expression of GLUT-2. Glucose, therefore, acts as the initiator of its own metabolism.

Secreted insulin enters the bloodstream and acts on hepatic, muscle and adipose cells. Binding of insulin to the extracellular domain of its receptor on these cells causes activation of tyrosine kinase domains (Bolander 2004), which act intracellularly by phosphorylating the tyrosine residues of specific proteins, including insulin receptor substrate-1 (IRS1). This leads to the production of glucose transporter-4 (GLUT-4), increasing facilitated glucose transport into the cells, and up-regulating enzymes involved in the transformation of glucose to glycogen, amongst other things (Bolander 2004). The α-cell is responsible for secreting the hormone glucagon, which acts

counter to insulin to increase blood sugar levels. At times of hyperglycemia glucagon release is inhibited by both the blood glucose concentration and the presence insulin (Leung et al. 2006). Glucagon acts on hepatic and adipose tissue, and activation of the glucagon receptor stimulates intracellular production of cyclic adenosine monophosphate (cAMP), initiating signaling cascades resulting in the activation of phorsporylase A kinase, the enzyme responsible for conversion of glycogen to glucose-1-phosphate, the first step in its conversion back to glucose.

In order to tightly regulate blood glucose levels, the secretion of insulin, glucagon and somatostatin is controlled through mutual inhibition and stimulation, depicted in Figure 2-2.

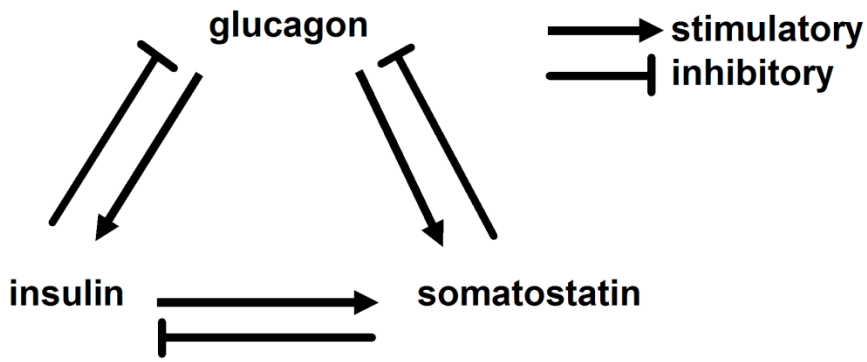

Figure 2-2. The inhibitory and stimulatory effects of the three main islet hormones on each other allows for strict control of hormone levels to maintain euglycemic conditions.

The directed flow of blood through the islet, contacting β-cells first, followed by α-cell and δ-cells, and the eventual recirculation of hormones back into the islets, allows for such regulation to occur. Hypoglycemia has obvious consequences in the body, as glucose is the primary source of energy for the cell. On the other hand, long term hyperglycemia has been shown to cause cardiovascular disease, as well as kidney and liver damage, amongst other things. The main cause of these is thought to be the formation of glycated proteins, disturbances of the polyol pathway due to intracellular hyperglycemia, activation of protein kinase C, and increased hexosamine pathway flux (Eiselein et al. 2004). Strict regulation of blood glucose levels is, therefore, vitally important.

2.2.3 Diabetes

Diabetes is a clinical syndrome affecting the body's ability to effectively produce or use insulin. It is estimated that over two million Canadians suffer from diabetes (Canadian Diabetes Association). Diabetes presents itself as either type I or type II. Complications that patients face due to both types of diabetes include an increased risk of cardiovascular disease, nephropathy, retinopathy, neuropathy, foot complications due to nerve damage or poor blood supply, skin complications, and gastroparesis. Medical interventions are sought to both control blood glucose levels and reduce patient morbidity caused by complications. Although type II diabetes can, for the most part, be managed through a combination of exercise and diet, treatment of type I diabetes requires the injection of exogenous insulin to maintain euglycemia. These interventions do prolong the lifespan of diabetics, however many negative side effects still contribute to a reduced quality of life. Alternatively, transplantation of donated islets of Langerhans can restore a patient's ability to independently regulate blood glucose, although the long term stability of these transplants is still an open challenge (Ryan et al. 2005).

Type I diabetes, or juvenile-onset diabetes, accounts for only 10% of diabetes cases and results from an inherited genetic susceptibility. The T-lymphocyte cells of the immune system mediate the destruction of the β-cells, leaving no source of insulin to regulate blood glucose levels. Activated T-helper cells are known to infiltrate the islet and produce characteristic cytokines that induce inflammation and β-cell destruction (Eiselein et al. 2004). Insulin depletion caused by loss of β-cell mass directly leads to hyperglycemia. Lack of circulating insulin prevents glucose from being taken up by target cells, as insulin is responsible for initiation of the production of the glucose transporter molecule GLUT-4. The lack of insulin also eliminates inhibition of glucagon release from α-cells, and therefore circulating glucagon causes production of glucose via glyconeolysis and gluconeogenesis pathways (Eiselein et al. 2004). Patients with type I diabetes are dependent on exogenous insulin injections to control blood glucose levels.

Type II diabetes can manifest itself much slower than Type I, and can be maintained in a pre-diabetic state for many years. Insulin target cells become resistant to insulin action, possibly due to a higher than normal amount of insulin constantly required to maintain euglycemia caused by consistently elevated glucose levels. This is likely the initiating step of type II diabetes (Martin et al. 1992). The body can cope with this resistance for some time as the β-cells compensate by secreting more insulin (Schinner et al. 2005), by an increase in cell mass through β-cell replication or neogenesis (Dickson and Rhodes 2004), or possibly by an increased efficiency of glucose stimulated insulin release (Liu et al. 2002). It is thought that during this initial stage of compensation that the β-

cell phenotype is kept in tact with the possible exception of the induction of genes required for β-cell replication (Weir and Bonner-Weir 2004).

When normal glucose levels can no longer be maintained due to sustained hyperglycemia, marked changes in β-cell gene and protein expression occur, such as up-regulation of enzymes that participate in gluconeogenesis and lactate production and down-regulation of genes responsible for normal β-cell function, including genes associated with secretory products, glucose metabolism and critical transcription factors, such as Pdx-1 (Weir and Bonner-Weir 2004). It has been hypothesized that even modestly higher levels of glucose may cause a β-cell glucotoxicity, which leads to alteration of normal β-cell function, most notably a loss of acute glucose stimulated insulin secretion (Weir and Bonner-Weir 2004). Diet, exercise and an appropriate drug treatment regime may allow a patient to stably remain in this pre-diabetic state, where glucose levels can still be controlled. Some critical point exists where stable decomposition occurs, such that there is roughly a 50 percent reduction in β-cell mass, although insulin is still secreted in a large enough volume to control blood glucose to a certain degree (Larsen 2004). Most type II diabetics remain at this stage for most of their life, and although glucose levels can be controlled somewhat, many negative effects of long term hyperglycemia remain, including retinopathy, nephropathy and neuropathy (Larsen 2004).

2.2.4 Diabetes treatment and therapies

Before the successful extraction of insulin by Frederick G. Banting and Charles Best in 1921, type I diabetes was fatal within 1-2 years of onset (Kobayashi et al. 2004). Soon after, insulin therapy was successfully implemented as a means of controlling blood glucose and prolonging patient survival. It is a necessary treatment for type I diabetes patients, but is not the only therapeutic option for type II diabetes. Other treatment options include an increase in physical exercise, a strictly controlled diet, or oral hypoglycemics (Eldor et al. 2005). It is clear that implementation of insulin therapy to control diabetes was one of the major advances in medicine in the twentieth century. The Nobel Prize was awarded to Banting and John J. R. Macleod in 1923 for discovery of insulin. Although the introduction of insulin therapy drastically increased life expectancy for sufferers of diabetes, complications remain in most cases as glucose level cannot be stringently controlled and therefore other treatment options are desirable as long term complications and risk of hypoglycemic episodes pose a major problem.

Although the administration of insulin to diabetic patients is successful in maintaining reasonable control of blood glucose levels, the morbidity caused by the aforementioned side effects leaves the need for alternative treatments to be explored and undertaken. Whole or partial pancreatic transplantations have been performed for several decades, alone or simultaneously with kidney transplantation, with engraftment rates at one year reaching 80% (Larsen 2004). However, the highly invasive nature of such a procedure along with exocrine gland associated complications had led to the development of islet-only transplant procedures. Although gradual improvement to islet isolation procedures and immunosuppressive regimens occurred from the first clinical transplant in 1974 through to the 1990s, insulin independence following transplant remained at very low levels. The major obstacles preventing successful islet transplantation were a lack of functional islet mass for transplant, inadequate prevention of graft rejection and autoimmunity, toxic effects of immunosuppressants, and inadequate islet potency (Shapiro et al. 2003).

In a significant trial at the University of Alberta, the above concerns were addressed in a new transplantation protocol performed on seven patients, all of whom achieved insulin independence for at least 4 months (Shapiro et al. 2000). Important aspects of the transplantation protocol included a new immunosuppressive regimen, the Edmonton protocol, revised recipient selection criteria, the use of islets isolated from two or three donor pancreata, and the development of an improved isolation procedure (Kobayashi et al. 2004). Two main problems of this transplantation approach were identified: the use of immunosuppressants and lack of available islets (Kobayashi et al. 2004). The latter poses the biggest challenge to islet transplantation in general and much current research is focusing on this issue, as even if long term insulin independence could be achieved by an optimized transplantation protocol, there would still be an extreme shortage of donor islets.

2.2.5 Islet regenerative potential

The need for transplantable islet cells has forced researchers to explore avenues such as the *in vitro* expansion of islet cell mass as well as production of functional islet cells from stem or progenitor cell sources. Importantly, only one islet cell type, the β-cell, is required to both sense blood glucose and produce insulin. It is possible, therefore, that intact islets may not be needed for transplant, but only β-cells. Current research concerning the regenerative potential of islet cells, the identification of

putative stem or progenitor cells, and embryonic pancreatic development may together lead to and understanding of how islet cells can be expanded or produced *in vitro*.

Under normal, healthy conditions, mature adult β-cells are essentially non-proliferating (Bouwens et al. 1997). However, under prolonged hyperglycemic conditions β-cell mass has been observed to increase to compensate for increased insulin requirements (Bonner-Weir et al. 1989). This increase in β-cell mass in both rodents and humans is attributed to an increase in cell replication and a decrease in apoptosis (Bernard et al. 1999). The decrease in apoptosis is attributed to the glucose stimulated synthesis of proteins that suppress apoptotic mechanisms (Hoorens et al. 1996). β-cell mass also increases dramatically during pregnancy and returns to normal levels as soon as 10 days post partum (Scaglia et al. 1995). Islets of Langerhans are also known to have regenerative potential in animal models of decreased β-cell mass (Bonner-Weir et al. 1993; Cantenys et al. 1981). β-cell regeneration has been observed experimentally in rodents in response to a loss of pancreatic β-cell mass due to partial pancreatectomy (Bonner-Weir et al. 1993), duct obstruction (Rosenberg et al. 1983a), duct ligation (Wang et al. 1995) or streptozotocin treatment (Banerjee and Bhonde 2003; Cantenys et al. 1981; Fernandes et al. 1997; Guz et al. 2001). In these *in vivo* studies however, it has proven difficult to implicate specific cells and clearly identify the mechanisms involved in the regeneration process. Importantly, harnessing the proliferative and regenerative potential of these cells *in vitro* will be required if these cells are to be used for transplantation.

A central goal of current diabetes research, therefore, is to explore the possibility of the generation of functional islet cells *in vitro*. The main issues regarding this avenue of research has been i) the identification of cell sources for *in vitro* culture, ii) the potential for expansion of cell populations, and iii) the hormone-expressing capabilities of these cells. Potential sources for proliferative *in vitro* cultures include donor islets (Gao et al. 2005; Gershengorn et al. 2004; Jamal et al. 2005), exocrine pancreas (Baeyens et al. 2005), prospective islet stem or progenitor cells (Banerjee and Bhonde 2003; Bodnar et al. 2006; Guz et al. 2001), and hESCs (Jiang et al. 2007; Liew et al. 2008; Shim et al. 2007). Recently, a viral-mediated *in vitro* reprogramming of non-islet adult mouse cells to insulin-producing β-cells has also been reported (Zhou et al. 2008). However, targeting cells of islet, and particularly β-cell origin for production of insulin expressing cells may be advantageous, as it has been suggested that these cells may maintain the chromatic structure important for β-cell function and, therefore, be capable of differentiation to functional insulin producing cells (Efrat

2008).

Replication of β-cells has been demonstrated *in vivo* in both rodents and humans (Cano et al. 2008; Dor et al. 2004; Teta et al. 2007). However, culture of human β-cells *in vitro* results in limited replication and complete loss of phenotype (Beattie et al. 1997). Although the *in vivo* results demonstrate β-cell replicative potential, it is apparent that *in vitro* culture conditions do not provide the appropriate environment, possibly due to a lack of cell-cell or cell-matrix contact or autocrine or paracrine signaling, to maintain the β-cell phenotype and induce proliferation. The focus of much recent research efforts has therefore been the identification of cells capable of both stable *in vitro* expansion and the ability to differentiate into a β-cell phenotype.

The existence of an islet stem cell has yet to be proven, but many studies have led to the belief that such a stem or progenitor cell does exist. Isolation of islet stem or progenitor cells may allow for their stable expansion and subsequent differentiation. Studies have differed in their conclusion as to where islet stem/progenitor cells reside, including the pancreas, either endocrine (Guz et al. 2001) or exocrine (Seaberg et al. 2004), or elsewhere in the body, such as the bone marrow (Hess et al. 2003). Islet cell budding during regeneration, presumably from islet stem or progenitor cells, has been observed to occur from the pancreatic ductal lining (Bouwens and Pipeleers 1998), which resembles the formation of islet cells during embryogenesis and post-natal growth (Madsen et al. 1996). These ductal regions express transcription factors known to be involved in embryonic development of islets, such as Pdx-1 (Kritzik et al. 2000). For these reasons, some have speculated that islet regeneration is a recapitulation of embryogenetic processes, and therefore the same factors that control the original development of β-cells would also be involved in β-cell regeneration. To further support this theory, pancreatic ductal cells can be expanded *in vitro* to form functional islet-like structures (Bonner-Weir et al. 2000; Ramiya et al. 2000), although with significantly lower physiologically stimulated insulin production compared to native islet cells.

It has also been suggested that regenerative competent stem or progenitor cells reside within the islet itself (Guz et al. 2001; Zulewski et al. 2001). A population of cells expressing the neural stem cell-specific marker nestin has been identified in rat and human islets as well as in pancreatic ducts (Zulewski et al. 2001). These cells can differentiate *in vitro* into cells expressing pancreatic endocrine and exocrine cell markers as well as hepatocyte markers and into insulin-producing cells

(Zulewski et al. 2001). Other presumptive precursor cells have been identified in *in vivo* regenerating mice islets following streptozotocin treatment, expressing GLUT-2 or Pdx-1 and somatostatin (Guz et al. 2001). A rare population of mesenchymal stem cell (MSC) has also been postulated as an islet-resident stem cell (Davani et al. 2007), but it has been suggested that these cells are contaminants of the islet isolation process and are, in fact, of pancreatic exocrine or ductal origin (Seeberger et al. 2006). It is apparent that many questions remain to be answered concerning the existence of islet stem cells, their identity and location and their involvement in islet regeneration.

The final, and most promising, theory of islet regeneration suggests that committed pancreatic cells undergo a transdifferentiation process by which they revert from a differentiated phenotype into a more primitive state before redifferentiating into islet cells. Transdifferentiation is the reprogramming of gene expression of differentiated cells resulting in a phenotypic switch, and has been observed physiologically in several systems (Li et al. 2005). Generally, there is an intermediate stage of dedifferentiation where the cell expresses either markers for both types of cells or neither. Support for the hypothesis of β-cell regeneration via transdifferentiation comes from the observation of transitional forms of cells that co-express duct and islet markers (insulin and amylase, proinsulin and proamylase) during regeneration (Bouwens 1998). Other studies have also shown transdifferentiation of pancreatic acinar cells (Song et al. 2004), hepatoma cells (Li et al. 2005), and hepatocytes (Grompe 2003) into insulin-expressing cells. The main hypothesis behind harnessing transdifferentiation for production of transplantable cells is that the cells can be stimulated to undergo all stages of transdifferentiation *in vitro*, including a prolonged, proliferative dedifferentiated state. *In vitro* expansion of dedifferentiated islet cells has become a major focus of diabetes research (Efrat 2008; Gallo et al. 2007; Gershengorn et al. 2004; Jamal et al. 2003; Lechner et al. 2005), and will be the main system discussed in this thesis.

2.2.6 *In vitro* expansion of prospective islet progenitor cells

Isolated islets have been induced to undergo transdifferentiation into duct-like epithelial structures (DLS), which begins with fractional β-cell apoptosis followed by a phenotypic change in some or all of the remaining islet cells (Jamal et al. 2003; Lu et al. 2005; Yuan et al. 1996). The DLSs show a complete loss of islet hormone immunoreactivity and increases in expression of duct epithelial markers (cytokeratin-19 (ck-19), nestin), and also have a high proliferation rate (Jamal et al. 2005).

In addition, a sub-population of these cells express Pdx-1, the marker of embryonic islet progenitors.

Jamal et al. (Jamal et al. 2005) also showed that DLSs can be induced to revert back into an islet-like structure (ILS) by the addition of islet neogenesis associated protein (INGAP). INGAP, first identified by Rafaeloff (Rafaeloff et al. 1997), is a member of the Reg family of proteins, known to be involved with the induction of islet neogenesis in animal models (Lipsett et al. 2007), and acts by enhancing the secretion of insulin and the transcription of islet genes involved with islet metabolism, β-cell mass, and neogenesis (Barbosa et al. 2006). The ILSs were characterized by the reappearance of islet hormones and loss of duct epithelial markers, showed similar number and arrangement of cell types as native islets, and secreted insulin in a physiological manner (i.e. glucose responsiveness). The potential for cell mass expansion was shown by Jamal et al. (Jamal et al. 2005) when DLSs were fragmented into small clusters that proliferated and were subsequently induced to revert back to ILSs. These results demonstrate how the proliferative nature of the DLSs may be harnessed to produce a scalable system of cell mass expansion. However, DLSs consist of a heterogeneous population of cells, containing α-, δ-, and PP- cell-derived $ck19^+$ epithelial cells, and β-cell derived $nestin^+$ cells (Hanley et al. 2008), and the contribution of each cell type to both the proliferative and redifferentiation stages of Jamal's protocol (Jamal et al. 2005), have not been investigated.

Long term culture of islets on tissue culture-treated surfaces results in a population of proliferative fibroblast-like islet hormone-negative cells (Schmied et al. 2001), which have been termed islet-derived precursor cells (IPCs). An epithelial-to-mesenchymal transition (EMT) of β-cells was originally postulated as the source of human IPCs (hIPC) (Gershengorn et al. 2004), along with the remaining islet cell types. However, lack of quantitative results led researchers to speculate that hIPCs were produced from MSCs normally present in very low numbers in islets (Davani et al. 2007; Gallo et al. 2007), although it has been suggested these cells arise from existing MSCs in nonendocrine pancreas (Seeberger et al. 2006; Seeberger et al. 2009). It is clear that β-cell EMT does not occur in mouse islets, as several groups have demonstrated that the IPC population from dedifferentiated islets were not of β-cell origin (Atouf et al. 2007; Chase et al. 2007; Morton et al. 2007; Weinberg et al. 2007). Recent studies, however, has definitively displayed that human β-cells do undergo EMT *in vitro* to produce hIPCs (Russ et al. 2008) (Russ et al. 2009), strongly supporting the transdifferentiation hypothesis of islet regeneration (Gallo et al. 2007; Gershengorn et al. 2004; Lechner et al. 2005).

hIPCs can be obtained either through dissociation of donor-derived islets into single cell suspension (Lechner et al. 2005), or by plating of intact islets onto tissue culture dishes, where they attach and spread before proliferating after the commencement of passaging (Gallo et al. 2007; Gershengorn et al. 2004). hIPCs display a similar heterogeneity to DLSs, as they are comprised of $ck19^{+}$/E-$cadherin^{+}$ epithelial cells and $nestin^{+}$/$vimentin^{+}$ spindle-shaped cells (Lechner et al. 2005). hIPCs also can be induced to differentiate to islet-like cell clusters that express insulin functionally at levels up to 34% of freshly isolated human islets (Lechner et al. 2005). A number of other studies have described the differentiation of nestin+ cells towards islet-like cells (Gallo et al. 2007; Gershengorn et al. 2004; Zulewski et al. 2001), but it remains unclear if the ck-19+ cell population possess similar differentiation potential. Regardless, efforts to redifferentiate hIPCs into insulin-producing β-like cells have yet to yield promising results (Kayali et al. 2007).

2.3 Human embryonic stem cells and the stem cell niche

2.3.1 Stem cells

Stem cells are defined by two unique properties: self-renewal and pluripotency. Self-renewal refers to the ability to maintain robust proliferation and give rise to more stem cells over extended culture periods. However, the cells must also retain pluripotency, which is the ability to be stimulated to produce differentiated, more committed progenies for all tissues. Somatic stem cells exist *in vivo* and reside in specific tissues, such as hematopoietic stem cells (HSC) (Orkin 2000), central nervous stem cells (Gage 2000), MSCs (Bianco et al. 2001), and epithelial stem cells (Blanpain et al. 2007). These somatic stem cells offer potential to treat tissue specific processes and significant current research is being undertaken to identify, expand and differentiate these cells into clinical grade cell therapeutic products.

2.3.2 Human embryonic stem cells

hESCs are derived from the inner cell mass of the pre-implantation embryo (Thomson et al. 1998).

Unlike adult stem cells, which are generally maintained in a homeostatic state through asymmetric cell divisions (Scadden 2006), hESCs are in a constant state of expansion. hESCs, therefore, represent a unique population of cells that hold promise in treating disease and injury due to their defining characteristics of expansion and pluripotency. hESCs are, in effect, an *in vitro* artifact of transient *in vivo* pluripotent cells, since *in vivo* pluripotent cells do not undergo long-term self-renewal. Pluripotency in hESCs is defined by the ability to be stimulated to differentiate into all three germ layers (mesoderm, endoderm and ectoderm) and is can be tested *in vitro* through embryoid body formation, or more stringently *in vivo* through teratoma formation (Amit et al. 2000). Although not definitive, a number of transcription factors, most notably Octamer-3/4 (Oct-3/4), Nanog, stage-specific embryonic antigen-3 (SSEA-3), insulin-like growth factor-1 receptor (IGF1R), and sex determining region Y-box2 (Sox2) are considered reliable markers for hESCs (Jaenisch and Young 2008). Despite their potential, clinical implementation of hESCs or hESC-derived cells has been delayed by the difficulty in fully defining the conditions required for long-term, stable expansion of hESCs and for effective and complete differentiation to desired cell types (Metallo et al. 2008; Skottman et al. 2007). The use of defined media for expansion of hESCs generally result in difficulty in maintaining a stable hESC phenotype, or conversely result in an increase in self-renewal capacity, but at the expense of differentiation potential (Draper et al. 2004).

hESC cultures are morphologically, phenotypically and functionally heterogeneous (Bendall et al. 2007; Stewart et al. 2006; Thomson et al. 1998; Xu et al. 2001). Spontaneous differentiation of hESCs occurs in all culture formats, but is more prevalent as the culture becomes more defined, but less optimal (i.e. moving from feeder layers, to conditioned media, to defined media) (Bendall et al. 2008). This highlights the fact that hESC culture methods are suboptimal at providing self-renewal conditions and that heterogeneity is an inherent characteristic of current hESC cultures. However, prospective isolation of hESCs from bulk cultures containing spontaneously differentiated progeny prior to analysis is rarely employed (Bendall et al. 2007; Enver et al. 2005; Stewart et al. 2006).

Heterogeneity within hESCs (i.e. excluding spontaneously differentiated cells) has also been documented, similar to that described in MSCs (Park et al. 2007), and HSCs (Mazurier et al. 2004). Heterogeneity, in terms of expression of transcription factors exists, in mouse embryonic stem cells (mESC), characterized by an interconvertibility between the two populations and distinct differentiation biases (Chambers et al. 2007; Hayashi et al. 2008; Nunomura et al. 2005; Singh et al. 2007). Heterogeneity has been described in hESCs, based on expression of SSEA-3 (Stewart et al.

2006), Oct4, Nanog, and SSEA-4 (Laursen et al. 2007). In the case of SSEA-3, heterogeneity exists based on active SSEA-3^+ and less active SSEA-3^- states, defined by expression of hESC transcription factors, clonogenic capacity, and cell cycle properties (Stewart et al. 2006). However, both cell types are capable of producing pluripotent hESC cultures. Cell cycle heterogeneity also exists within hESC cultures based on $GCTM^{high}$, $GCTM^{low}$ and $GCTM^{neg}$ (an antibody specific to pericellular hESC matrix proteoglycans) subpopulations, which correlates to increased cell cycle times and decreased proportions of $Oct4^+$ cells, respectively (Filipczyk et al. 2007).

2.3.3 The hESC niche

Stem cell developmental potential is maintained by self-renewal, which is thought to be controlled *in vivo* through the extrinsic activity of specific microenvironments or niches. Signals from the niche provide cues for resident stem cells to undergo expansion, maintenance, or depletion divisions (Bendall et al. 2008). Stem cell niches are generally comprised of differentiated cells, providing both cell-cell contact and paracrine signaling, and a three-dimensional extracellular matrix secreted by the differentiated cells or stem cells themselves. The concept of the stem cell niche was first proposed in the mammalian hematopoietic system (Schofield 1978), and most direct evidence for the concept has come from studies in Drosophila and *C. elegans* (Crittenden et al. 2002; Xie and Spradling 2000). Stem cell niches are now associated with a number of organs and tissues, including the testis, intestinal crypt, and hair follicle (Li and Xie 2005).

In contrast to their *in vivo* counterparts, hESCs were originally thought to be able to maintain their phenotype in the absence of a niche. However, recent evidence has demonstrated that hESCs both create and are reliant on a microenvironment or *in vitro* niche (Bendall et al. 2007). Similar to *in vivo* stem cell niches, the hESC *in vitro* niche consists of supportive differentiated cells, including hESC-derived fibroblast like cells (hdFs), paracrine signals and interactions with extra-cellular matrix (ECM) components (Bendall et al. 2007; Greber et al. 2007; Peerani et al. 2007). Niche-independent hESC cultures can arise after a significant number of passages (Werbowetski-Ogilvie et al. 2008), demonstrating a variety of features suggestive of early transformation events, including growth factor independence, increased proliferation and dramatically reduced differentiation potential (Werbowetski-Ogilvie et al. 2008). This clearly demonstrates the importance of the *in vitro* niche and that niche components and dynamics are defining factors regulating hESC fate within the culture.

Paracrine signals, a critical component of the stem cell niche, are subject to diffusion limits and tend to affect cells in the immediate vicinity of their origin (Francis and Palsson 1997). Increasing distance from the niche results in differentiation of stem cells in *in vivo* systems, both invertebrate and vertebrate (Jones and Wagers 2008; Scadden 2006). Though the hESC niche is an *in vitro* phenomenon, the underlying function of this niche to maintain stem cell properties is retained; thus distance limitations surrounding paracrine niche effects are likely also present. In support of this, it has been observed that some hESC colonies exhibit internal/central differentiation suggesting that a minimum colony to niche distance is required to maintain hESCs (Peerani et al. 2007). Those findings suggested that the distance of hESC cells to supportive niche cells and colony size are each important factors in maintaining healthy hESC cultures. The molecular mechanisms of niche regulation of hESC self-renewal and pluripotency are still not well understood. A complete understanding of the factors involved may lead to development of improved defined media. Originally, mouse embryonic fibroblast (MEF) feeder layers were required to maintain hESCs in cultures. However, MEF conditioned media, with the inclusion of basic fibroblast growth factor (bFGF), in combination with extracellular matrix such as matrigel, provides a feeder-free option (Xu et al. 2001). The actions of exogenous bFGF on hdFs, which provides signals for hESC self-renewal and pluripotency.

The factors produced and secreted by hdFs have not been fully characterized, but are known to include insulin-like growth factor-II (IGF-II) and member of the transforming growth factor-β (TGF-β) family (Bendall et al. 2007). Furthermore, little is known about the signals that drive the differentiation of hESC to produce hdFs. It remains unclear if hdFs are a requisite component of hESC cultures, or if the development of an optimal culture media is possible that would eliminate the signals driving hdF differentiation.

Chapter 3
Design and Analysis of a Long Term Live Cell Imaging Chamber for Tracking Cellular Dynamics within Cultured Human Islets of Langerhans

3.1 Preamble

This chapter details the design considerations for the imaging chamber that is predominantly used for the LCI experiments that follow in subsequent chapters. The chamber was introduced previously for imaging monolayers of neural stem cells and mouse embryonic stem cells (Ramunas et al. 2006; Ramunas et al. 2007). Here, its use is extended to three-dimensional cultures of human islets of Langerhans.

3.1.1 Objective

Because the imaging chamber had not been utilized for LCI experiments on three-dimensional cell cultures, introduction of growth and metabolism limitations due to the confined nature of the chamber and new culture requirements has to be considered. A numerical model of the diffusion-based transport within the imaging chamber was developed to consider if the confined imaging system would negatively affect cell viability. Specifically, transport of media nutrients and oxygen to the islet are considered, as they are embedded in a collagen matrix, unlike previous monolayer cultures. Furthermore, the intra-islet diffusion of nutrients and oxygen are also considered. Cells within an islet experience concentration gradients as nutrients diffuse within the islet and are simultaneously taken up by cells. Of critical importance is to determine under what conditions islet metabolism is adversely affected by the imaging chamber configurations. Specifically, both chamber dimensions and islet sizes are considered. This is particularly important as the islet transformation phenomenon being studied involves a significant amount of internal β-cell death, and therefore observation of the process alone does not allow for the discrimination between the cell death caused by the inclusion of cholera toxin in the media and cell death caused by sub-optimal transport conditions.

3.1.2 Justification

Live cell imaging in three dimensions has been performed previously to assess cell migration through extracellular matrix in attempt to mimic *in vivo* conditions, which two-dimensional cultures cannot (Friedl and Brocker 2004; Niggemann et al. 2004; Niggemann et al. 1997). Such experiments, however, are performed by tracking the migration of only single cells in three-dimensions and are not capable of tracking multi-cellular aggregates. Recent developments in both genetic modifications to enhance cell tracking (Hadjantonakis and Papaioannou 2004; Kanda et al. 1998) and three-dimensional imaging technologies (Keller et al. 2008; Reynaud et al. 2008) have enabled characterization of multi-cellular aggregates at the single cell level. However, such imaging systems are relatively new and therefore may not be a justifiable expense for many biology labs. More significantly, genetic modification of input cells may not be possible or desirable. Indeed, this is the case for donated human islets of Langerhans. Although post-isolation modification of islet cells has been implemented (Hanley et al. 2008), this likely would not be desirable for any system that hopes to involve characterization or production of clinical grade cells for transplant. Therefore, an imaging system enabling characterization of unmodified three-dimensional islets of Langerhans was developed.

3.1.3 Approach

Because of the tedious and time consuming nature of imaging chamber construction, loading and imaging, assessing the range of chamber configurations and islet sizes experimentally was not feasible. Furthermore, as stated above, for the DLS transformation, it would not be possible to distinguish between expected and unwanted cell death. Computational modeling was therefore implemented. A three-dimensional diffusion/reaction model was developed using Comsol Multiphysics™ to consider appropriate chamber dimensions and maximum islet sizes. These chamber and islet parameters were then tested experimentally to ensure that future imaging experiments can be designed to provide appropriate conditions.

This chapter contains materials (sections 3.2 – 3.7) from:
Biotechnol Bioeng. 2007 Aug 1;97(5):1138-47.

Design and analysis of a long-term live-cell imaging chamber for tracking cellular dynamics within cultured human islets of Langerhans

Duane Moogk[1], Stephen Hanley[2], John Ramunas[1], April Blaylock[1], Jana Skorepova[1], Lawrence Rosenberg[2*], Eric Jervis[1*]

[1] Department of Chemical Engineering, University of Waterloo, Waterloo, Ontario N2L 3G1
[2] Department of Surgery, McGill University, Montréal, Quebec H3G 1A4

[*]Corresponding authors

Eric Jervis
Department of Chemical Engineering
University of Waterloo
200 University Ave. West
Waterloo, ON, Canada
N2L 3G1
Email: ericjj@cape.uwaterloo.ca
Phone: 519-888-4567 ext. 33928
Fax: 519-7464979

Lawrence Rosenberg
Montreal General Hospital
1650 Cedar Avenue
Montreal, PQ, Canada
H3G 1A4
E-mail: lawrence.rosenberg@mcgill.ca
Phone: 514-934-1934 ext. 42945
Fax: 514-934-8289

*Note regarding copyright permission from publisher – "Re-use in other publications. The right to re-use the final Contribution or parts thereof for any publication authored or edited by the Contributor (excluding journal articles) where such re-used material constitutes less than half of the total material in such publication. In such case, any modifications should be accurately noted." - http://media.wiley.com/assets/1540/87/ctaaus.pdf

Modifications to original publication:

- Materials and Methods section moved to end of chapter
- Additional figure added for clarity (Figure 3-1)
- Additional equations added for clarity (boundary and initial conditions)
- A small number of additional sentences were added for clarity
- Terminology of DEC changed to DLS to match remaining chapters
- Abstract was removed
- Reference list was included at end of thesis

Contribution of authors:

Stephen Hanley – islet isolation, purification and sorting
John Ramunas – image acquisition set-up
April Blaylock – image acquisition software
Jana Skorepova – provided figure 3-1a
Lawrence Rosenberg – manuscript review
Eric Jervis – manuscript review and editing

All other aspects of this chapter, including all writing, were performed by Duane Moogk

3.2 Introduction

Type I and II diabetes are associated with the autoimmune destruction of insulin producing β-cells or impaired β-cell function and resistance of target cells to insulin, respectively. Recent success in clinical trials has led many to believe that long-term independence from insulin therapy is achievable through islet transplantation (Ryan et al. 2005; Shapiro et al. 2000). Indeed, researchers are currently exploring means of expanding donor islet cell mass *in vitro* (Gao et al. 2005; Gershengorn et al. 2004; Jamal et al. 2005) and the production of functional islet cells from differentiated stem or progenitor cells (Banerjee and Bhonde 2003; Bodnar et al. 2006; Guz et al. 2001) with the objective of supplementing limited donor islet availability. Islet β-cell regeneration has been observed experimentally in rodents in response to a loss of pancreatic β-cell mass due to various interventions (Bonner-Weir et al. 1993; Cantenys et al. 1981; Rosenberg et al. 1983b; Wang et al. 1995) and i*n vitro* experiments have revealed an inherent plasticity of islet cells (Gao et al. 2005; Jamal et al. 2005). However, the specific cells and mechanisms involved in tissue regeneration and transformation processes remain unresolved (Dor et al. 2004).

Collagen-embedded human islets of Langerhans can be induced to transform into DLS, a process that progresses first as a wave of β-cell apoptosis followed by a phenotype change in some or all of the remaining islet mantle cells (Jamal et al. 2003; Lu et al. 2005; Yuan et al. 1996). The DLS show a complete loss of islet hormone immunoreactivity and increases in expression of the duct epithelial markers ck-19 and carbonic anhydrase II (Jamal et al. 2003). Significantly, DLS-resident cells have a high proliferation rate and a sub-population of these cells are hormone^{-}/PDX1^{+}, a marker of embryonic islet progenitors (Jamal et al. 2005). DLS can be induced to revert back into ILSs by the addition of INGAP (Jamal et al. 2005), first identified by Rafaeloff, et al. (Rafaeloff et al. 1997). The ILS are characterized by the reappearance of islet hormones and loss of duct epithelial markers, similar numbers and arrangements of cell types as intact islets, and secretion of insulin in a glucose-responsive manner.

Understanding cellular activities, interactions and processes in heterogeneous aggregated cell populations, such as islet of Langerhans, is an important goal in tissue engineering, embryology and stem cell biology (Khademhosseini et al. 2006). Implication of specific cell subpopulations in dynamic processes and long-term fate determination of individual cells is often difficult in these

systems. Herein we hypothesized that the ability to track cells in real time within a three-dimensional aggregate using robot-assisted time course imaging could further the understanding of tissue transformation events such as the islet to DLS and DLS to ILS transformation processes. Live cell bright field imaging has previously been utilized in monolayer cultures for studying cell behavior (DiMilla et al. 1993; Hsu 1960; Karpowicz et al. 2005) and morphological phenotypes (Geng et al. 2004), as well as for tracking single cell locomotion through three-dimensional substrates (Demou and McIntire 2002; Niggemann et al. 1997; Rabut and Ellenberg 2004). However, it is a less effective mode for studying cell aggregates as identifying and tracking individual cells in thick three-dimensional clusters becomes difficult.

Described herein is an imaging chamber designed to enable time course imaging of human islet of Langerhans with controlled aggregate thickness. Diffusion processes were modeled considering the imaging chamber's dimensions to evaluate the chamber design's effect on mass transport and to determine the appropriate dimensions to avoid introduction of metabolite transport limitations. Human islets of Langerhans were cultured in appropriately sized imaging chambers for 5 days to verify the utility of the design. Structure and phenotype were maintained in islets cultured in maintenance media, and cystic transformation was observed in islets cultured in islet-to-DLS transformation media. This approach sets the foundation for bioengineering at the single cell level that will enable the analysis of tissue biogenesis from tissue-resident stem and progenitor cell populations.

3.3 Mathematical models

Mass transport models were developed to consider the effects of the imaging chamber geometry on glucose and oxygen transport to isolated islets. The model considers diffusion as the only transport process, as isolated islets no longer receive metabolites through vasculature and convective fluxes are small enough to be considered negligible in a collagen-embedded islet. Grid convergence of the finite element solver was validated, as there were no significant changes in simulation results with varied grid sizes. Also, note that the geometry of the imaging chamber effectively isolates the gap-confined cells from any thermal-induced convection in the outer reservoir chamber (Figure 3-1).

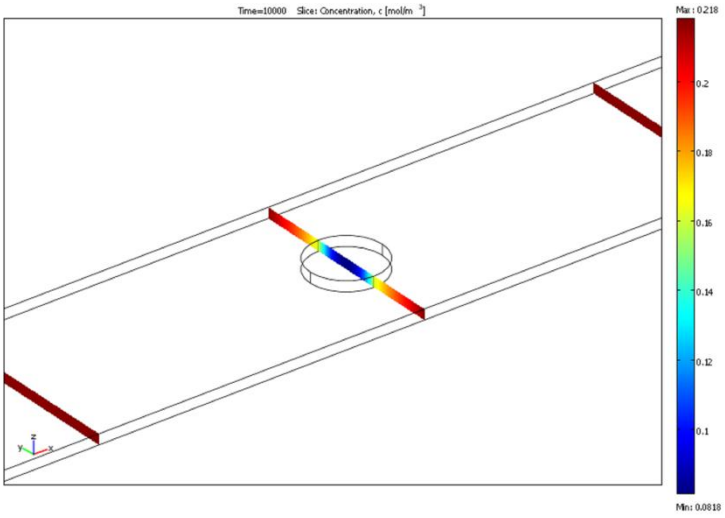

Figure 3-1. Schematic of the imaging chamber model. Color scale represents oxygen concentration within the collagen in the imaging chamber and within the islet extracellular space.

3.3.1 Glucose considerations

The partial differential equations describing the diffusion of glucose within a spherical islet were previously developed (Bertram and Pernarowski 1998) and have been modified here to consider a cylindrical coordinate system, as it is assumed that a spherical islet compressed in the imaging chamber would take on a roughly cylindrical structure; the curvature of the islet is considered small compared to the radius of the cylinder, while total islet volume is conserved.

Equations 1-4 represent the transport of glucose to and within the islet, as well as within the islet cells. Equation 1 describes the change in extracellular glucose concentration outside of the islet over time as the glucose diffuses from the media to the islet surface, whereas equation 2 describes the change in extracellular glucose concentration over time within the islet as the difference between the diffusion of glucose and the uptake of glucose into the islet cells, the latter being described by Equation 3. Equation 4 describes the change in intracellular glucose concentration as a summation of the diffusion of glucose between cellular gap junctions and the uptake of glucose from the extracellular space.

$$\frac{\partial C_{ge}}{\partial t} = D_c \frac{1}{r}\frac{\partial}{\partial r}\left(r \frac{\partial C_{ge}}{\partial r} \right), \qquad r > R,\ t > 0 \qquad (1)$$

$$\frac{\partial C_{ge}}{\partial t} = pD_c \frac{1}{r}\frac{\partial}{\partial r}\left(r \frac{\partial C_{ge}}{\partial r} \right) - \frac{1}{\rho} F\left(C_{ge}, C_{gi}\right), \qquad r < R,\ t > 0 \qquad (2)$$

$$F\left(C_{ge}, C_{gi}\right) = V_{\max} \frac{\left(C_{ge} - C_{gi}\right) K_m}{\left(K_m + C_{ge}\right)\left(K_m + C_{gi}\right)} \qquad (3)$$

$$\frac{\partial C_{gi}}{\partial t} = \frac{D_i}{r}\frac{\partial}{\partial r}\left(r \frac{\partial C_{gi}}{\partial r} \right) + \frac{1}{\rho} F(C_{ge}, C_{gi}), \qquad r < R,\ t > 0 \qquad (4)$$

Here C_{ge} represents the extracellular glucose concentration, p is the dimensionless islet porosity, D_c is the diffusivity of glucose through collagen, r is the radial distance from the centre of the islet, ρ is the dimensionless islet volume fraction (volume of extracellular space / cell volume), and R is the islet cylindrical radius. The function $F(C_{ge},C_{gi})$ represents glucose transport into the islet β-cells by the GLUT-2 transporter (Bertram and Pernarowski 1998). Here, C_{gi} is the intracellular glucose concentration, V_{max} is the maximum glucose uptake rate and K_m is the GLUT-2 transporter dissociation constant. Equation 4 considers the concentration of glucose inside the cells; however it does not include any consideration of glucose metabolism. Whitesell et al. (Whitesell et al. 1991) showed that glucose transport was in great excess of glucose metabolism in an insulin secreting cell line. We have therefore assumed that the glucose metabolism term is negligible when considering the glucose mass balance. Further, glucose transport should not limit metabolism over physiological ranges of glucose concentrations (3-15 mol/m^3) (Whitesell et al. 1991). The diffusion term is included in equation (4) to account for transport of intracellular glucose via gap junctions or by other means (Bertram and Pernarowski 1998), where D_i is the diffusivity of glucose through cellular gap junctions and is assumed to be somewhat smaller than extracellular glucose diffusivity.

The cylindrical system developed here, representing an islet in an imaging chamber, was modeled using COMSOL™ to investigate whether imaging chamber geometry adversely affects glucose transport to the islet. For design sensitivity analysis parameter values were set to an initial C_{ge} concentration of 5.2 mol/m^3 for r < R, to match normal islet culture conditions, and a C_{gi} concentration of 4.16 mol/m^3 (80% of extracellular glucose concentration). Values for the GLUT-2 dissociation rate, K_m, and GLUT-2 maximum uptake rate, V_{max}, were set to 17 mM and 0.53 mM/s,

respectively (Johnson et al. 1990). The diffusivity of glucose in collagen, D_c, was set to a value of 1.44 x 10^{-10} cm^2/s (Wu et al. 2005) and the intracellular glucose diffusivity, D_i, was set to a value of 1.44 x 10^{-12} cm^2/s. The islet volume fraction, ρ, was set to a value of 0.02 (Bonner-Weir 1988) and islet porosity, *p*, was set to a value of 0.03. The initial concentration of glucose within the collagen surrounding the islet was varied, as it depends on the amount of media initially mixed with the collagen during islet embedding. Boundary conditions assume zero flux at the islet centre for both C_{gi} and C_{ge}, continuity of C_{ge} at the islet edge, and a zero flux condition for C_{gi} at the islet edge. The two long edges of the imaging chamber were assigned a constant glucose concentration of 5.2 mol/m^3 to represent the bulk media. The width of the chamber (w) was varied between 1 and 3 mm. These boundary conditions are explicitly stated in equations 5-9.

$$\frac{\partial C_{gi}}{\partial r} = 0\,, \qquad r = 0 \qquad (5)$$

$$\frac{\partial C_{ge}}{\partial r} = 0\,, \qquad r = 0 \qquad (6)$$

$$\frac{\partial C_{gi}}{\partial r} = 0\,, \qquad r = R \qquad (7)$$

$$C_{ge} = 5.2\frac{mol}{m^3}\,, \qquad r > w \qquad (8)$$

$$C_{gi}(t = 0) = 4.16\frac{mol}{m^3}, \qquad r < R \qquad (9)$$

3.3.2 Oxygen considerations

A model of oxygen transport to islets in the imaging chamber was also developed in a cylindrical coordinate system to determine if oxygen transport was limited. Equation 10 describes the change in oxygen concentration over time as it diffuses to the islet surface from the surrounding media under the imaging chamber. Equation 11 describes the change in oxygen concentration over time within the islet as the difference between the diffusion of oxygen and its utilization by the islet cells.

$$\frac{\partial C_o}{\partial t} = D_o \frac{1}{r}\frac{\partial}{\partial r}\left(r\frac{\partial C_o}{\partial r}\right), \qquad r > R\ ,\ t > 0 \qquad (10)$$

$$\frac{\partial C_o}{\partial t} = pD_o \frac{1}{r}\frac{\partial}{\partial r}\left(r\frac{\partial C_o}{\partial r}\right) - Rxn\ , \qquad r < R\ ,\ t > 0 \qquad (11)$$

Here, C_o is the oxygen concentration, D_o is the diffusivity of oxygen in collagen, and *Rxn* is the oxygen consumption rate, a zeroth order term for which a volumetric rate is estimated by using the literature value of 5 pmol/min/islet and an average islet diameter of 150 µm (Sweet et al. 2002). Because the sizes of islets and imaging chamber that we could practically implement, based on technical issues such as image resolution and chamber construction, were considerably below the critical thresholds determined, sensitivity analysis was not performed for the model parameters. The initial concentration of oxygen in all regions is 0.218 mol/m^3, considering equilibrium with a 21% oxygen gas phase. Boundary conditions assume zero flux at the islet centre, due to spherical symmetry, continuity of C_o at the islet edge and a constant concentration of 0.218 mol/m^3 maintained along the two long edges of the imaging chamber representing the bulk media, and are presented explicitly in equations 12-13.

$$\frac{\partial C_o}{\partial r} = 0\ , \qquad r = 0 \qquad (12)$$

$$C_0 = 0.218\ \frac{mol}{m^3}\ , \qquad (13)$$

3.4 Results

3.4.1 The imaging chamber culture system

Initial efforts to image islets at single cell resolution in the absence of the imaging chamber were limited by the ability of bright field microscopy to focus through multiple layers of islet cells, such that only peripheral cells could be imaged. In those trials, islets were embedded in a collagen matrix in Petri dishes or flat bottom wells. Islet transformation to DLS was induced and observed under these culture conditions; however the underlying mechanisms of this process could not be

characterized because a majority of internal islet cells could not be identified or tracked during the transformation process (Figure 3-2a). Also, only those islets embedded very near to the dish bottom could be imaged at high resolution because of focal distance limitations. Thus, it was apparent that new culture strategies were required to enable tracking of all cells during time course imaging of intact islets.

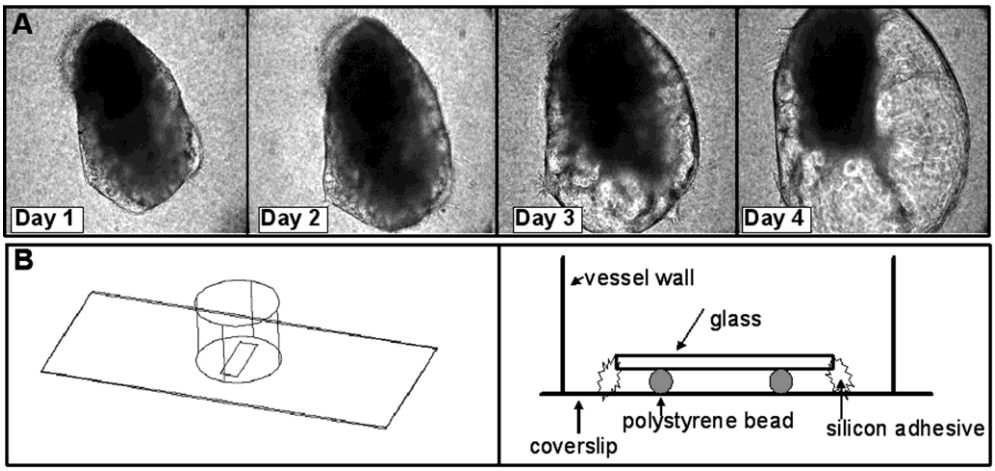

Figure 3-2. a. Initial time course imaging experiments were conducted with relatively large islets embedded in collagen in petri dishes or flat-bottom wells. Due to the thickness of the islet it is not possible to identify or track individual cells as the islet undergoes transformation to a DLS. b. Left: The imaging chamber is constructed on a coverslip. The actual culture surface is roughly 2 mm by 8 mm. Right: A side view of the imaging chamber shows how polystyrene microbeads are inserted under the gap to dictate the z-axis culture thickness. Elastic silicon adhesive is used to pull the top glass downward to maintain a tight and uniform gap spacing.

An imaging chamber, which functions to restrict the z-axis thickness of the culture, was implemented to facilitate time-course imaging of islets (Figure 3-2b). Previous studies have utilized the imaging chamber to restrict neurosphere growth to a two-dimensional monolayer and facilitate time course imaging and lineage informatics-based analysis (Ramunas et al. 2007). Although compression of an islet under the imaging chamber inevitably alters its structure, it was thought that cell-cell and cell-ECM connectivity and overall islet cell functions could be maintained by appropriate selection of both initial islet size and imaging chamber gap spacing. For imaging purposes, the maximum allowable islet thickness would likely be 3-4 cells thick, which would

translate to an imaging chamber thickness of 25-50 µm. A z-axis DIC focus series of a human islet in a 25 µm imaging chamber is shown in Figure 3-3.

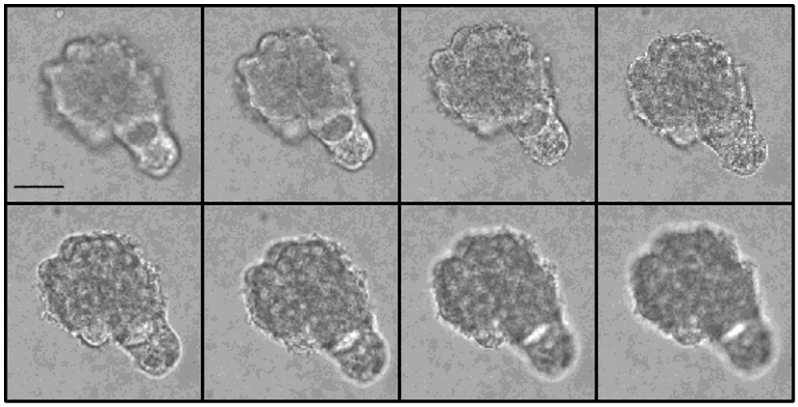

Figure 3-3. Z-axis optical sections of a human islet in a 25 µm gap thickness imaging chamber. The optical sections are 5 µm apart and include an extra section both below (top left) and above (bottom right) the islet to ensure the entire islet was imaged. Scale bar equals 25 µm.

3.4.2 Effect of glucose transport limitations on imaging chamber design

Numerical simulations of the mathematical model were performed in COMSOL™ to test the effect of the imaging chamber culture system on diffusive transport to the islet. In the simulations, the islet confined under an imaging chamber of a given size was exposed to a bulk media solution with a glucose concentration of 5.2 mol/m^3 to match normal islet culture conditions. For simplicity, the entire islet was modeled as a single solid object, instead of a group of individual cells, and therefore glucose concentrations are considered continuous throughout the cell mass and cellular uptake of glucose was assumed to occur as distributed point reactions throughout the entire islet. This was done because we were interested mostly in determining if the islet boundaries (edge and centre) were limited, for which we could then surmise if the cells are actually limited. Although this approach is a simplification over modeling a number of individual cells that together form an islet, it is useful because islet size can be varied easily without the need to alter the model geometry. It was determined that a sensitivity analysis of the parameters in the set of equations was not necessary, as this was a trivial situation, where the recovery time to equilibrium was the only issue and the initial conditions dictated this time. Diffusivities within the collagen were examined to determine the effect

of embedding the islets, and to model the diffusion of glucose through the extracellular islet space, also composed mainly of collagen.

Simulations were performed to determine whether islets in the imaging chamber experienced glucose concentrations below a set threshold of 2.5 mol/m^3, below which islet function is adversely affected (Schuit et al. 2001), for no longer than 50 minutes, as similar cell types can recover from glucose starvation times below this threshold (Kriat et al. 1992). Further, we wished to identify the minimum dimensions of the imaging chamber and maximum islet size at which mass transport limitation occurred, and to what extent the initial glucose concentration in the surrounding collagen affected results. It must be noted that these simulations ignore vasculature and convective flux, as may be the situation encountered by islets cultured under typical long term collagen-embedded cultures (Wang and Rosenberg 1999).

The simulations showed that the initial glucose concentration in the collagen was the most important parameter affecting glucose starvation times, as variation of both the imaging chamber size and the islet size had little effect. Regardless of the islet or imaging chamber sizes, the islet cells do not experience glucose levels below 2.5 mol/m^3 if the initial glucose concentration in the collagen is above this level. If the initial concentration is below this level the islet cells experience undesirable glucose concentrations. Thus initial islet loading protocols require that the collagen be prepared with appropriate substrate concentrations to avoid initial glucose starvation as the glucose diffuses from the bulk media through the glucose-depleted embedding collagen.

3.4.3 Effect of oxygen transport limitations on imaging chamber design

The COMSOL™ model for oxygen transport in the imaging chamber was used to determine if islets in the system experience hypoxic conditions due to transport limitations with the proposed design. With initial oxygen concentrations of 0.218 mol/m^3 throughout, we investigated whether the islets in the imaging chamber would experience oxygen concentrations below values that affect normal islet function, assumed to be 0.082 mol/m^3 (Dionne et al. 1989). We determined the minimum gap sizes acceptable for a range of initial islet sizes that maintain islets above this target oxygen concentration (Figure 3-4a). The results clearly show that, for imaging chambers in the desired range of thickness (25-50 μm), the maximum initial islet radii range from 80-100 μm, for a chamber width of 2 mm.

The simulations also allowed us to determine the maximum size a cylindrical islet could grow to before becoming oxygen limited for given imaging chamber sizes (Figure 3-4a). It can be seen that, regardless of the imaging chamber z-axis depth, for a chamber width of 2 mm the maximum aggregate radius is roughly 156 µm. Simulations of imaging chamber widths varying between 1 and 3 mm showed that the maximum aggregate thickness ranges from 177 µm to 148 µm for these respective extremes (data not shown). However, production and use of chambers with widths smaller than 2 mm becomes technically challenging. The simulated oxygen concentration profiles for a limiting and non-limiting case are shown for the islet edge and centre (Figure 3-4b).

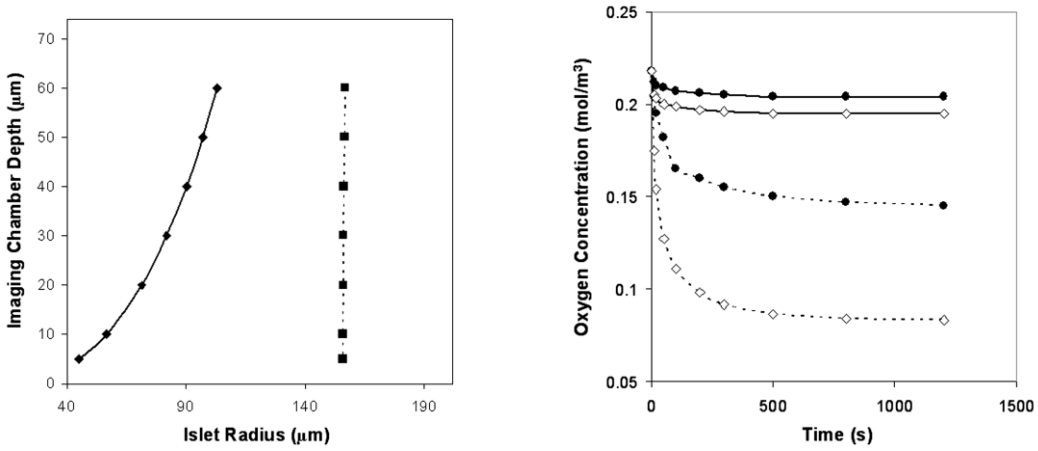

Figure 3-4. Left - Numerical simulations provided values for the maximum initial (spherical) radius of an islet for a given chamber size (solid line), and the (cylindrical) radius that the islet would be compressed to (dashed line). If an islet radius smaller than the maximum is chosen, the dashed line then represents the maximum radius that a proliferating islet could grow to before becoming oxygen limited, which is dependent only on the width of the imaging chamber. Right - Simulations of oxygen concentration profiles at the islet centre (diamond markers) and edge (round markers) over time. The solid line is for a 40 µm radius islet compressed into a 25 µm imaging gap. The dashed line is for a 100 µm radius islet compressed into a 50 µm gap.

3.4.4 Islet structure and phenotype can be maintained in a 25 μm imaging chamber for at least five days

The simulations showed that a 25 μm imaging chamber, which would result in an islet thickness of 2-3 cells, could maintain islets as large as 80 μm in initial radius before transport limitations arose. However, the smallest range of islet sizes was selected, generally between 35-45 μm in diameter, both to reduce the deformation of the islet structure during compression and to reduce the total number of islet cells to be tracked. Further, this size allows cell proliferation to occur without immediate limitations arising.

Time course image sets of human islets in a 25 μm imaging chamber were obtained at three minute intervals for a period of 5 days before islets were fixed and stained for islet hormones. Analysis of the time courses revealed that individual cells could be identified and tracked over time. Indeed, it is the movement of the cells from frame to frame that makes identifying the cells much easier than in static images. Cell borders can easily be identified and dense secretory vesicles within the cells are also very clearly observed in cytoplasmic flow using DIC bright field imaging. [see Appendix D - Movie 1: Islet maintained in 25 μm gap chamber for 5 days. scale bar = 25 μm]

Islets in the imaging chamber containing islet maintenance medium were imaged over 5 days at a single optical section with no significant changes observed regarding islet size, morphology and cell viability. Further, no cell divisions or death was observed at any point during the culture (Figure 3-5a). Thus, extended time course imaging is feasible in this non-proliferative culture. At a randomly selected time point near the beginning of the experiment 29 cells could be positively identified (Figure 3-5b). Although there is significant cytoplasmic motion, it did not appear at any time that cells were migrating, as they generally remained in the same location relative to the surrounding cells, making it trivial to follow individual cells in intact islets over time.

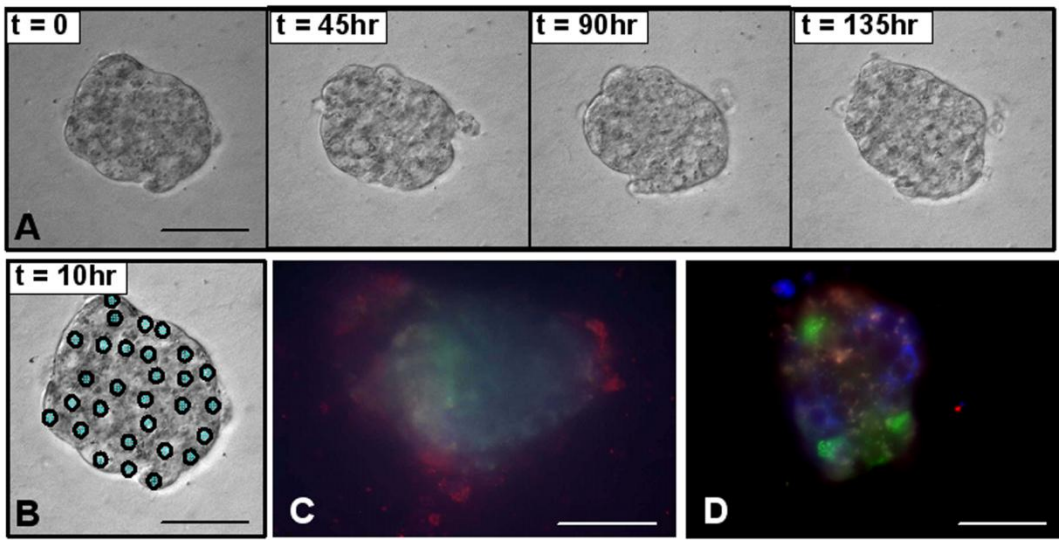

Figure 3-5. An islet embedded in collagen in a 25 µm gap thickness imaging chamber was cultured in islet maintenance media for five days. A. No changes in islet structure, cellular organization, or cell viability were apparent over the culture period. B. Islet cells can be identified and tracked over time; here, 29 cells are identifiable. Immunostaining for islet hormones after five days culture (insulin - green, glucagon - blue, somatostatin - red) – C. Islet cultured in absence of imaging chamber. D. Islet cultured in 25 µm gap thickness imaging chamber. Scale bars equal 25 µm.

The islets were fixed and permeabilized in place in the imaging chamber and stained for the islet hormones insulin, glucagon and somatostatin. Imaging showed cells positively stained for each islet hormone, with no co-staining observed, confirming that islet α-, β-, and δ-cells were viable and expressed glucagon, insulin and somatostatin, respectively, and verifying that islet cell phenotype was maintained over the 5 day culture period during imaging (Figure 3-4d). Islet hormone expression appeared similar to islets cultured in normal open chambers, but cultured exactly the same otherwise (Figure 3-5c), leading us to conclude that the imaging chamber does not significantly alter the physiological state of the islet.

Islet cells identified with fluorescent imaging could be related to the final time point of the DIC time course. This allows for the movies to be observed with the knowledge of cell phenotype.

Because the islet cells are relatively inactive while cultured in the islet maintenance media, it was not possible to identify distinct morphological or behavioral traits related to specific cell types.

3.4.5 Islet to DLS transformation induced and observed under a 25 µm imaging chamber

Islets were cultured in a 25 µm imaging chamber containing islet transformation media. Cystic transformation was observed in roughly 30% of these islets (Figure 3-6). The overall cystic structure of the transformed islets appears to form from the combination of a number of smaller cysts within the islet and through a combination of cell death and the stretching of viable cells throughout the islet. [see Appendix E - Movie 2: Islet phenotype transformation in a 25 µm gap chamber for 5 days. scale bar = 25 µm] These smaller cysts eventually merged, although the exact mechanism of this event cannot be fully discerned from the single focal plane time course. The cystic structure collapsed at two separate time points due to a lack of collagen matrix support surrounding part of the islet. The islet cells pulled the remaining surrounding collagen matrix inward, observable using the polystyrene beads within the collagen gel as tracers, at a rate of 0.2 µm/min. Following culture, transformed islets were fixed and stained in the imaging chamber at the same time as the non-transforming islets. Imaging showed no appreciable positive staining for any of the three islet hormones (data not shown), confirming that the remaining viable cells were no longer expressing islet hormones at the time of fixing. These observations, coupled with the change in morphologies seen in the time courses confirm that the islet cells have indeed undergone a phenotypic transformation.

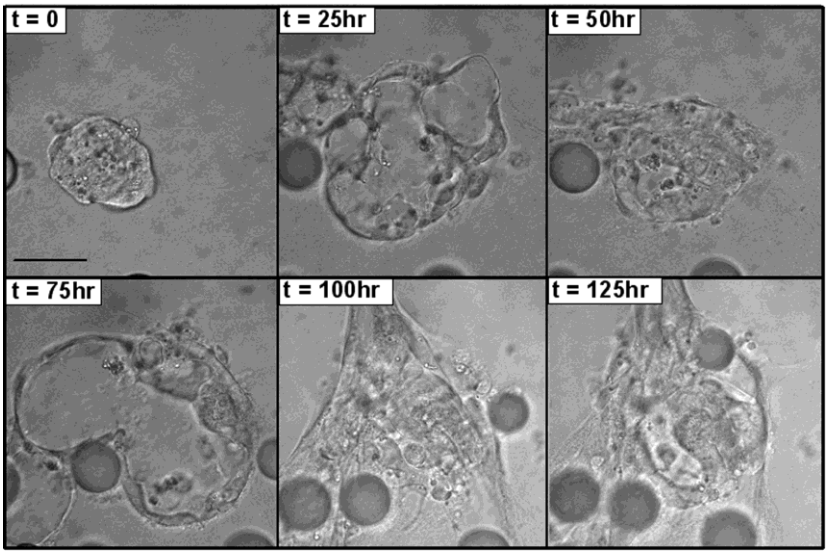

Figure 3-6. Time course shows the transformation of islet to cyst. The collapse of the cysts, as seen at 50 hours and 100 hours onward is due to the breakdown of the collagen surrounding the islet. By 25 hours no collagen is visible along one side of the islet (top of image). By 100 hours, islet cells begin to pull collagen (and beads within it) inwards. Scale bar equals 25 µm.

All cystic structures were observed to initiate formation between 0 and 17 hours following addition of the transformation media. Most cells could be tracked over time by identification and tracking of cell borders and/or secretory vesicles. Unfortunately, some cells became untrackable as they migrated to out-of-focal plane segments of the islet. The incorporation of automated three-dimensional time course imaging will eliminate this problem and is currently under development.

Cyst formation coincided with cell death, as previously reported (Jamal et al. 2003). During cell death the surrounding viable cells detach from the dying cells and begin to stretch and spread away from the dead cells. Dead cells remained inside the cystic structures that formed around them. Over time these dead cells shifted out of focus and the long term fate of this debris remains unclear. However, cell debris is not typically observed in three-dimensional sections of cystic structures so degradation of this material must be occurring. Cell death was observed in 6 of 16 and 4 of 12 cells tracked from two islets (data not shown), the majority of which (8 of 10) were originally located in the core of the islet. This agrees with previous reports suggesting that the wave of cell death during cystic formation is primarily β cells (Jamal et al. 2005). However, other cells originally located

within the islet core did remain viable and became part of the cystic structures, eventually relocating to the periphery.

Thinly stretched cells were observed either above or below (z-axis) the cysts, confirming that cysts were enclosed completely by cells, and not the imaging chamber walls. This is an important observation as it suggests that the cyst formation process is not altered significantly by the presence of the imaging chamber boundary surface (i.e. cysts appear to be completely enclosed by cells and not the chamber walls). After formation, most of the cystic structures grew and shrank in a pulsing manner, as peripheral cells comprising the cysts stretched and compressed in a cyclic progression. This is routinely observed in larger embedded transformed islets cultured in much thicker preparations. It was observed that some of the viable cells remained round and compact on the periphery of the cystic structures, while others stretched into elongated cells that formed the cyst boundaries. The evaluation of the nature of these different cells and their significance in islet regeneration is currently underway.

3.5 Discussion

As tissue engineering and regeneration research advances it will become imperative to observe and characterize individual cellular activities within three-dimensional, heterogeneous multi-cellular aggregates intended for transplant. Long-term live-cell imaging, cell tracking, and lineage analysis will be a useful tool in characterizing the dynamic events of tissue transformation and biogenesis. To this end, we have designed and implemented an imaging chamber that facilitates live cell imaging of cellular aggregates while maintaining the three-dimensional structure required for cell-cell and cell-extracellular matrix interactions. This design has the significant advantage of preserving dynamic processes including growth, death and transformation. Although confocal microscopy has been used to image islets at the single cell level, only single time point studies have been reported (Boffa et al. 2005; Brissova et al. 2005; Hermann et al. 2005). The dependence of this imaging modality on fluorescence means that long term live cell imaging for the purposes of single cell tracking is not feasible as phototoxicity will undoubtedly affect long-term cell viability.

The imaging chamber described herein has previously been implemented to study monolayer cultures (Karpowicz et al. 2005; Ramunas et al. 2007). Herein, chamber design criteria were

investigated to ensure the imaging chamber could be used for collagen-embedded three-dimensional cultures of human islets of Langerhans. Mathematical modeling was used to validate the design and determine the limits of the chamber dimensions and islet sizes which ensure that metabolite transport limitations do not create culture conditions unfavorable to islet survival and function. Models of glucose and oxygen transport were developed and tested to evaluate these critical culture parameters.

The simulations reveal that, regardless of the imaging chamber dimensions and islet size, glucose limitation can be prevented by ensuring that the collagen surrounding the islets has an initial glucose concentration of at least 2.5 mol/m^3. Glucose diffusion to the islet is not a limiting process, as the surrounding collagen reaches an equilibrium concentration of the bulk media, 5.2 mol/m^3, for all cases. It is, however, for the cases where the initial collagen glucose concentration is less than 2.5 mol/m^3 that the islet experiences low glucose for lengths of time considered unfavorable for islet survival and proper function. If the collagen is prepared in glucose free media an islet would experience glucose limitation for several hours. Providing the same initial glucose concentration in the collagen as the bulk media would ensure that the islets were exposed to this concentration over the duration of culture (Lu et al. 2005). For the islet imaging experiments, the islets were left in a small amount of media prior to suspension in collagen. The exact volume of the media is not known (~3-6 µL), and therefore the initial glucose concentration cannot be determined. However, because the islets remain viable and functional for long periods, it can be assumed that the initial glucose concentration in the collagen is sufficient to avoid glucose starvation during the initial phase of the experiments.

For oxygen transport we determined the minimum gap size for a range of islet sizes required to prevent hypoxic conditions within a non-proliferating islet, as well as the maximum radius to which a proliferating islet could grow to before becoming hypoxic for different chamber widths. For imaging and cell tracking purposes it is desired to have an imaging chamber that creates a three to four cell thick cell mass, requiring 25-50 µm chamber gap spacing. The simulations show that islets with an initial radius of up to 80-100 µm can be cultured in imaging chambers with these dimensions without experiencing oxygen transport limitations. For larger islets, oxygen supplementation to increase the bulk concentration is possible (e.g. a doubling of dissolved oxygen allows islets with an initial radius of 110-140 µm to be cultured). In general, oxygen transport is affected predominantly by the width of the imaging chamber (i.e. distance of the islet to the gap opening), and therefore altering these dimensions will allow for the culture of larger islets within the desirable chamber

spacing for imaging and tracking – although chambers of smaller dimensions are considerably more difficult to fabricate and use.

The mathematical models implemented to examine the imaging chamber's effect on metabolite transport incorporate several simplifications and assumptions. Diffusion is likely the only mode of metabolite transport to the islets in the imaging chamber; however, it remains unclear if cellular movement within the transforming islet introduces local convective fluxes with an order of magnitude equal to or greater than the diffusive flux. The model was also simplified by considering an islet as a single solid object with a porosity specified to account for extracellular space. Both extracellular and intracellular oxygen and glucose concentrations were considered continuous throughout the entire islet mass and uptake of these components by the cells was modeled as distributed point reactions; intracellular metabolism of these components was not considered. Although simplified, the model allowed us to select islet and imaging chamber sizes for long term imaging experiments, and we have validated that human islets can be maintained under these conditions for periods of up to 5 days.

Significantly, we have also shown that human islets can be induced to transform into DLS within the imaging chamber. Although only a single optical section time course was obtained, several observations regarding the mechanisms of the transformation process were made. First, observation of cell death, predominantly in the core of the islet, agrees with previous descriptions of the islet to DLS transformation (Jamal et al. 2005). Here we were able to show that cyst initiation results from the detachment of transforming cells from dead cells and the subsequent morphological change of these cells from round and compact to elongated. Other key observations include that not all internal islet cells died, but some migrated to the islet periphery during transformation, and that after cystic transformation was apparently complete, a range of cell sizes and shapes, both round and stretched, existed. The phenotypic identity of these cells before, during, and after the islet to DLS transformation remains unclear, although it was confirmed that no cells expressed insulin, glucagon or somatostatin after islet transformation.

The time course images described herein were obtained from single optical sections of islets, however, a complete understanding of the dynamics of islet transformation can only be gained from imaging and tracking all islet cells. Such z-stack optical section time courses can be attained with the implementation of a robotic microscope stage. These systems will allow for 3-axis panning of the

imaging chamber to obtain three-dimensional time course images of multiple islets. Robotic stages enable a greater number of islets to be imaged, as the current static experiments described here can image only one full islet transformation at a time. It must be noted that the chamber was designed solely as a tool for imaging islets, as recovery of transformed islets from the chamber is difficult. Future bioreactor configurations aimed at expansion and recovery of islet cells for clinical use will have to be designed as a more open system and clearly at a much larger scale. The imaging chamber, however, will aid in gaining a more fundamental understanding of human islet plasticity and potential for expansion. Further, it will facilitate the analysis and tracking of every cell in the tissue mass. Such detailed analysis of cells will likely be required as bioengineered processes move toward the cell as therapeutic product. Clearly new levels of quality assurance will be required because bioengineered transplanted cells and their progeny should remain with the patient for the patient's lifetime. Over such extended periods product quality control and assurance take on new significance – what is the penalty for transplanting one bad cell, and how can processes be engineered to minimize this potential?

3.6 Materials and methods

3.6.1 Imaging chamber construction and preparation

To construct the imaging chambers (Figure 3-1b) a 2 mm by 8 mm rectangle cut from a microscope slide was glued at the short ends to a cover slip with silicon adhesive glue. A 15 mm length of 12 mm inside diameter glass tubing was glued to the cover slip, enclosing the rectangular microscope slide to form a well. The chambers were autoclaved submerged in deionized water and then rinsed with phosphate buffered saline (PBS) prior to use. Polystyrene microspheres (Polysciences, Warrington, PA, USA) with a mean diameter of 25 μm were sterilized by suspension in 70% ethanol followed by rinsing three times in phosphate buffered saline (PBS). The imaging chambers were conditioned with a 1% bovine serum albumin (BSA) (Sigma, St. Louis, MO, USA) in PBS solution containing the 25 μm microspheres at a concentration of 10^6 microspheres/mL. Tweezers were used to gently lift one edge of the top surface and 5-10 μL of the solution was pipetted between the surfaces. The chambers were filled with 1 mL of 1% BSA in PBS and incubated at 37ºC with 5% CO_2 for at least 4 hours. Prior to use, the chambers were rinsed three times with PBS.

3.6.2 Isolation and culture of human islets of Langerhans

Human islets were isolated from cadaveric donor organs at the Montreal General Hospital, as previously described (Jamal et al. 2005). CMRL-1066 medium with antibiotics and antimycotics (Gibco, Burlington, ON, Canada) and 10% foetal bovine serum (FBS) (MBI, Amherst, NY, USA) was used as islet maintenance culture medium. The islets were sorted by size and approximately 600 islets were isolated from the smallest size fraction (diameter range 35-45 μm) and then shipped overnight from Montreal, QC to Waterloo, ON at room temperature in a 1 mL Eppendorf tube containing islet maintenance media. To induce transformation, islets were cultured in DMEM/F12 (Gibco) with 10% FBS, antibiotics and antimycotics, 1 μM dexamethasone, 10 ng/mL epidermal growth factor, 24 mU/mL insulin and 200 ng/mL cholera toxin (Sigma).

3.6.3 Loading and culture of islets in imaging chambers

For each gap to be loaded, 50 μL of the islet suspension was pipetted into a 1 mL Eppendorf tube and centrifuged briefly at ~600 rpm. The supernatant was removed, leaving only a small volume of media (~3-6 μL). The islets were then resuspended in 6 μL of chilled collagen, followed by the addition of 1 μL of a 10^7 microspheres/L suspension of 25 μm microspheres. Immediately prior to loading, 1 μL of collagen neutralizing solution (600 μL 10x Waymouth media, 400 μL 0.34 N sodium hydroxide (NaOH)) was added to the suspension and mixed well. To load the islets under the imaging chamber the top surface was lifted from the bottom cover slip using tweezers and 5-10 μL of the suspension was pipetted onto the cover slip at the opening of the imaging chamber, which was then drawn into the gap space by capillary action. The top surface was gently lowered to minimize ejection of the loaded islets and microspheres. The chamber was incubated at 37º C for at least 20 minutes to allow for collagen gelling. The chamber reservoir was then topped with 1 mL of the appropriate media, maintenance or transformation, and a glass lid was placed over the top of the vessel to maintain sterility.

3.6.4 Long-term live cell imaging

Islets were imaged on an inverted microscope (Axiovert 200, Zeiss Germany). Chambers were maintained at 37^{o}C in a 5% CO_2 humidified air atmosphere. To minimize phototoxicity, a shutter was used to ensure incident light from the microscopes only reached samples while images were being acquired. Images were captured at three minute intervals using a digital camera (XCD-SX910, Sony Japan). The islets were manually focused on an optical section deemed to be near the centre of the islet. The focus was locked, but readjusted from time to time to account for slight focal plane drift.

3.6.5 Immunocytochemistry

After imaging, islets were washed three times for 10 minutes with PBS in the imaging chamber, fixed with 4% paraformaldehyde for 15 minutes, permeabilized with 0.1% Triton X-100 (Gibco, Grand Island, NY, USA) for 10 minutes, and blocked with 10% goat serum in PBS for 1 hour, all steps at room temperature. All subsequent washes were performed with 10% goat serum in PBS. Islets were treated simultaneously with rabbit anti-somatostatin (1:50) (Cedarlane, Hornby, ON, Canada), guinea pig anti-insulin (1:50) and mouse anti-glucagon (1:1000) (Sigma, St. Louis, MO, USA) primary antibodies for 2 hours at room temperature. The islets were washed three times for 10 minutes before simultaneous exposure to fluorescein isothiocyanate (FITC) -conjugated goat anti-rabbit IgG (1:200) (Cedarlane, Hornby, ON, Canada), tetramethyl rhodamine iso-thiocyanate (TRITC) -conjugated goat anti-guinea pig IgG (1:200), and 7-amino-4-methylcoumarin-3-acetic acid (AMCA) -conjugated goat anti-mouse IgG (1:200) for 2 hours and then washed 3 times for 10 minutes.

3.7 Supplemental data and discussion

The main focus of this chapter was the development of a model specifically considering human islets of Langerhans. The model therefore focused on a three-dimensional, multi-layer aggregate of cells embedded within collagen. However, given the desire to perform live cell imaging on a number of cell types with varying configurations (i.e. monolayer, multilayer, aggregating and non-aggregating colonies), some of the results from this islet-specific model can be generalized for this purpose. The model parameters could easily be changed to represent different cell types or matrix components, provided the appropriate values could be attained from literature or independently measured. For aggregating cell colonies, the depth of the imaging chamber, as dictated by the spacing beads, has no effect on nutrient transport. The only consideration that is needed, as in the islet case, is that aggregates are compressed when loaded into the chamber. The chamber depth is only of importance because it will dictate to what dimensions the aggregate will be compressed, and therefore if radial transport limitations will occur. Because of this, the model results apply equally to monolayer and multilayer cell configurations.

In the case of cholera toxin-induced DLSs, cell death is expected for the majority of core β-cells (Jamal et al. 2003). Therefore, experimental testing of culture parameters based on observation would not be feasible, as discrimination between cell death due to cholera toxin versus sub-optimal culture conditions would not be possible. However, for a culture of cells under stable growth or maintenance conditions, cell death, particularly at the centre of the colony, would be a clear indication of chamber-induced cell death. Therefore, in future studies, particularly of hESCs (Chapter 5), the maximum colony diameters determined from these simulations as a reasonable first guess at the limits to which hESC colonies could grow. Although a number of conditions were different, including a lack of ECM embedding and likely different cell uptake rates, these results at least allowed us to select colonies of appropriate small sizes and predict roughly to what size we could track their growth before apoptotic conditions were introduced.

Chapter 4
Live Cell Imaging, Cell Tracking and Analysis in Two and Three Dimensions with Applications to Islet-Derived Precursor Cells

4.1 Preamble

This chapter describes the design and development of the cell tracking and analysis tools used for two- and three-dimensional LCI data sets. The imaging chamber introduced in chapter 3 was implemented as a three-dimensional culture system for derivation of hIPCs, while a standard culture system was employed to characterize the two-dimensional hIPC derivation process.

4.1.1 Objectives

The first objective of the chapter is to develop and test a comprehensive cell tracking and analysis system for LCI data. Given raw LCI image data as an input, the goal is to enable fast, accurate and detailed tracking and analysis. The first aspect to consider is manual cell tracking, where a user identifies, tracks, and scores individual cells for either predetermined or emergent features, with the overall objective of creating a comprehensive database detailing the cell-level properties of every cell within an LCI image set. An important aspect of the design was incorporation of cell relationships to enable lineage analysis. Colony tracking tools were also developed to include colony-level information.

The second objective is to develop a set of tools for analyzing the tracked data and incorporating cell, lineage, and colony measures together for analysis. Of particular interest are methods to query very large data sets with specific hypotheses in a quick and informative manner. To achieve this, a system incorporating data queries and interactive visualizations was developed.

To implement and test these features, LCI of human islet of Langerhans was performed to investigate the production of hIPCs, recently demonstrated in two- and three-dimensional culture

systems (Gallo et al. 2007; Gershengorn et al. 2004; Jamal et al. 2003; Lechner et al. 2005). The objective is to observe and characterize hIPC derivation and proliferation to assess the contribution of different cell types to each culture phase. Both two-dimensional and three-dimensional hIPC derivation processes were studied and compared using the cell tracking and analysis tools to test the feasibility and utility of each combination of culture method, LCI strategy, cell tracking approach and analysis tool.

4.1.2 Justification

While software packages are available for analyzing LCI data, most require very specific input image data formats, to which the LCI data obtained in these experiments may not match, since the system developed here produces two- and three-dimensional tiled arrays. Furthermore, analysis packages are often inflexible and therefore new ideas and strategies for data analysis and presentation are difficult or impossible to implement. Because part of the objective is to consider new methods for querying and visualizing LCI data, a system was developed in-house to ensure flexibility and compatibility with the existing LCI image data structure.

Islets of Langerhans consist of well characterized cell types (hormone-secreting α-, β-, δ-, and PP cells), as well as a number of less characterized types (Petropavlovskaia et al. 2007). The contribution of these cells to hIPCs, regardless of the derivation process, remains unclear. hIPCs consist of at least two distinct sub-populations of cells (Hanley et al. 2008; Lechner et al. 2005). Recently, the cellular origins of DLS (hIPCs derived in collagen embedded cultures) cells were shown (Hanley et al. 2008), but the contribution of individual cell types to the expansion phase of DLS culture is still unknown. Live cell imaging provides the ability to identify how individual cells contribute to both the hIPC derivation and expansion phases. Identification of sub-populations of cells that contribute to hIPCs may aid in further understanding the physiological relevance of these cells. Furthermore, identification of sub-populations better suited for expansion and/or redifferentiation to islet-like cells may aid in the development of strategies and protocols for large-scale production of islet progenitors or functional islet-like cells.

4.1.3 Approach

Two- and three-dimensional live cell imaging and cell tracking was performed to characterize both hIPC derivation methods. The methods for two-dimensional culture were followed as presented by Gallo and colleagues (Gallo et al. 2007), and therefore imaging and cell tracking was performed without the need for culture optimization. Three-dimensional experiments were performed using methods developed in chapter 3. Methods for tracking and analyzing the LCI data in two and three dimensions were developed and evaluated. Finally, strategies and tools for analysis and visualization of tracked LCI data were developed and implemented to examine the nature of hIPC derivation and proliferation.

*Note: Design of the cell tracking and analysis tools was done collaboratively with Darik Gamble, who was also responsible for:

- all design aspects involved with image archiving and retrieval
- all design aspects involved with the database creation, updating, and structure
- software coding for the cell tracking, lineage tracking, and analysis tools

4.2 Development of LCI tracking and analysis tools

The methods that can be used for tracking LCI data depend on the imaging system employed and other considerations such as ease of automation and the inclusion of markers, as discussed in the literature review. For DIC or phase contrast LCI, manual tracking is often employed, and was done so here. A significant design aspect to consider when implementing manual cell tracking is the speed at which tracking can be performed. Because LCI produces very large raw image files, the speed at which a user can open, browse, and switch between image files, track cells and include observable properties and observations into the database can largely affect the productivity and throughput of the post-LCI analysis.

Analysis of tracked LCI data has historically been limited to single cell properties being investigated, such as migration rates, lifespan, or size (DiMilla et al. 1993; Hsu 1960; Killander and Zetterberg 1965a). These measurements could then be analyzed in a standard fashion. However, tracked LCI datasets that incorporate a number of cell properties over a number of generations present

a unique challenge for analysis. Lineage-based analytical techniques are not well developed. In fact, a recent paper by Glauche and colleagues (Glauche et al. 2009) was the first to establish a set of statistical measures tailored to analyzing cell lineage data. These measures are a useful tool for characterizing lineages and sub-lineage components, and generally produce a reduced set of parameters to describe individual lineages (e.g. number of leaves, number of divisions, branch lengths, cell death index). Therefore, the result is a smaller number of measures that still require interpretation and analysis, and do not retain the generational information that the lineage provides. Further development of such measures will certainly improve the quality of LCI data analysis.

4.2.1 LCI data structure

The cell tracking system was designed to handle the structure of the LCI data sets. During imaging, individual regions of a culture are imaged as tiled arrays of individual field of view (FOV), either as two-dimensional mosaics or three-dimensional hypercubes. These multi-FOV regions are termed 'blocks' and are stored as separate raw image files. Each block is accompanied by a comma-separated value (CSV) file that contains image meta-data: the x-y-z location of each frame FOV (the top left of the image, in robotic motor units from a preset home position) and the acquisition time of each image. Individual blocks can have unique hypercube dimensions and image intervals, which can be altered in real time. A master file is also created, which contains experimental meta-data: the settings for each block including imaging frequency, block dimensions, robotic step sizes, and camera settings. This meta-data also contains the manufacturer-specified conversion between robotic motor units and micrometers, microscope magnification levels, and digital image size. The image coordinates are converted to a set of (x,y,z) points that describes an image's spatial extent in terms of micrometers, relative to a preset 'home' point (0,0,0). This allows for accurate measurement of cells and sub-cellular components, with sub-micron resolution.

The LCI image files and corresponding image and experimental meta-data are loaded together into a Matlab-based, structured query language (SQL) database-backed cell tracking and analysis program. The block structure is maintained in the database relational model of the experiment, but is further divided into 'layers'. The original set of images provides the basis for the first layer of the block. Additional layers are created by extracting information from the image raw data. For example, tracked cell positions comprise a second layer, and cell outlines another. The

layers are presented together, but can be isolated or ignored depending on the current layers of interest. For example, during single cell tracking the DIC and tracked cell layers are displayed together. Significant consideration regarding the management, archiving, retrieval, display, and updating of the database during tracking were taken into account by the software programmer, Darik Gamble.

4.2.2 Navigation and cell tracking

LCI blocks are loaded sequentially by the tracking software for viewing and the image sequences are progressed forward or backward using keyboard shortcuts for easy navigation during manual tracking. Images can be zoomed to any level and the screen can be scrolled in the x- or y- direction at any zoom level. For z-slices, at any time point the user can scroll through the z-stack and place a tracking point at any level. Users can manually jump to any time point by entering the frame number, and shortcuts are also available to jump to the first or last frame of the image set (Figure 4-1).

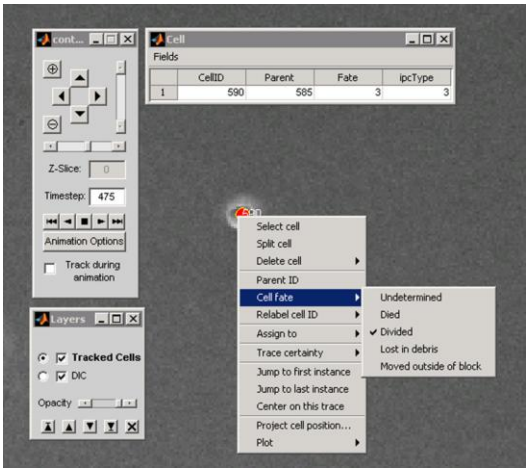

Figure 4-1. Screen shot of cell tracking software. Single cell located at centre of image with cell tracking marker (red) and cell ID (590) overlaid. Top left - navigation panel for panning, zooming, and stepping through time. Bottom left - layers panel (here both DIC image layer and tracked cell layers are on). Top right - Cell property table, where manually scored properties are entered and all other properties (e.g. parent ID) are displayed. Bottom right – cell options appear by right clicking on the tracked cell.

Each tracked cell requires a unique identifier that is associated with all data extracted from the LCI images, including first and last instance, identity of parent cell, identity of progeny (daughter cells), cell fate (died, divided, lost), all instances of tracked (x,y,z) co-ordinates, and all other observed, scored and extracted properties. Cells are tracked by clicking over the image at the location of the cell, at which point the (x, y, z) co-ordinates, relative to the home position (0,0,0), are logged into the tracking database. Qualitative data, such as morphology, are entered manually into a table, which can contain cell-state properties (those that don't change over the life of the cell) or trace-state properties, for which a unique value can be inputted for every tracked time point (Figure 4-1). Measurements of cell or sub-cellular component sizes can be made by creation of a new layer in the tracking database. Measurements require the user to manually outline the region of interest and the co-ordinates of the resulting polygon are stored in the data table for the specific layer it represents (see 'Colony tracking' below for example of outlines). Each outline can then be assigned to and associated with a tracked cell in the database. Because the LCI meta-data is retained in the tracking software, feature sizes can be measured with sub-micron resolution by association of the outline co-ordinates with the image magnification and corresponding micron/pixel values.

4.2.3 Lineage tracking

New cell identities can be created at any time point to begin tracking a new lineage. When a cell that is being tracked divides, the user can automatically create two new cell identities by using the 'split cell' feature, at which point the parent identity of the new cells is automatically entered into the database. Conversely, the new progeny identities are added to the parent cell's data (Figure 4-2). This is a quick and easy way to track through divisions, instead of manually creating new cells and entering the parent identity into the database. The lineage relationships between the tracked cells are, therefore, maintained in the database, and lineage visualizations can be produced at any point in the cell tracking process (Figure 4-2). This is an important feature, especially when tracking very large lineages, as it aids the tracker in identifying regions of the lineage that still need to be tracked.

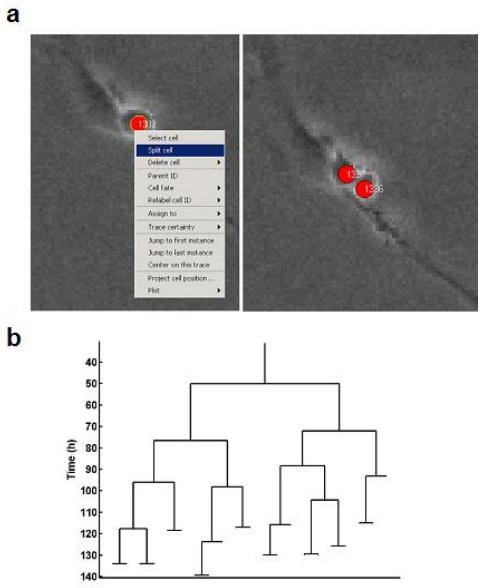

Figure 4-2. a) left – Final frame before division of a single cell, when 'split cell' option is selected. right – Two daughter cells are automatically created and relationships recorded to the database. b) Plotted lineage tree. Bifurcations in the tree represent cell divisions. In this example, terminating lineages represent untracked cells. Cell death is displayed as a red X at the terminating end (not shown here).

The plotted lineage figure is active and the user can click on any point of a lineage and be directed to that time point in the image file. The lineage can also help the user identify possible tracking errors based on expected cell lifetimes. All tracked lineages from a block can be plotted in the same visualization, enabling identification of sub-lineages that can be connected. This feature is most useful when all cells in a block have been tracked as best they can without completion of the lineages. Invariably, some cells cannot be fully tracked because they are lost in debris or undergo quick movements between frames. Often, however, an incomplete lineage, tracked from the other direction (i.e. forward or backward in time) and lost at nearly the same time, exists in the same spatial location. Provided there are not a number of 'lost' cells in the same area at the same time, the two disconnected cell lineages can be connected. In this respect, the lineage information is useful in aiding the cell tracking process and in interpreting and analyzing experimental results, as discussed below.

4.2.4 Colony tracking

In the absence of single cell tracking, whole colonies can be tracked and their sizes measured by outlining the colony at any given time point. The colony is given a unique identifier and can incorporate any other colony-level properties required for data analysis. As described above with cell outlines, colony outline co-ordinates can be used to measure the colony size with sub-micron accuracy. Changes in outline area over the LCI time course can be converted to apparent colony growth. Furthermore, multiple outlines can be assigned to the same colony to track separate aspect of colony growth (Figure 4-3).

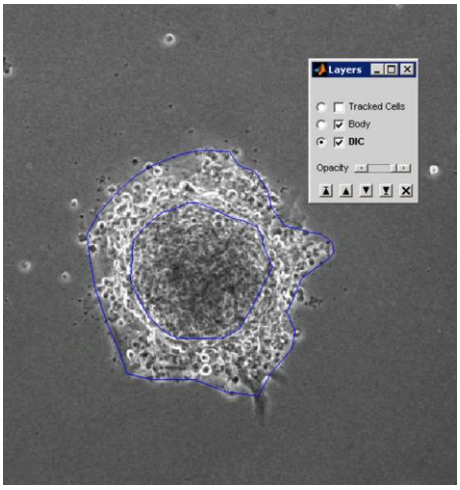

Figure 4-3. Outlines tracking the initial phases of hIPC derivation. Outlines are created in a separate database layer (labeled 'body' here). Multiple outlines can be used, in this case to track the area of the islet core and the monolayer of cells spreading away from the core.

Given a completely tracked colony of cells, colony outlines can be automatically produced, using Matlab's convex hull algorithm, to allow for estimation of colony size and overall growth rate (Figure 4-4). This is important, as individual cell cycle times do not necessarily correlate directly to overall colony growth, as cell death must also be considered. The outlines combined with cell counts also provide information on colony density, and possibly the degree of cell-cell contact within a colony.

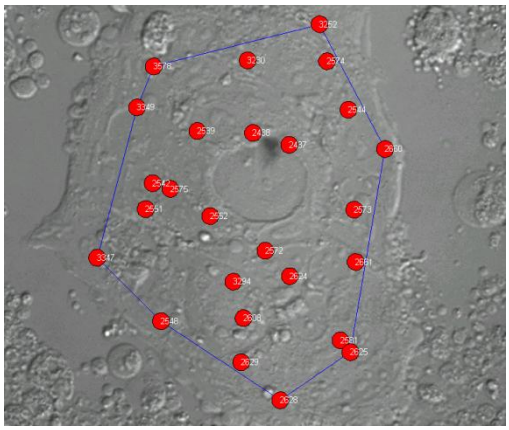

Figure 4-4. Automatic colony outline estimation based on complete manually tracked colony. The Matlab convex hull (convhull) was implemented.

Together, the cell, lineage and colony tracking process produces a detailed data set within the relational database that maintains the spatial and temporal information within the system being tracked through the (x, y, z) and lineage data, respectively. Individual cells and colonies contain as many extracted or measured properties as created by the user during the tracking process. This results in a highly dimensional and highly connected data set, requiring unique tools for analysis and interpretation.

4.2.5 Visualizations

Upon completion of tracking and scoring of LCI images, the data is analyzed through queries and image-based visualizations made available in the cell tracking software. The combination of queries, property gating and visualizations enables efficient investigation of the large amount of tracked data. Analysis of cell tracking data can present problems due to the unique structure of the data itself. Visualization of the data in a number of forms can help the user to form hypotheses that may not be obvious by looking at numerical data or the recorded image sequences alone. Such visualizations allow the user to apply their innate pattern recognition skills to discover underlying patterns in the tracked data. This approach can be useful for general interpretation of data for which there is not necessarily a strict hypothesis, for example the hypothesis that observable cell properties can be used to distinguish sub-populations of cells, yet the specific property or set of properties is unknown. The four main visualization techniques that were identified and developed for analysis of tracked LCI data are lineages trees, property population histograms, property scatter plots and image overlays.

While lineage trees offer an ideal visualization to aid in the tracking process, they can also be used to further analyze the cell system being studied. Any cell data in the tracking database can be displayed on the lineage, including cell state properties (Figure 4-5) or dynamic cell trace properties, where the display attribute (line thickness, color, or distance from axis) corresponds to the trace property value. The lineage view allows users to identify temporal/generational trends in the data.

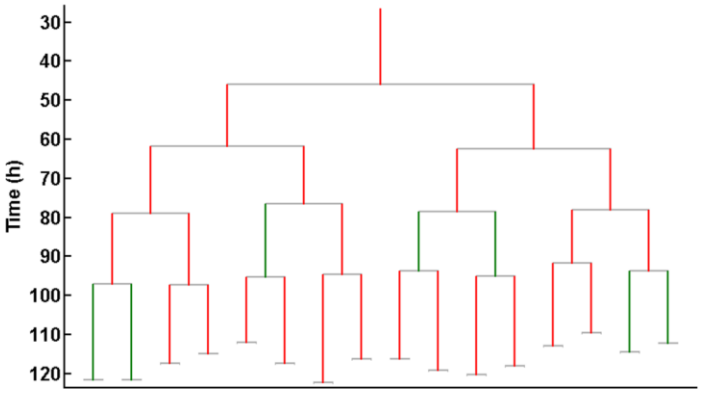

Figure 4-5. Cell properties displayed on a lineage tree. Here, the scored morphology of hIPC cells is displayed. Red – epithelial-like morphology, green – spindle morphology.

Data can be extracted from lineages to produce other useful plots. Some of these, as previously proposed by Glauche and colleagues (Glauche et al. 2009), will reduce the lineage data to single measures, such as number of deaths or number of branches. This concept was extended here to consider these measures dynamically, to produce informative visualizations. For example, this approach makes it possible to analyze how a given lineage property changes over the course of its development (Figure 4-6).

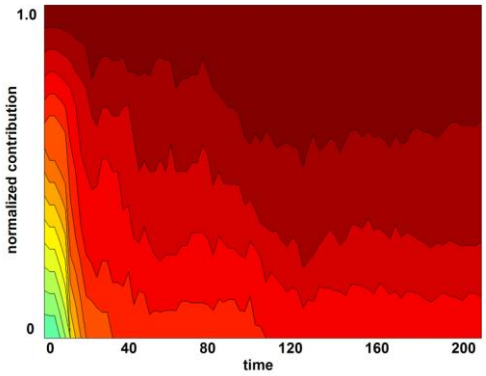

Figure 4-6. Normalized contribution of clonal colony founders to total colony population. In this example, of 14 colony founders (each represented by a different color), 4 contribute to the colony population at 200 hours.

Histograms provide a simple visualization of the frequency of any given parameter occurring over a given distribution of values. Here, histograms are used to visualize both continuous and discrete cell properties (Figure 4-7). For continuous measurements, such as cell cycle time, histograms require binning. The total range of which values may fall is divided into bins of equal sizes. Histogram visualization allows the user to view the overall distribution of a given parameter and possibly to identify sub-groups of cells based on multimodal distributions. As in the lineage view, cell properties can be overlaid on the histogram to compare the distribution of the plotted parameter with existing properties.

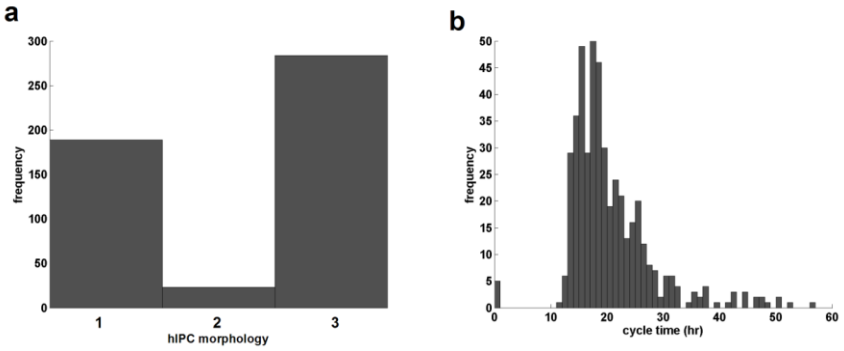

Figure 4-7. Cell property histogram display. a – Discrete cell property, hIPC morphology, in which no user defined binning is required (here, each bin represents a unique morphology that was scored). b – Continuous cell property, cell cycle time, in which bin sizes are manually set by the user.

Scatter plots are another way to visualize and analyze lineage data. The most common scatter plots utilized during this research was cell cycle scatter plots, with a given cell on one axis and its sister, mother, cousin, or grandmother on the other (Figure 4-8). Scatter plots can be used to assess the degree of correlation between the two variables plotted. Plotting multiple scatter plots of the same property, but with different cell relationships (i.e. cell cycle plots of sister-sister, mother-daughter, and cousin-cousin) can display how properties converge or diverge based on their lineage relationship.

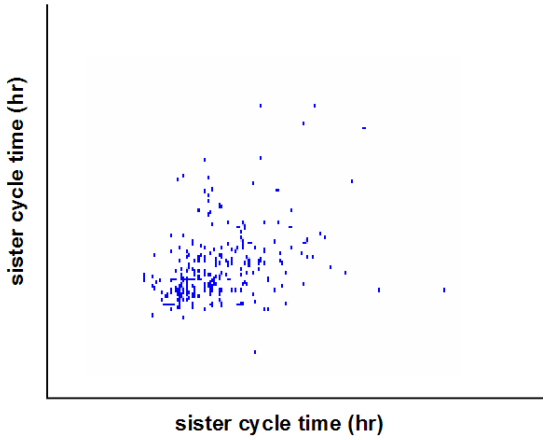

Figure 4-8. Scatter plot of sister-sister pair cell cycle times

Visualizations can also be incorporated within the LCI images themselves. For example, the cell tracking marker, based on its color or size, can represent any scored cell property. The user can view the LCI time courses and observe the spatial and temporal distribution of the visualized property. Such visualization allows the user to visually interpret the dynamic LCI data, which can be valuable in forming new hypotheses and leading to specific quantitative analyses.

4.2.6 Gates and queries

The power of the visualization methods described above is increased with the incorporation of gating. Gates are used, much as in FACS, to separate data based on a predetermined value (for discrete measures) or threshold (for continuous measures) of a given property into sub-groups, which can then be analyzed and compared using standard concepts of union, intersection, and

exclusion. Here, gates are most often used to separate cells, but can also separate lineages, blocks, or entire experiments. Gates can be created and manually manipulated on any visualization including lineages, histograms, scatter plots, or the LCI images (Figure 4-9).

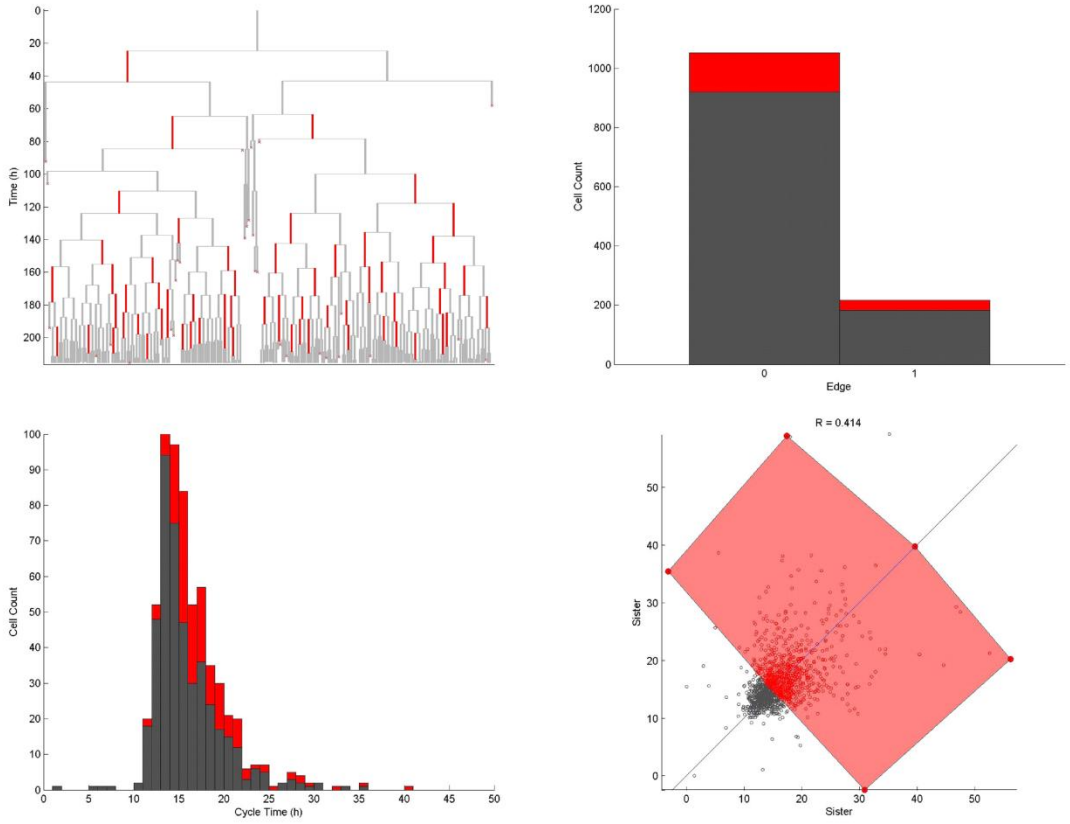

Figure 4-9. Cell gating and display across all visualizations. Gates can be created over any of the visualizations. Here, a gate is created in the scatter plot view (bottom right, red polygon) and cells within the gate are colored red in all other visualizations.

A set of gates were identified that would likely be useful for any project, including gating by project (if multiple projects are being analyzed simultaneously), block, colony, or lineage. The gates were made available to be automatically produced from the software gate menu. Properties that are always included in the tracking database, such as cell fate (divided, died, lost) can easily be used as gates. In the case of multiple, overlapping gates, the priority for how cells will be displayed in the visualizations can be manually controlled.

More complex gates that cannot be created easily with standard visualizations, for example that have multiple parameters that must be met, can be manually created using a MySQL query. For example, a gate may include cells that exist in a given experimental block, with mother cells of a given morphology, and sister cells that have a cell cycle time longer than a predetermined threshold. These gating methods are invaluable considering a given experimental data set may contain thousands of tracked cells. Implementation of specific gates allows the user to identify very small populations of cells that meet specific gating criteria. Gating also allows the user to isolate or exclude data from further analysis. Complex gates can be created that consider cell membership in all other existing gates in combination using IN and NOT IN clauses along with AND and OR statements. The membership in the resulting conjugate gate can be counted and visualized. This method of analysis, therefore, expands on the lineage measures set forth by Glauche and colleagues (Glauche et al. 2009), as it provides flexibility to characterize lineages based on any combination of properties. Similar to their measures, most of these will produce an output based on a 'count', or the number of cells, branches, sub-lineages, or divisions that possess the properties of interest. However, the ability to further view these identified sub-groups over visualizations allow the user to explore their spatial and temporal dynamics, which was previously not possible.

4.2.7 Statistics

One of the challenges of LCI data analysis is putting the data into a form that lends itself to statistical analysis. For analysis of individual cell properties, standard statistical analysis can be performed, as most of the data analyzed in such a manner (most often cell cycle times) had normal distributions. The ability to perform two-sample t-tests or ANVOA tests was incorporated into the histogram visualization. However, if the user needs to include the lineage data structure so as to retain information about the cell generation, standard statistical techniques are not appropriate. Unfortunately, statistical analysis of lineage-structured data is not well developed (Glauche et al. 2009).

4.3 Implementation of tracking and analysis tool to characterize human islet-derived progenitor cells

The tools for tracking and analysis of LCI data were implemented and tested on LCI data sets of hIPC derivation processes. Proliferative human islet-derived cells represent an attractive cell source for diabetes-related cell therapies, as they may be epigenetically similar to beta cells and may be more amenable to be stimulated to functionally produce insulin (Efrat 2008). Derivation of these proliferative cells can be achieved in standard flask cultures or in collagen-embedded three-dimensional cultures (Gallo et al. 2007; Gershengorn et al. 2004; Jamal et al. 2003). Both derivation processes produce heterogeneous hIPC populations (Hanley et al. 2008; Lechner et al. 2005), but the proliferative potential of the different cell types remains unclear. This is an important consideration given the possibility that sub-populations may also possess different differentiation potentials. Furthermore, β-cell derived hIPC sub-populations may be more attractive than others, since the main goal is the production of functional insulin-producing cells. Culture strategies for expansion and differentiation will depend on the distribution of proliferative and differentiation potentials in the hIPC population.

4.3.1 Human islets contribute unequally to monolayer hIPCs

The multiple stages of monolayer hIPC derivation – the process by which fresh islets attach to and spread out onto the culture dish surface, followed by culture as proliferative single cells (Gallo et al. 2007; Gershengorn et al. 2004) were examined. Of interest during the first stage was the distribution of islet sizes and their relative contributions to the day 14 population of monolayer cells. During this process, a low resolution wide-field tiled array (5x objective lens, 4x20 array) was imaged to capture as many islets as possible. Using the colony outline tool initial islet sizes were measured, which ranged from 40 – 320 μm in diameter, a range and distribution which agree with previous reports (Lehmann et al. 2007). The progression of islet attachment and spreading into monolayer configuration for the first 6 days of culture was then tracked, again using the colony outline tool (Figure 4-10).

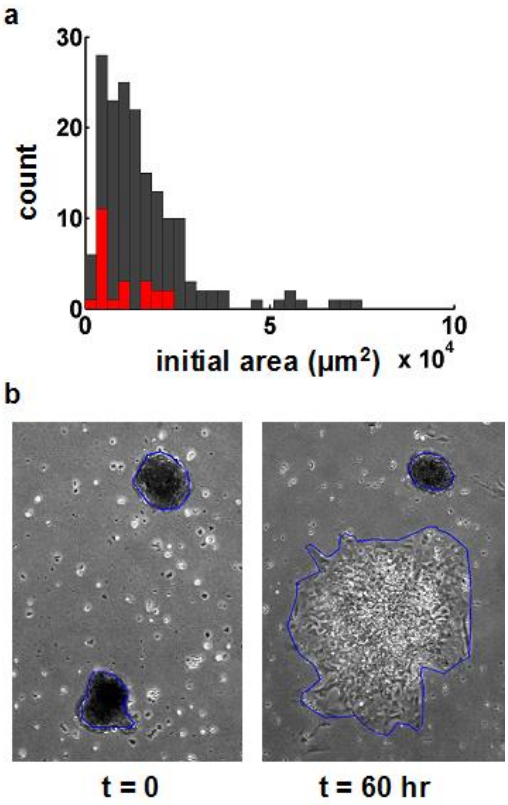

Figure 4-10. Initial stage of hIPC derivation. a – histogram of initial islet sizes (cross-sectional area), red indicates islets that did not contribute to the eventual hIPC population. b – images of two similarly sized islets immediately after seeding onto culture dish (left) and after 60 hours of imaging (right).

The main islet core and the spreading monolayer perimeter were both outlined to track the fraction of islet cells that contributed to the monolayer of cells that would eventually contribute to proliferating hIPCs. All islets (166/166) attached to the culture dish, as none were removed during media changes. After 6 days, 14% (23/166) of islets did not have any cells spreading away from the islet body. In these cases the islets did not change in size, shape or appearance from day 0. Conversely, 67% (112/166) of islets spread completely out by day 6, with little or no apparent cell death. The remaining islets (31/166) spread partially onto the surface, as a number of dead cells remained. Of the islets that did not spread out at all, none of them were larger than 80 μm in radius (Figure 4-10). However, there was an even distribution over all islet sizes for those that spread onto to the surface, either partially or fully. This result shows that not all islets contribute equally to the initial hIPC formation stage.

4.3.2 Monolayer-derived hIPCs may exist in dynamic equilibrium

Following trypsinization and passaging of the attached islet monolayers into dispersed, proliferating single cell cultures, two distinct cell morphologies were observed, as previously reported (Lechner et al. 2005). Cells were imaged at high resolution (20x) for up to six days after each passage, for three passages. Individual cells were tracked over their lifetime and scored for their morphology as either *epithelial-like* or *spindle-shaped* cells (Lechner et al. 2005). Analysis of cell cycle data shows that epithelial and spindle cells possess unique cell cycle properties that change over the course of multiple passages (Figure 4-11).

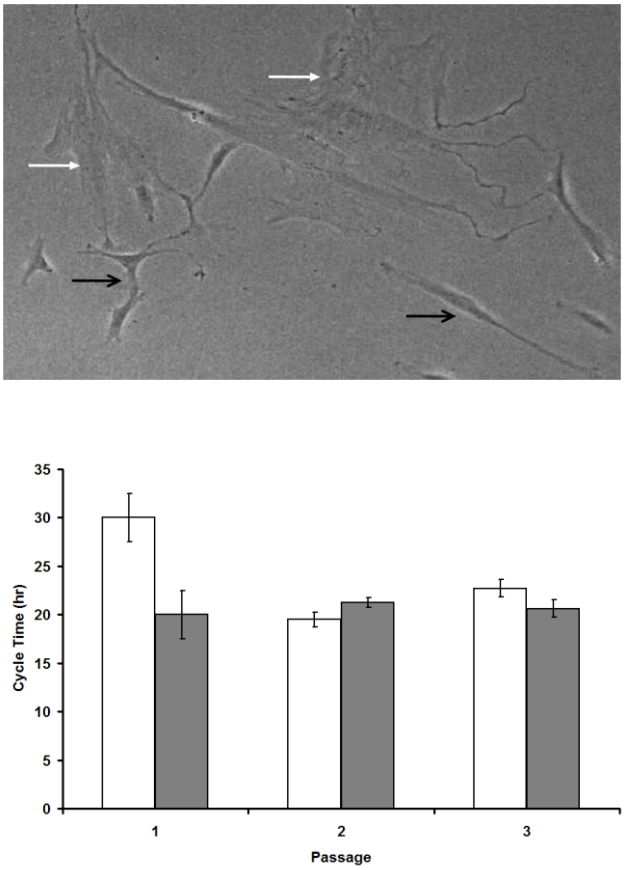

Figure 4-11. Top – Phase contrast image of epithelial-like (white arrows) and spindle-like cells (black arrows). Bottom - Cell cycle times of spindle-like (white) and epithelial-like (grey) hIPCs over the first three passages of expansion (for spindle-like and epithelial-like, respectively, passage 1 n = 192 and 73, passage 2 n = 284 and 212, passage 3 n = 237 and 92).

The most significant difference in the cell cycle analysis is the average cycle time of spindle-like cells during the first passage. Importantly, not included in this plot are a number of spindle-like cells present in the first passage that were tracked for longer than 30 hours , but not to the point of division (LCI halted before cells divided). These cells were identified on lineage visualizations as well as a query on cells that existed at the end of the LCI data set. As no cell proliferation occurs during the first phase of hIPC derivation (islets attaching and spreading over the culture surface), the process of passaging into non-adherent cell monolayers induces proliferation. The commencement of proliferation is likely due to disruption of the islet cell's normal structure due to altered cell-cell and cell-matrix contact (Russ et al. 2009) and activation of the NOTCH signaling pathway (Bar et al. 2008). These results show that the spindle-like sub-population of hIPCs begin proliferation at a slower rate than the epithelial-like sub-population. If the spindle-like cells that were not tracked to division during the first passage possessed longer cycle times than 30 hours, the discrepancy between the two cell types would be greater in the first passage. It is also possible that this sub-population of spindle-like cells were not proliferative at all, which would suggest that a fraction of these cells could not be induced to proliferate after trypsinization. In either situation, longer LCI experiments are required to investigate this open question. Unlike the first passage, after subsequent passages the proliferation rate of both sub-populations is similar.

Lineage analysis of proliferating hIPCs revealed that the scored epithelial and spindle morphologies did not always exist as separate, distinct lineages (Figure 4-12). This was identified after the scored morphologies were overlaid on the lineage visualizations. Unfortunately, it was not possible to determine individual cell expression of either ck-19 or nestin through immunocytochemistry; the cells could not be fixed and permeabilized in place on either cover slip or plastic culture surfaces immediately following imaging (existing protocol in literature requires centrifugation of cell on surfaces immediately prior to fixation).

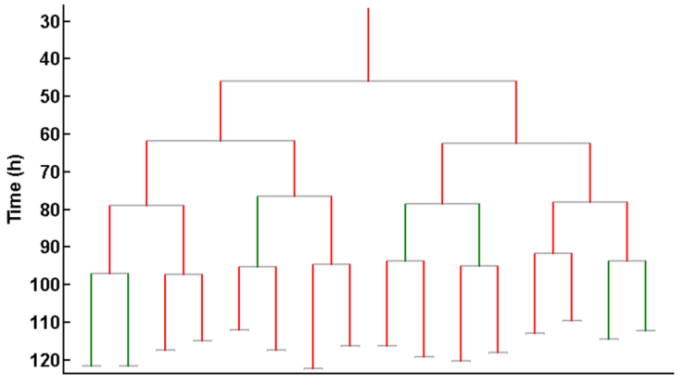

Figure 4-12. Visualization of cell morphology on tracked lineage trees shows an apparent interconvertibility between spindle-like (green) and epithelial-like (red) hIPCs.

The main assumption here was that morphology alone could be used to discriminate between the two sub-populations. However, if the morphologies are interconvertible, but expression of ck-19 and nestin are restricted to distinct lineages, then cell-level analysis is not sufficient to investigate this system.

4.3.3 Maintained islets imaged and tracked in three dimensional culture

It was previously shown that islets cultured under maintenance conditions in the imaging chamber retain structure and islet hormone expression (Moogk et al. 2007) (Chapter 3). It was also shown that individual cells could be identified and visually tracked over the time course, although only in a single imaging plane. Here, islet cells were successfully imaged and tracked in three dimensions using the cell tracking software under similar conditions (Figure 4-13).

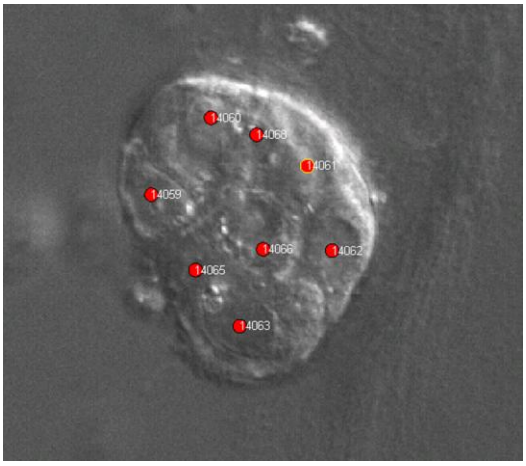

Figure 4-13. A single optical section of a human islet of Langerhans imaged in a 25 µm imaging chamber under maintenance conditions. Cells can be easily identified and tracked.

For three dimensional cell tracking, the user generally will scan through the z axis image stack and identify the most in focus image of each cell nucleus. As the time course progresses, the user tracks the cell nuclei through the z axis optical sections if there is cell migration in that axis. There was a high level of confidence that all cells were identified and correctly tracked, as multiple users viewed and tracked this data set. All cells maintained a compact morphology and no significant cell motility or migration was observed within the islets. Surrounding collagen was visible and remained intact and fully surrounded the islets for the duration of the experiments. As expected, no cell death or divisions were observed, and therefore islets were maintained stably with no noticeable changes for over 24 hours. As such, only cell tracking was performed on this data set, as no other cell or colony properties were of interest. Although this is not an informative data set, in terms of understanding islet behavior, it shows that three-dimensional aggregates can be tracked successfully from LCI image data.

4.3.4 Three-dimensional imaging and tracking of islet to DLS transformation

Comparison of the results from the monolayer hIPCs to the three-dimensional DLS derivation process was performed to determine if the derivation processes yield unique cell types, or if they appear to produce similar cell populations. Three-dimensional LCI was performed on islets embedded in collagen in the gap chamber imaging systems. Under DLS-formation conditions, which require the

inclusion of cholera toxin to the media, some cells underwent dramatic dynamic morphological transformations from round, compact cells to extremely elongated (Figure 4-14). Cell death was observed for islet core cells - most likely β-cells, as previously described by (Jamal et al. 2005).

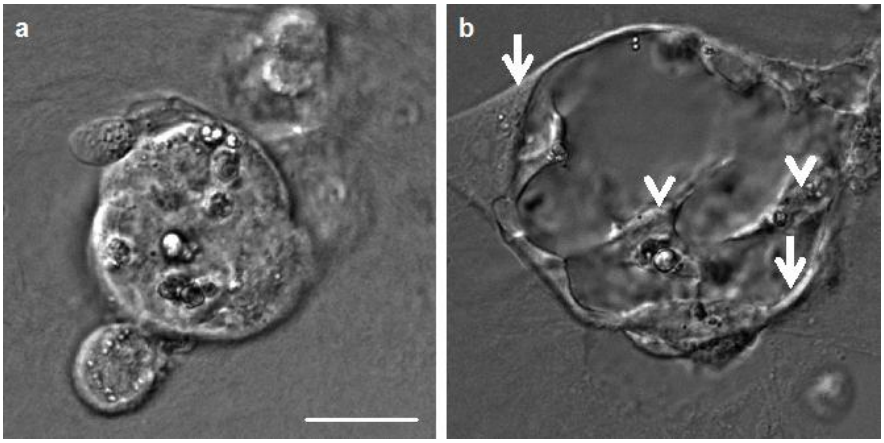

Figure 4-14. Collagen embedded human islets under a) maintenance conditions b) cholera toxin-induced DLS formation conditions. Arrows show extended cell phenotype and arrowheads show compact cell phenotype. Scale bar equals 25 µm.

Due to the extreme morphologies observed and the fact that rapid morphological changes occurred at time scales similar to the imaging rate, identification of cell nuclei and cell tracking was difficult. Although the LCI was performed with intervals of three minutes between images, this was not sufficient for trackers to manually track all cells from frame to frame. Cell morphology was scored based on the display of the elongated cystic morphology characteristic of DLS cells (Jamal et al. 2003). Some cells did not display this morphology at any point during DLS formation, while others cycled between compact to extremely elongated. These morphologies are reminiscent of the epithelial and spindle morphologies observed in the two-dimensional hIPC culture system.

Under DLS formation conditions, however, no cell divisions were observed. It was noted that the collagen matrix that the islets were embedded in did not maintain its support throughout the duration of the culture due to the cystic pulsing of cells during DLS formation. The lack of complete matrix support may explain why apparent DLS transformation was achieved, but cell proliferation was not observed. Wang et al. (Wang and Rosenberg 1999) concluded that both elevated cAMP, a known effect of cholera toxin, and integrin-ECM interactions were required for the apoptosis,

phenotypic transdifferentiation, and proliferation associated with the islet to DLS transformation. Therefore the initial stages of DLS transformation – cell death and phenotypic transformation – were observed, but the effects of long term culture, such as collagen matrix degradation or disruption, likely prevented cell proliferation, which does not initiate until around 36 hours (Jamal et al. 2003).

4.3.5 Imaging and tracking DLS to ILS transformation

Although DLS cell proliferation was not observed, the second stage of the protocol, presented by Jamal and colleagues (Jamal et al. 2005), that induces the formation of islet-like structures (ILS) from DLSs and the eventual re-expression of islet hormones, stimulated by the removal of cholera toxin and inclusion of INGAP to the culture media, was implemented. During the immediate period following this media change the DLS still underwent rapid cystic pulsing, again confounding cell tracking. Instead, the LCI data set was tracked backwards from the end of the ILS formation phase, as cell identification was aided by inclusion of the fluorescent nuclear indicator 4',6-diamidino-2-phenylindole (DAPI) following fixing. The fluorescent DAPI images were overlaid with the final LCI time point. Edge detection using ImageJ® was performed on the DAPI images to aid in detecting the hard edges of cells in, or very near to, the focal plane of the images (Figure 4-15).

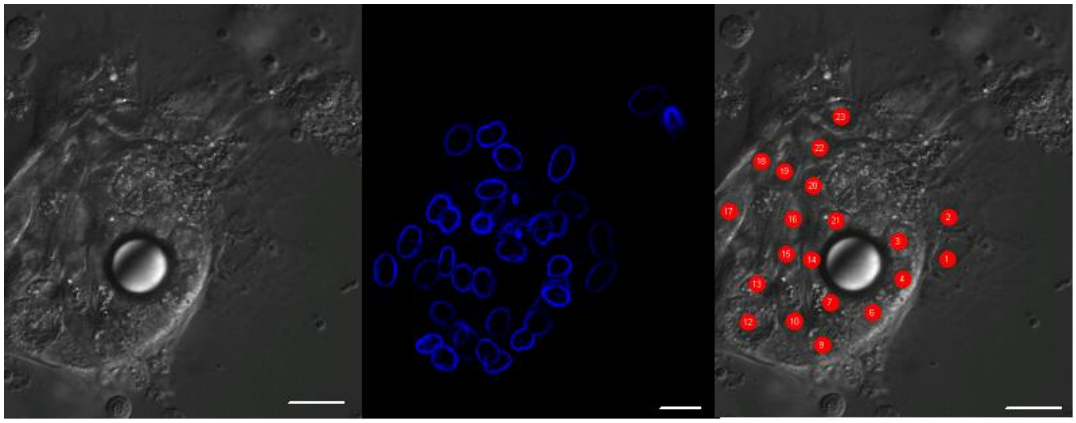

Figure 4-15. Combination of final LCI image (left) and edge-detected DAPI nuclear stain fluorescence image (middle) to aid in cell identification (right). Following identification, cells are tracked backwards through the LCI time-course.

Though this aided in initial identification of all cells, the tracking certainty of a number of cells remained low, although better than at the DLS formation stage, where the motility of the cells

and overall cystic pulsing of the islets confounded the tracking process. The imaging chamber, while successful in maintaining islet structure and functionality (Moogk et al. 2007) and enabling cell tracking under maintenance conditions, is not ideal for motile cell aggregates due to tracking issues and disruption of support matrix.

Simultaneous to DAPI inclusion, immunofluorescent staining was performed to probe the expression of c-peptide, glucagon and somatostatin (all indicators of physiological islet hormone expression). Immunofluorescent images were overlaid with the final LCI time point and expression of individual cells was manually scored (Figure 4-16).

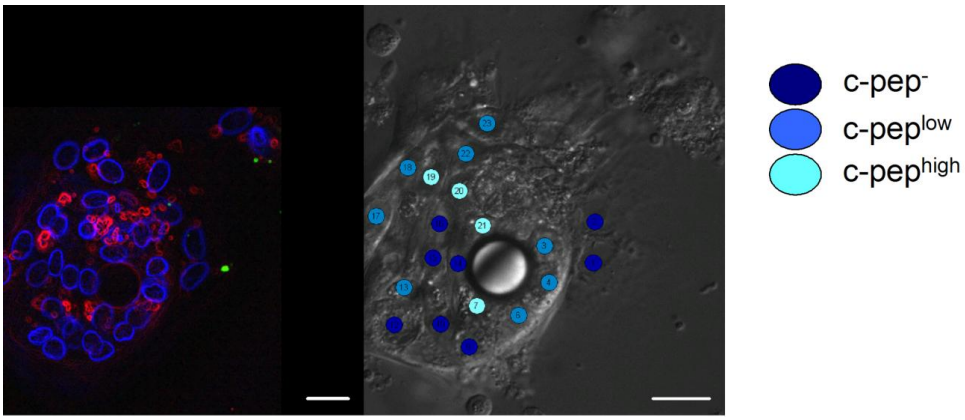

Figure 4-16. Immunocytochemistry of c-peptide expression following INGAP treatment (left) is combined with the final image of the tracked LCI to score individual c-peptide expression levels (middle). Scale = 25 µm.

There was no notable expression of glucagon or somatostatin (not shown). However, c-peptide expression was observed. As noted above, the DLS transformation process may not have been complete, and previous data (not shown) has shown instances of c-peptide expression in clustered regions of non-cystic cells, with no expression in cystic regions.

If cells expressing c-peptide after ILS formations had previously displayed a cystic phenotype during cholera toxin treatment, this would suggest, however not definitively prove, that the c-peptide was re-expressed in these cells during INGAP treatment. However, by performing a query incorporating both morphology and c-peptide expression information, it was determined that nearly all cells that were scored as expressing high levels of c-peptide did not, at any point during the

treatment, display a highly cystic phenotype. Therefore, c-peptide positive ILS cells were likely cells that retained expression, possibly at low levels, during the islet-DLS transformation process.

4.4 Discussion

The large data sets produced by LCI required the development of a package of tools for tracking and analysis. The main requirements were that image data could be viewed and tracked quickly with the incorporation of observable and extractable properties and that analysis could provide informative results considering the unique lineage structure of the data. Furthermore, the tracking system required the capability to view and track both two- and three-dimensional data sets. The process of deriving progenitors from human islet of Langerhans was used as a cell system to implement and test the tracking and analysis tools, as both two- and three-dimensional protocols had previously been developed. The open question of the source of hIPC sub-populations of cells and their proliferative potentials provided the opportunity to investigate the hypothesis that LCI, cell tracking and analysis tools could be used to characterize heterogeneous and dynamic cell systems.

The use of cell property display on lineage plots revealed the dynamic heterogeneity in the two-dimensional hIPC system. Without the implementation of LCI and cell tracking and scoring, this result would not have been revealed. However, the fact that, in the three-dimensional system, ck-19 and nestin populations derive from distinct islet cell types suggests that interconvertibility is unlikely. However, in the two-dimensional system the exact islet cell-source of the sub-populations remains unclear. The significantly different cell cycle times during the first passage of hIPC culture suggests that morphology alone does discriminate between two distinct populations. Further investigation is required to confirm cell type by protein expression to determine if morphology alone is sufficient to distinguish the two sub-populations. In this case, cell-level properties alone were not enough to definitively distinguish between hIPC sub-populations and it is apparent that incorporation of molecular-level information with the LCI results would further this course of investigation.

The three-dimensional LCI experiments did not provide completely trackable results, and therefore did not provide insight into the proliferation potential of DLS cells. However, combining the tracked data set with end-point immunocytochemistry images verified that c-peptide^{+} cells identified after INGAP treatment were likely cells that had not undergone complete DLS conversion

and may have retained c-peptide expression throughout the treatments. LCI and tracking of maintained islets showed that three-dimensional cell tracking is possible under the appropriate conditions. The major considerations for implementing three-dimensional LCI on other cell systems are that they can be supported by matrix requirements within the imaging chamber, and that cell and colony spatial dynamics do not occur on a time scale similar to image acquisition. Here, rapid islet cell morphological changes caused both disruption of the surrounding matrix and confounding of the tracking processes.

While some questions remain open regarding human islets of Langerhans and their culture-derived progenitors, this chapter has shown that cell- and colony-level tracking and analysis can be a useful tool for characterizing heterogeneous cell systems. The introduction of active visualization methods combined with gating and queries allows for general and specific hypothesis testing. Coupled visualizations and gates also enable the user to view and interpret data in a form that conveys both the spatial and temporal structure of the data that is unique to lineage and colony tracking. This allows the user to use their natural pattern recognition skills to identify trends and form new hypotheses.

4.5 Methods

4.5.1 Isolation of human islets of Langerhans

Human islets were isolated from cadaveric donor organs at the Montreal General Hospital, as previously described (Jamal et al., 2005) and maintained in CMRL-1066 medium, antibiotics, antimycotics (Gibco, Burlington, ON, Canada) and 10% FBS (MBI, Amherst, NY, USA). Islets were shipped overnight from Montreal, PQ to Waterloo, ON on ice in a 15 mL tube.

4.5.2 Generation and culture of hIPCs

hIPCs were generated as previously described by Gallo (2007). Briefly, islets were plated in tissue culture-treated flasks at a density of roughly 1 islet/cm^2 in modified RPMI-1640 medium (11.1 mM glucose) (Invitrogen, Burlington, ON), supplemented with 10% FBS (ATCC, Manassa, VA). Flask were incubated at 37˚C, 5% CO_2 and 95% humidified air, and media was replenished every 3 days. After roughly 15 days, once most islets had spread into a monolayer, cells were detached from the surface with 0.25% Trypsin EDTA and replated as single cells at a density of 12 000 cells/cm^2 for two passages, with subsequent passaging at 4000 cells/cm^2. hIPCs were imaged by seeding onto 100 mm plastic dishes under similar conditions.

4.5.3 Generation and culture of DLS and ILS

Islets were embedded in collagen in 25 μm imaging chambers, as previously described (Moogk et al. 2007). To induce DLS formation, islets were cultured in DMEM/F12 (Gibco) with 10% FBS, antibiotics and antimycotics, 1 μM dexamethasone, 10 ng/mL epidermal growth factor, 24 mU/mL insulin and 200 ng/mL cholera toxin (Sigma). Chambers were incubated at 37˚C, 5% CO_2 and 95% humidified air and media was exchanged once every 8 days while the chambers were in the incubator, and once every 4 days during imaging to account for evaporation of media. ILS transformation was induced by inclusion of 167 nM INGAP to the maintenance media.

4.5.4 Live cell imaging

Imaging chambers and dishes were contained in a controlled 37˚C, 5% CO_2 humidified air atmosphere on the microscope stage of an inverted microscope (Axiovert 200, Zeiss Germany) equipped with 3-axis robotic motors. Images were acquired using a digital camera (XCD-SX910, Sony Japan) and Visual C++ in house-developed software.

hIPCs were imaged with a 10x objective and 0.5x camera adapter at 10 minute intervals, generally as a single 10x10 block. Media changes were performed every second day, by pausing image acquisition and removing the dish to a laminar flow hood. Immediately following imaging,

cells were fixed for immunocytochemistry. For DLS and ILS transformation, optical section z-stacks were collected at 4-minute intervals, each stack consisting of 10-18 images spaced by roughly 2 µm. A 40x objective lens and a 0.5x camera adapter were utilized and 6-8 islets were imaged per microscope, depending on the distances between the islets in the imaging chamber. Each islet was imaged as an individual block, generally as a single (x, y) field of view with multiple z-slices.

4.5.5 Immunocytochemistry

Islets were fixed, permeabilized, and stained for islet hormones and with the nuclear stain DAPI. The imaging chambers were washed briefly with PBS, and the cells were then fixed with 4% paraformaldehyde for 15 minutes, permeabilized with 0.1% Triton X-100 (Gibco, Grand Island, NY, USA) for 10 minutes, and blocked with 10% goat serum in PBS for 4 hours, all steps at room temperature.

Islet-derived DLSs and ILSs were treated simultaneously with rabbit anti-somatostatin (1:50) (Cedarlane, Hornby, ON, Canada), guinea pig anti-c-peptide (1:1000) and mouse anti-glucagon (1:1000) (Sigma, St. Louis, MO, USA) primary antibodies overnight 4˚C. The cells were washed three times for at least two hours before simultaneous exposure to FITC-conjugated goat anti-rabbit IgG (1:50) (Cedarlane, Hornby, ON, Canada), TRITC-conjugated goat anti-guinea pig IgG (1:1000), and AMCA-conjugated goat anti-mouse IgG (1:200) overnight at 4˚C and then washed three times for at least two hours. DAPI with antifade was added 24 hours before imaging and the samples were stored at 4˚C.

Chapter 5
Human embryonic stem cell colony formation is dependent on interplay between self-renewing stem cells and unique precursors responsible for niche generation

5.1 Preamble

This chapter implements monolayer live cell imaging, using the imaging chamber developed in Chapter 3, to investigate human embryonic stem cells and the process by which they produce differentiated niche cells.

5.1.1 Objective

The concept of the *in vitro* hESC niche is relatively new, but is supported by results showing that hESCs differentiate to produce hdFs that provide factors required for maintenance of hESC self-renewal and pluripotency (Bendall et al. 2007). The main objective of this chapter is to use LCI to track hESC colonies at the single cell level to observe and characterize hESC differentiation to hdFs. This is of significant interest because it was unclear if all hESCs possessed equal potential to produce hdFs. Furthermore, it was unclear if there was an identifier of hdF differentiation commitment, before hdFs actually formed away from the colony that could be detected through lineage tracking and analysis.

5.1.2 Justification

The first hESC lines were isolated about a decade ago (Thomson et al. 1998). While many groups aim to develop protocols for effective differentiation of hESCs to committed mature cell types, much remains unknown about the properties of hESCs and the conditions required to maintain and expand them *in vitro*. The development of an optimal defined media may enable the culture and expansion of

pure hESCs. However, it is also possible that hESC pluripotency and self-renewal is dependent on the *in vitro* niche, including hdFs, and therefore pure hESC cultures may not be possible. In this case, culture protocols should be designed with niche requirement in mind. Understanding the process of niche production and maintenance from hESCs, and the dependence of the hdF and hESC populations on each other should aid in such considerations.

5.1.3 Approach

Because hESCs cultured in open flasks generally grow in near-monolayers (i.e. two or three cells thick at the most), it was assumed that monolayer culture in the imaging chamber described in Chapter 3 would be acceptable, provided the chamber was treated with appropriate matrix proteins. LCI and single cell tracking and classification were implemented to observed hESC colony growth and hdF production.

5.2 Introduction

Stem cell developmental potential is maintained by self-renewal, which is thought to be partially controlled *in vivo* through extrinsic signals that regulate stem cell survival, self-renewal and differentiation. Similarly, recent evidence has demonstrated that hESCs both create and are reliant on a supportive *in vitro* niche (Bendall et al. 2007; Peerani et al. 2007). Similar to *in vivo* stem cell niches, the hESC *in vitro* niche consists of supportive differentiated cells, including hdFs, paracrine signals, and interactions with extra-cellular matrix (Bendall et al. 2007; Greber et al. 2007; Peerani et al. 2007). Recently, multiple niche-independent hESC cultures have demonstrated a variety of features suggestive of early transformation events, including growth factor independence, increased proliferation and dramatically reduced differentiation potential (Werbowetski-Ogilvie et al. 2008). These results illustrate the importance of the *in vitro* niche, and that niche components and dynamics are defining factors regulating hESC fate within the culture. However, the mechanisms by which hESC colonies create and maintain their niche, and respond to disruptions of their microenvironment, so as to maintain self-renewal and pluripotency is not well understood.

Differentiation of hESCs to hdFs is observed in all hESC culture formats, but is more prevalent as the culture becomes more defined and feeder layer-free (i.e. moving from MEF layers, to conditioned media, to defined media) (Bendall et al. 2008). Repeated passaging for expansion of hESC cultures causes disruption of the hESC microenvironment and requires the re-establishment of the cellular and non-cellular niche (such as ECM produced by hESCs) (Bendall et al. 2009). To establish a cellular niche in the absence of MEFs, hESCs generate hdFs (Bendall et al. 2007; Xu et al. 2001). This re-establishment period, in which niche signals for survival are sub-optimal, appears to invoke significant cell death, based on observed cell debris following passage and the established disparity between hESC colony doubling time (30-36 hours) (Stojkovic et al. 2005; White and Dalton 2005) versus the observed cell cycle times of hESCs and hdFs (15-25 hours). Therefore, the period of hESC culture immediately following passaging provides the opportunity to investigate the mechanisms of hESC colony establishment, which represents a highly inefficient process for hESCs (Stewart et al. 2006; Watanabe et al. 2007).

LCI was implemented in combination with the previously reported culture system (Karpowicz et al. 2005; Moogk et al. 2007; Ramunas et al. 2006; Ramunas et al. 2007), cell tracking and phenotype scoring methodologies to investigate how hESC colonies re-establish following disruption of their microenvironment during passaging. The results show a previously unappreciated level of morphological and behavioral heterogeneity at the hESC colony perimeter that corresponds to presence or absence of adjacent co-transferred hdFs. A distinct hESC-derived cell was identified at the colony periphery and was observed to function as a reversible intermediary in the intrinsic differentiation of hESCs to niche hdFs. Both induction of hdF differentiation and cell death increased without adjacent hdFs. Thus, hdF co-transfer following passage promotes colony expansion while decreasing clonal selection within the colony.

5.3 Results

5.3.1 Live cell imaging of hESC colonies following passage

Wide field live cell DIC microscopy was employed to image multiple hESC colonies at high spatial and temporal resolution for up to 200 hours. A total of 29 colonies were imaged from H9 (n=11) and

H1 (n=18) hESC cell lines in the previously described monolayer culture chamber. Starting colonies ranged in diameter from 60-140 μm and contained between 6 and 25 colony founder cells. Growth rates were compared between hESCs seeded inside and outside the imaging chamber to confirm that use of the monolayer culture system did not affect the growth of hESC cultures. No significant differences were observed between these two conditions (data not shown) and, importantly, both configurations yielded growth rates that agreed with previously reported values (Becker et al. 2006; Mantel et al. 2007). This, in combination with previously reported use of this culture system to analyze stem cell properties (Ramunas et al. 2007), ensured that culture of hESCs in the monolayer culture system was comparable to normal hESC culture conditions, with the significant advantage of facilitating cell tracking and phenotype scoring.

Colony lineages were produced by manually tracking cell positions, divisions and deaths in the time course image sequences to assess generational relationships. Cells were initially classified as either hESC colony cells, or colony-local hdF cells co-transferred during passaging (approximately 300 μm from the colony perimeter) [see Appendix F - Movie 3: hESC colony (red) and hdF (green) in 4.7 μm imaging chamber]. A third distinct cell morphology was observed, characterized by a thin and extended cell body that stretched along the perimeter of the colony (Figure 5-1a). The morphology appeared following cell migration to the colony periphery. As these cells remained attached to the hESC colony, in contrast to hdFs, they were labelled as *"edge cells"* to distinguish them from *"internal cells"* cells that never displayed this morphology. Any cell that displayed the edge cell morphology at any point in its lifetime was scored as an *edge cell*, since a number of edge cells that originated from the internal hESC colony displayed in internal morphology before migrating to the colony periphery and taking on the edge cell morphology. However, no instances were observed of an edge cell changing morphology to an internal cell.

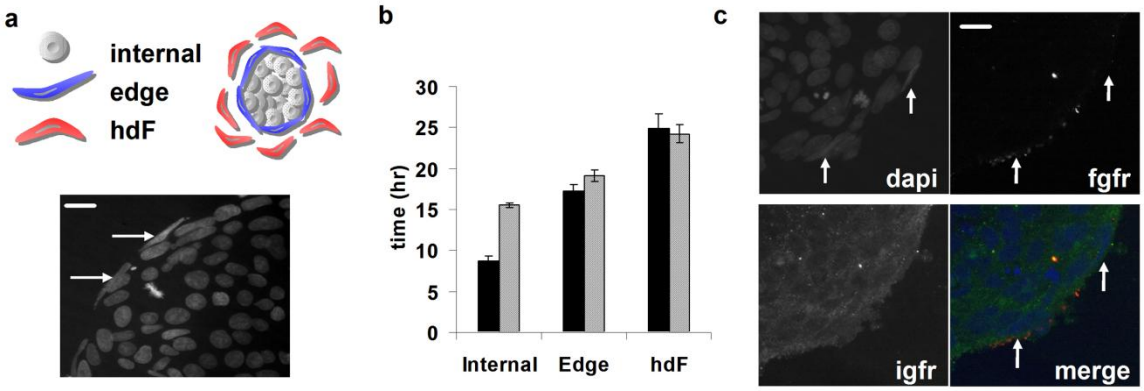

Figure 5-1. hESC colony heterogeneity. (a) Schematic (top) and DAPI nuclear stain (bottom) showing the distinct morphological differences between internal colony cells, edge cells (arrows), and hdFs. (b) Mean time to death (black) and mean cycle times (grey) for all three cell types. Error bars indicate 95% confidence intervals. (c) Immunocytochemistry of hESC colony periphery - merged in bottom right panel, showing DAPI (blue, top left), FGFR (red, top right), and IGFR (green, bottom left). Arrows depict FGFR+ (left) and FGFR- (right) edge cells. Scale bar = 25µm.

5.3.2 hESC colony periphery produces biologically distinct hESC-derived cells

To determine whether the edge cell did indeed represent a distinct subset of colony cells, cell cycle times, time to death and immunoreactivity of internal cells, edge cells and hdFs surrounding the colonies were analyzed. In addition, parent morphology influence on the morphology, cell cycle and/or cell death of the resultant progeny was assessed. The three cell types identified have significantly different cell cycle times ($p < 0.001$) (internal 15.4 hrs ± 0.3 hrs (n=1985); edge 18.9 ± 0.7 (n=327); hdF 24.1 ± 1.1 (n=129)) (Figure 5-1b). Also, in contrast to hdFs and edge cells, internal colony cells that died exhibited a significantly shorter lifetime compared to those internal cells that divided ($p < 0.001$) (i.e. internal cells where much more likely to die soon after division). Thus, it is apparent that edge and hdF cells die at or near M-phase, whereas internal cells die most likely in S-phase. These results show that the edge cell is not solely distinguished by morphology but that they possess cell cycle properties distinct from both internal hESCs and hdFs.

To further characterize the edge cell phenotype, immunocytochemistry was used to determine the expression of the pluripotency markers Oct4, IGF1R and fibroblast growth factor receptor (FGFR1) by the edge cells (Figure 5-1c). Consistent with previous reports, all edge cells expressed IGF1R and most also expressed Oct4; however a fraction of cells on the colony periphery also expressed FGFR1, which was not observed on internal cells. Overlay of a FGFR1 stained colony with the final live cell imaging time point revealed that the majority of cells expressing FGFR1 were independently scored as displaying the edge cell morphology (82%); however, a large fraction of cells scored as edge cells did not stain for FGFR1 expression (62%). Comparison with conventional open culture systems revealed morphologically and phenotypically similar cells (not shown), verifying that the edge cell phenotype is not an artifact of the culture system.

5.3.3 hESC-derived edge cells are a niche differentiation-competent subpopulation of hESCs

Cell cycle times and marker expression patterns suggest that edge cells, or a fraction thereof, possess hdF differentiation potential. Analysis of parent-progeny relationships (Figure 5-2a) revealed that 10.2 % of edge cells (43/420) gave rise to hdFs compared to 0.6 % of internal cells (15/2416). It was also observed that edge cells gave rise to internal ($e \rightarrow i$) (51.2%, 215/420) and edge ($e \rightarrow e$) (38.5%, 162/420) progeny in almost equal proportion. Analysis of cell cycle times of edge cell progeny revealed that internal cells arising from edge cells ($e \rightarrow i$) displayed an average cell cycle time only 0.5 hours longer than internal cells that arose from internal cells ($i \rightarrow i$) (Figure 5-2b). Combined, these observations show the degree of cell plasticity that exists within hESC colonies and that colony cells respond dynamically to signals, or lack thereof, from the local microenvironment by generation of edge cells, which possess hdF developmental potential.

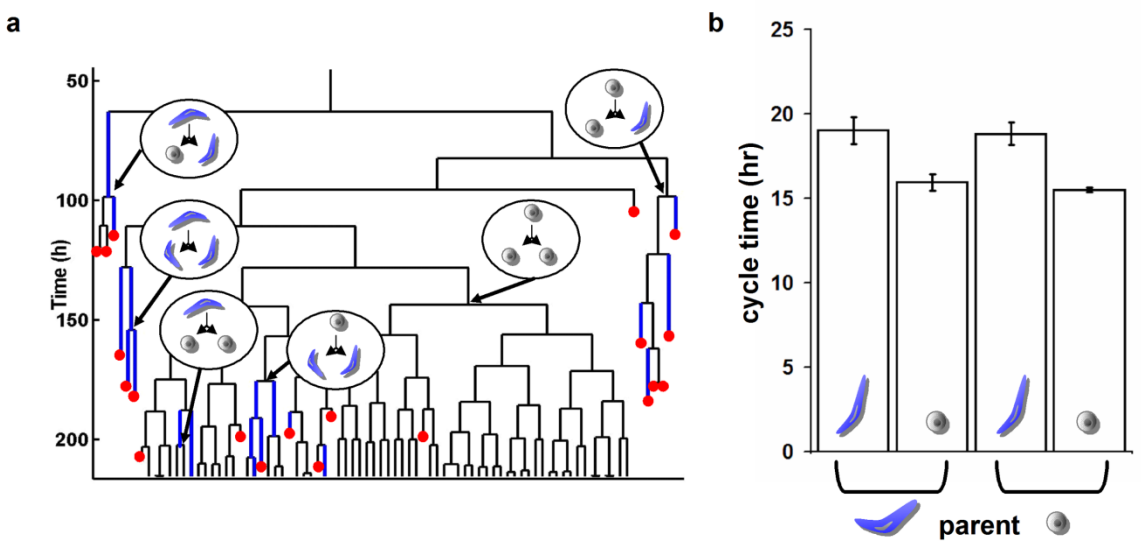

Figure 5-2. (a) Six different mother-daughter phenotype outcomes are possible (depicted in circles). Blue lines in the lineage tree represent edge cells. Red circles indicate cell death. (b) There are no significant differences between cell cycle times of internal and edge cells based on the morphology of their parent. Error bars indicate 95% confidence intervals.

The appearance of edge cells during colony re-establishment suggested that the post-passage conditions may be driving hESCs to become edge cells, similar to the production of hdFs by peripheral hESCs (Bendall et al. 2007). Therefore, the influence of the initial presence of co-transferred hdFs on the number of edge cells that arose was assessed. This analysis revealed that edge cells appeared at a higher frequency (20% edge cells (319/1694 total cells)) in colonies that had no post-passage local hdFs compared to colonies with surrounding hdFs (14% edge cells (164/1145 total cells)) ($p < 0.001$). Subsequent spatial analysis revealed that colonies with no surrounding hdFs had a uniform angular distribution of edge cells, while in colonies with non-uniform distributions of surrounding hdFs, edge cells tended to arise on the colony side away from hdFs (Figure 5-3). As co-transferred hdFs were not in direct contact with the colony, these results suggest that edge cells arise due to the absence of paracrine signaling from local hdFs.

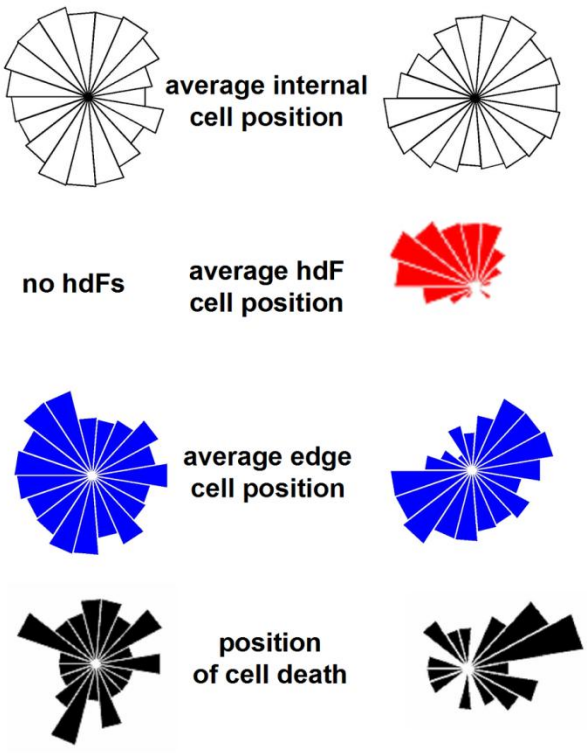

Figure 5-3. Area proportional rose plot of the spatial distribution of cell types in two colonies - one with (right) and one without (left) co-transferred surrounding hdFs: edge cells (blue), internal cells (white) and hdF cells (red), cell death (black). The area of each angular bin is proportional to the average number of cells present or the total number of cells deaths that occur within a given angular section over the first 100 hours. Edge cells and cell death were primarily localized to the colony side opposite co-transferred hdFs.

5.3.4 Local hdFs enhance colony expansion

Based on previous reports that hdFs secrete supportive survival factors in response to FGF stimulation (Bendall et al. 2007; Dvorak et al. 2005; Greber et al. 2007), the relationship between local hdF presence and colony expansion was asssessed. This analysis revealed that the number of cell deaths within a colony was inversely proportional to the number of surrounding hdFs; significantly more cell death occurred in colonies that lacked surrounding hdFs. The impact of hdF

presence on cell death within the colony was further confirmed upon analysis of the angular distribution of hdFs and location of cell death in individual colonies (Figure 5-3). Similar to edge cell distribution, in colonies with non-uniform distributions of surrounding hdFs, the cell death rates of both edge and internal cells tended towards the colony side away from hdFs. It should be noted that edge cells were much more likely to die under conditions lacking hdFs (39% die without hdFs vs. 16% with hdFs) compared to internal cells (9% die without hdFs vs. 6% with hdFs).

To investigate the overall effect of co-transferred local hdFs on colony expansion, the overall growth rates and cumulative number of deaths in colonies with and without local hdF support was directly compared. For example, two specific colonies from the same imaging chamber with and without local hdFs, and with similar starting size (11 and 14 cells, respectively) showed a significant difference in colony growth rate (Figure 5-4a). While both colonies had similar cumulative deaths over the first 100 hours, the colony with no surrounding hdFs had more than 3-fold more deaths within the first 20 hours of passage; this early death drastically slowed colony expansion. Thus, increased cell death, due to lack of hdFs and subsequent edge cell formation, negatively influences the initial recovery and expansion of hESC colonies immediately following passage. Significantly, this will also positively select for those clones able to survive suboptimal conditions following passage.

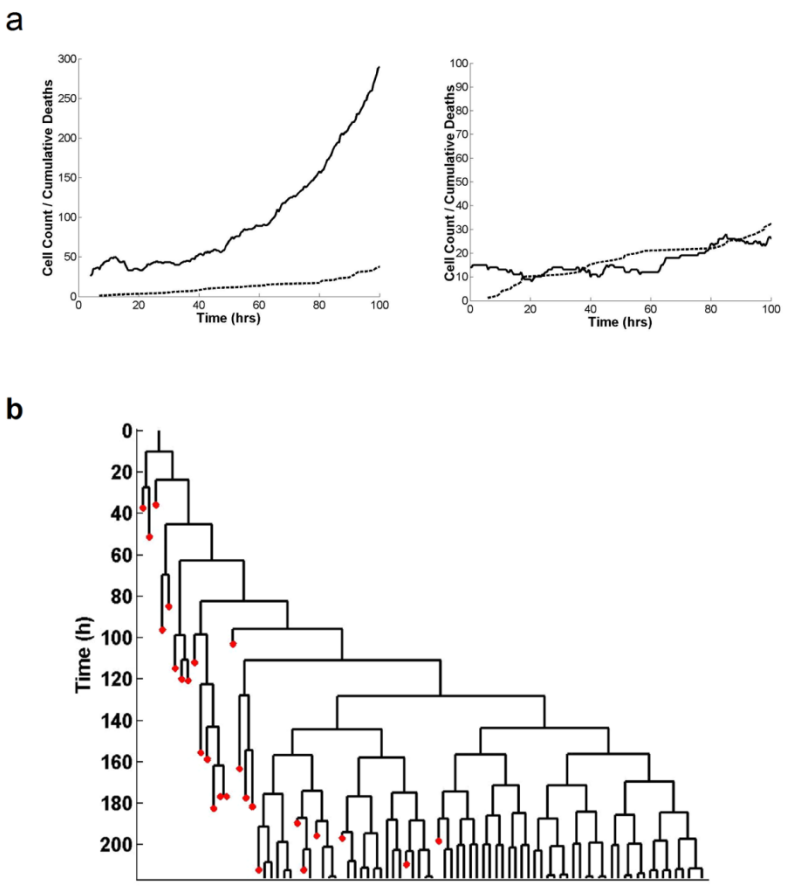

Figure 5-4. (a) Cell count (solid) and cumulative deaths (dotted) versus time of two colonies - one with (left) and one without co-transferred hdFs (right). (b) Lineage tree of single founder cell (from a colony with 14 total founder cells) showing pruning of sub-lineages due to cells death (red) and the resulting overall contribution to final colony population.

Early cell death following passage affects the proportional contribution of colony founder cells to the final colony population, causing clonal selection. Lineage trees were constructed from the tracked cell data from colonies that had starting populations of between 3 and 30 cells; all of which achieved varying degrees of growth or extinction due to cell death. In nearly all colonies (14/16), regardless of starting cell numbers, less than five founder cells contributed progeny to the final colony population (~200 hours). Of the lineages that contribute a significant fraction to the final colony, some experience very little early cell death, and therefore have stable expansion throughout. In contrast, some lineages underwent significant cell death early in colony development, without

complete lineage extinction, that then went on to achieve relatively stable expansion (Figure 5-4b) following re-establishment of the supportive niche, which was assessed by the presence of either passaged or colony-derived hdFs. This shows the uneven contribution of colony founders to the established colony population. Of colonies that at least doubled in size, the contribution of individual founder cells ranged between 1 and 70 percent of the final colony population. In all colonies tracked, the maximum number of starting cells that contributed lineages to the final colony was just over half of the starting cell number. Examination of lineage trees clearly reveals the high level to which cell death influences the clonal diversity of the subsequent culture.

5.4 Discussion

To retain self-renewal and pluripotent potential, hESCs require and can create a supportive microenvironment that is comprised of extracellular matrix, paracrine signaling and non-hESC cells. Under suboptimal conditions, such as those that may be experienced immediately after passaging, there is a higher rate of transition of hESC colony cells towards cells which possess hdF developmental potential. This is supported by results showing niche-associated FGFR1 expression of some edge cells and the fact that edge cells are much more likely than internal hESCs to give rise to hdFs. While continuous monitoring of hESC cultures has previously been used to quantify colony growth and distinguish between differentiated and undifferentiated cell populations (Narkilahti et al. 2007), these results show that the boundary between hESC colony and differentiated hdFs may not be as distinct as previously thought, as the edge cell sub-population that possess hdF differentiation potential appears to exist in a dynamic equilibrium with the remaining hESCs.

Heterogeneity within ESCs (Chambers et al. 2007; Filipczyk et al. 2007; Hayashi et al. 2008; Nunomura et al. 2005; Singh et al. 2007; Stewart et al. 2006) and other stem cells (Mazurier et al. 2004; Park et al. 2007) has been well documented. The interconvertability between internal and edge cells across multiple generations highlights the dynamic that exists between the two sub-populations of the hESC colony. We suggest that this equilibrium is regulated by paracrine signals produced from hdFs in a feedback loop, as depicted by the model proposed in Figure 5-5. This model fits with the observation that more hdFs are produced under less optimal culture conditions (Bendall et al. 2008; Greber et al. 2007), and adds an intermediary to the hESC-niche model previously proposed by Bendall and colleagues (Bendall et al. 2007). The observation that edge cells are more likely to die

than internal hESCs suggests that the edge subpopulation may be less responsive to survival and self-renewal signals, and therefore that suboptimal niche microenvironment depletes the pool of self-renewing hESCs and possibly selects for hESC with greater niche independence.

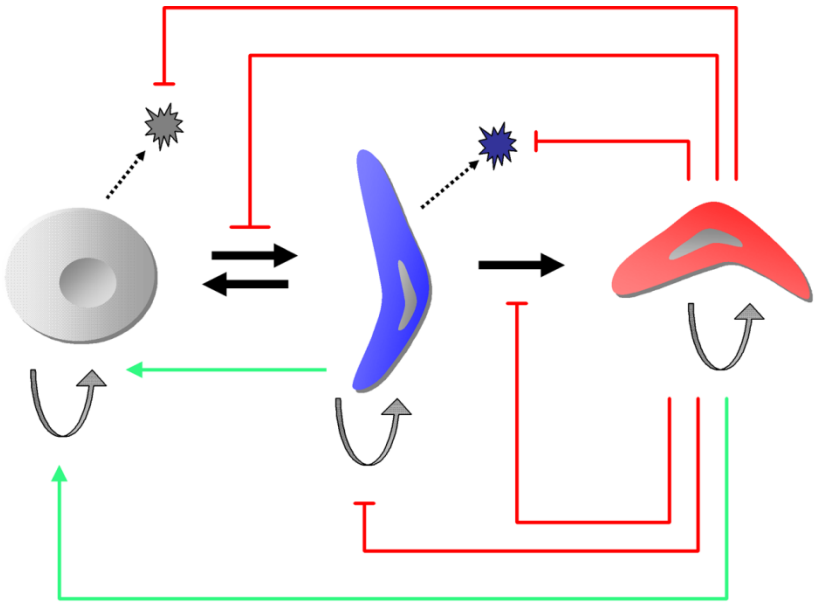

Figure 5-5. Proposed model of niche regulation. Transition of cell phenotype through division (black arrows), self-renewal (grey arrows), and cell death (dotted arrows) of internal (grey), edge (blue) and hdF (red) cells is regulated by stimulatory (green lines) and inhibitory (red lines) paracrine signaling.

The re-establishment of hESC colonies immediately following passage is highly dependent on the formation of edge cells and rate of cell death, both influenced by the surrounding microenvironment. Broadly, two colonies identical in terms of their composition, size, and cell density at the time of passage, will differ in their long term outcome based on their post-passage microenvironment. The presence of co-transferred hdFs promotes colony recovery and expansion, resulting in decreased clonal selection during passaging. Edge cell formation, cell death and clonal selection resulting from the absence of co-transferred hdFs highlights that hESC culture strategies, including future large-scale expansion systems (Nie et al. 2009; Oh and Choo 2006), must include consideration of microenvironment to decrease selective pressure and minimize hESC transformation.

The appearance and behavior of the edge cell is a result that likely would not have been uncovered solely through molecular-level interrogation. The combination of features that define the edge cell here are emergent cell-level properties, observed through LCI, and analyzed and interpreted best through cell and lineage tracking. Cell-level properties, such as morphology and cell-cycle are manifestations of numerous pathways. Non-destructive analysis of these complex, interacting molecular pathways is not yet feasible. As such, emergent behaviors analyzed through LCI and tracking in the context of lineage can be used to reveal trajectories in cell cultures across generations. In this chapter, this approach lead to a new understanding of the re-establishment of a supportive niche in hESC cultures following disruption during passage.

5.5 Experimental procedures

5.5.1 hESC culture

hESC lines H9(WA01) and H1(WA02) were maintained as previously described (Chadwick et al. 2003) in mouse embryonic fibroblast-conditioned media (MEFCM)+ 8ng/ml bFGF on Matrigel (BD Bioscience) coated tissue culture plates. No significant difference in cell cycle times was present between the two cell lines (supplemental). hESCs were cultured until confluent where upon they were passaged in clumps following Collagenase IV treatment. For time lapse imaging, hESC cultures were treated for 5min with Collagenase IV prior to collection. Collected hESC aggregates were gently triturated to clumps of approximately 10-20 cells and seeded into matrigel-coated gap-chambers. Gap chambers were assembled and loaded as previously described (Moogk et al. 2007). Gap chambers were pre-coated with 1:30 Matrigel in KO-DMEM containing 4.7 μm polystyrene beads (Polysciences) at 10^6 beads/mL for 2-5hrs uncovered at room temperature, rinsed gently and then coated either at room temperature for 1hr or overnight at 4^oC with 1:15 Matrigel. hESCs in tissue culture plates or gap chambers were incubated at 37^oC in 5%CO_2. Media was changed every other day during imaging.

5.5.2 Live cell imaging

LCI of hESCs under standard culture conditions using (DIC) microscopy does not yield trackable data (i.e. cells cannot be unequivocally identified at all time points) (data not shown). Therefore, hESC colonies were cultured using a monolayer culture system (Ramunas et al. 2006) to enable cell and lineage tracking. hESCs were imaged on an inverted microscope (Axiovert 200, Zeiss Germany) with a 40x objective lens. The microscope stage was enclosed to maintain a 5% CO_2 humidified air atmosphere, while the entire microscope was enclosed in thermal insulation to enable maintenance of 37˚C by an automated controller. Images were captured with a digital camera (XCD-SX910, Sony Japan) equipped with a 0.5x adapter using in-house software at 3 minute intervals. Individual hESC colonies and surrounding area were imaged as tiled image array mosaics, enabling high resolution imaging of areas larger than a single field of view, which were collected and stored as individual image files. Acquisition was paused briefly for media changes, during which the chamber was removed to a laminar flow hood, or to refocus the image blocks.

5.5.3 Extraction of image data: Cell tracking and scoring

Post-imaging analysis of DIC image data was performed using custom software developed in Matlab® (Mathworks, Natick, MA) that acted as a front end to a SQL-based database of all collected and derived data. Users manually identified and tracked individual cells, which were assigned unique identifiers, over the time course sequences. The cells' absolute positions, relative to a preset stage origin, were logged into the database along with cell fate (died, divided) and generational information (mother ID, daughter IDs) allowing for the construction of lineages. Cells were also manually scored as edge cells or hdFs. A query-based approach to data analysis facilitated comparisons of multiple datum types across time.

5.5.4 Calculation of cell lifespan

Cycle times and time-to-death were calculated only for cells whose birth and death or division was observed during the course of an experiment. Times were calculated as the difference in image

acquisition times between the cells' first and last tracked instances. Cells whose births were not observed (e.g. colony founder cells) and cells whose final instances were not observed (e.g. cells that migrated out of an imaging region, or cells that were still alive when the experiment was terminated) were not assigned a cycle time or time to death. These cells represented a very small fraction of the total number of cells imaged.

5.5.5 Assessment of IGF1R, FGFR1, and Oct-4 expression in hESC by immunocytochemistry

hESCs were cultured in gap-chambers as described above for 4-9 days. Cells were rinsed twice with PBS before fixation with 4% paraformaldehyde and permeabilization with 0.1% Triton X-100. Cells were blocked with 10% Normal Donkey Serum (NDS) + 5% BSA at room temperature (RT). The antibodies used were 10μg/ml chicken anti-IGF1R (Abcam), 2μg/ml mouse anti-FGFR1, clone VBS1 (Chemicon) and 3μg/ml goat anti-Oct3/4(N-19) (Santa Cruz Biotechnology). Cells were incubated with primary antibodies followed by secondary detection with Alexa Fluor 488 goat anti-mouse IgM, 594 goat anti-chicken IgG (Molecular Probes) at 3μg/ml and 647 goat anti-mouse IgG (Invitrogen) at 5μl/ml. Chamber slides were mounted and counterstained using Vectashield Mounting Medium with DAPI (Vector Laboratories). Immunofluorescent images were aligned with endpoint LCI data to identify and score each cell at the end of the culture.

5.6 Supplemental data and discussion

This chapter utilized the imaging chamber described in chapter 3 and the tracking and analysis tools developed in chapter 4 to investigate hESC-niche dynamics using monolayer LCI. Of particular note was that the edge cell morphology was not known or expected prior to the tracking process. Its morphology was noted and subsequently scored during the tracking process, but it was not until the combination of morphology scoring with cell cycle times and end-point immunocytochemistry that the hypothesis of the edge cell as an hdF progenitor was formed. The inclusion of lineage-related information revealed the most significant aspects of the hESC/edge cell/hdF dynamic - that hdFs are more likely to arise from edge cells and that there exists an interconvertibility between internal and edge hESCs across generations.

In addition to single cell tracking of colonies, overall hESC colony growth rates were estimated using colony outlines (Figure 5-6). For this experiment, LCI was performed at a much lower frequency of only one image per day, since tracking of individual cells was not required. However, at each time point individual hdFs were identified to quantify the local hdF presence around each tracked colony.

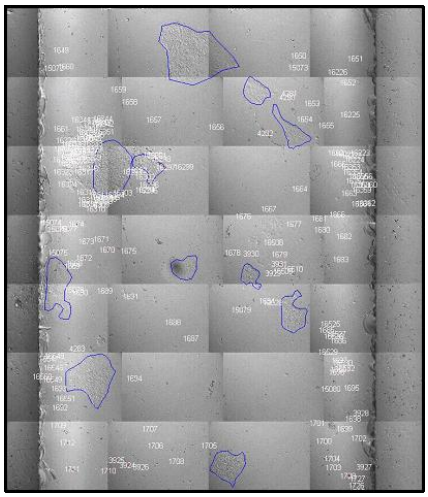

Figure 5-6. Tiled array of the entire width of an imaging chamber containing hESC colonies (manually outlined with blue circles) and co-transferred hdF (individually identified and numbered).

The data shows that, in general, colonies that have a higher number of hdFs in their immediate vicinity have higher average specific growth rates (Figure 5-7).

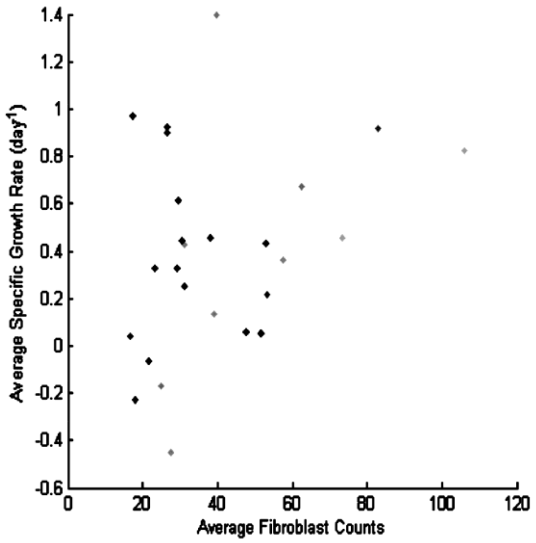

Figure 5-7. Average specific growth rate (based on area) of manually outlined hESC colonies plotted against the average number of fibroblasts within 300 μm of the colony.

The spread of the data is likely due to the absence of single cell measurement of colony size. Here, growth rate is calculated from manually outlined colony areas, and therefore does not account for variability in colony cell density. Indeed, upon inspection of a number of individual colonies, varying colony densities were observed. This is reminiscent of the colonies tracked at the single cell level, as a number of them dispersed within the first day or two. These were not included in the analysis, as it was concluded that these were likely pre-existing hdFs present at high density from the previous passage of hESC culture. Therefore, outlined colonies of such cells would appear to have a high growth rate, regardless of the presence or absence of local hdFs. This explains the occurrence of colonies with apparently high growth rates and low hdF counts in the data. Although supportive of the overall conclusion reached in the chapter, this data further highlights how the absence of single cell-level data can lead to spurious interpretations. Here, cell density could not be taken into consideration and therefore the true growth rate of the colonies could not be calculated.

To complement the area proportional rose plots presented in this chapter, the same information can be presented as cell property image overlays (Figure 5-8). Although single frame image overlays cannot provide as much information as the rose plots, which show the average spatial distribution of properties over a given time range, viewing the image time courses with properties overlaid can help the user understand the spatial dynamics of a given property.

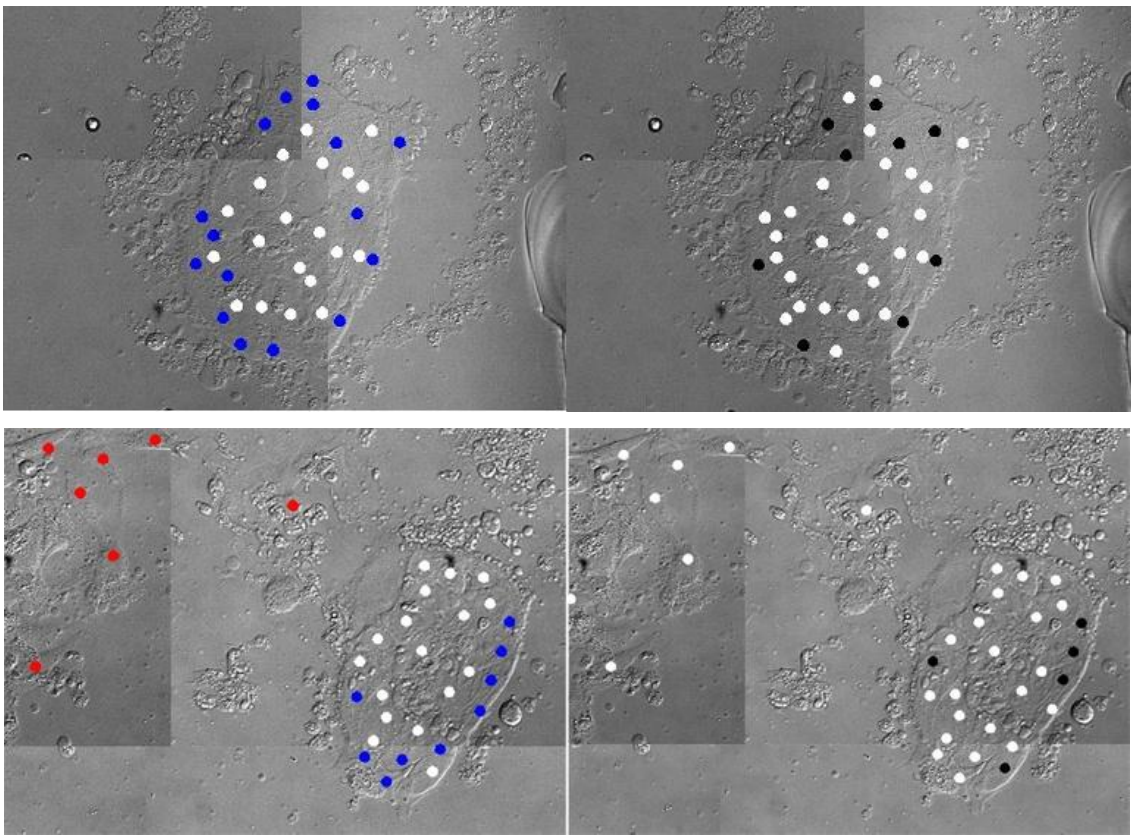

Figure 5-8. Cell property image overlays of two hESC colonies, one with (bottom) and one without (top) surrounding hdFs (red). These images highlight the spatial dependence of edge cells (blue) and cell death (black represents cell alive in this frame but that eventually die) on surrounding hdFs.

Multiple cell properties can be displayed for a single cell for a given time point by using cell marker color and size to represent individual properties (Figure 5-9). Multiple colors can be displayed on a single cell marker as well, by dividing each cell marker into multiple sections. Although identification of cells with a given combination of properties can be accomplished through

manual queries, the image overlay, again, may aid the user in identifying further dynamic trends within a sub-population of cells, or between multiple sub-populations displayed on the same overlay.

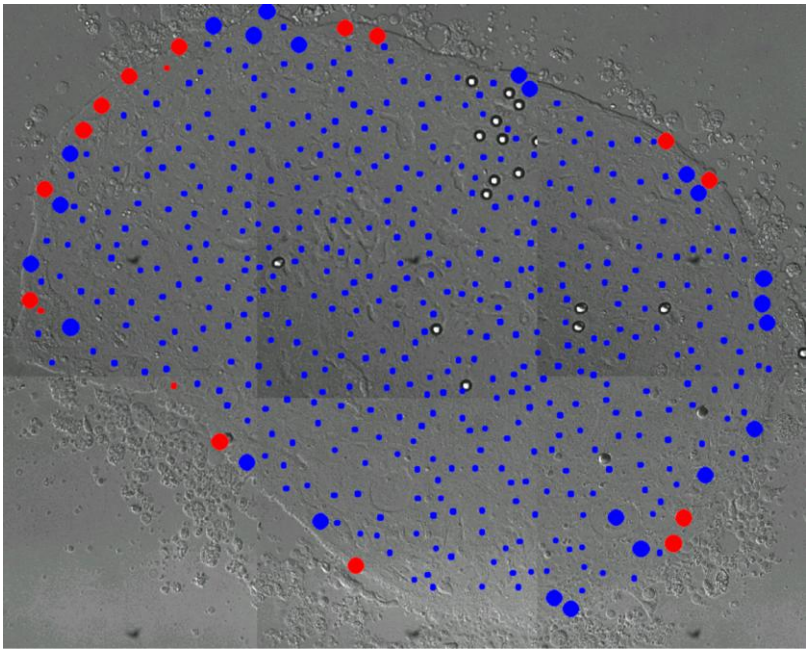

Figure 5-9. hESC colony displaying edge cells (large) and internal cells (small) in combination with immunocytochemistry scoring for FGFR positive (red) and FGFR negative (blue) cells.

Chapter 6
Conclusions and Future Work

This thesis presents the development of live cell imaging and analysis tools and techniques, enabling the study of multicellular, heterogeneous *in vitro* cultures. These developments were combined to test the hypothesis that underlies this thesis. Recall, the hypothesis:

> ***Heterogeneity within in vitro cellular systems, which may not be known or measurable at the molecular level, can be uncovered and described at the cell and lineage level to identify emergent properties and behavioral phenotypes resulting from dynamic spatiotemporal cell-cell and colony interactions.***

This was developed from the reasoning that observable cell-level properties are manifestations of molecular-level events, and are therefore generalized descriptors of highly connected, complex molecular interactions. Dynamic heterogeneity, immeasurable or unpredictable at the molecular level, could therefore be uncovered by characterizing individual cells, their interactions with other cells, and entire multicellular colonies. Of particular importance to this study was the inclusion of lineage, providing an intermediate level of information as a temporal connector of generational relationships. In this respect, lineage-based data connects the cell-level information spatially and temporally to colony-level information, and can provide information about the dynamic trajectory of cell traits over multiple generations. Live cell imaging, combined with cell, lineage, and colony tracking was identified as a means to characterize cell systems at this level, and was implemented here to investigate heterogeneity within human islets of Langerhans-derived cells and human embryonic stem cell colonies.

Three main objectives were identified to develop strategies and tools to test the overall hypothesis. First, as discussed in chapter three, culture conditions for three-dimensional, matrix-embedded imaging of islets of Langerhans were examined to determine the feasibility of single cell tracking in three-dimensional cell aggregates. The main design considerations were as follows:

i) Both imaging chamber and islet dimensions must ensure that transport of nutrients to all islet cells is not limited, producing adverse physiological conditions

ii) Imaging chamber depth must allow optical sectioning using DIC imaging to enable identification of every cell within an islet

iii) Islet sizes must be selected to ensure that the imaging chamber dimensions do not disrupt their existing cell-cell and cell-matrix interactions

iv) The system enables stable, long-term imaging for periods of days to weeks

Nutrient transport was considered by modeling the imaging chamber/islet system in COMSOL™ Multiphysics. The model considered diffusion from the bulk media to the islet through collagen, diffusion within the intra-islet space, uptake of nutrients into the cells, and transport within the islet cells through gap junctions. The major conclusions from simulations are as follows:

i) Providing an initial glucose concentration at or near the physiologically required concentration, 5.2 mol/m^3, is sufficient to ensure glucose limitation is not reached, provided the bulk media is replenished when required.

ii) Given a standard imaging chamber width of 2mm, oxygen transport becomes limited once the islet radius, imposed by compression in the imaging chamber, surpasses 150 µm.

These results led to the selection of input islets with sizes ranging between 35-45 µm in diameter, generally the smallest range of human islets available, to ensure that transport of nutrients would not be an issue. DIC optical sectioning produced trackable time course image sequences with an islet compressed to roughly 5 cells thick, or less. Therefore, it was concluded that with 25 µm imaging chambers, which would provide this degree of compression, 35-45 µm input islets would not experience any adverse conditions. This was confirmed by showing that islets could be cultured and imaged in 25 µm chambers for several days under maintenance conditions and retain their structure, surrounding matrix support, and expression of islet hormones.

The main objectives of chapter four were to develop cell, lineage, and colony tracking tools, as well as methods for visualizing and analyzing tracked LCI data. These features were implemented and tested using human islet of Langerhans and their derivatives. Islets were chosen because of existing protocols for derivation of islet progenitor cells in both two- and three-dimensional culture

systems. hIPCs also met the criteria of being a dynamic, heterogeneous system with which to test the overall hypothesis of this research. The heterogeneity is also of significant interest in diabetes research, as the identification and isolation of specific cells capable of *in vitro* expansion and re-differentiation to cells of clinical-grade therapeutic potential is a major goal in the field.

The development of methods for tracking, visualizing, and analyzing LCI data lead to the following general conclusions:

i) The discovery of unpredictable trends, properties, and events is aided through the interactive display of cell and colony properties on visualizations such as lineages and population property histograms

ii) The incorporation of other analytical data, such as immunocytochemistry, can increase the power of LCI analysis

The most significant development from the cell tracking and analysis design was the implementation of interactive visualization and gating. The combination of large, highly dimensional data sets with general hypotheses (i.e. heterogeneity exists and can be identified) requires that the data can be viewed quickly and display a variety of information together. This allows the user to visually interpret the data and use their innate pattern recognition skills to look for both spatial trends (e.g. using cell property overlaid on the LCI images) or temporal trends (e.g. using lineage visualization). The value of such visualizations in conveying the dynamics of the systems being studied cannot be overstated.

The monolayer hIPC derivation process was studied using two-dimensional LCI, colony and single cell tracking, morphology scoring, and cell cycle analysis. The analysis was achieved by implementing analysis features including histograms and population gating. Colony-level analysis revealed unequal islet contribution to the hIPC population. It remains unclear if there are distinguishing properties of islets that do not contribute to hIPCs, as no colony-level trends appeared during analysis, such as islet size or morphology. Single cell tracking and morphology scoring confirmed the morphologically different cell types previously reported and revealed dynamic proliferative properties of the cell population.

Three-dimensional DLS and ILS transformation was also studied, implementing the design considerations from chapter three. Tracking of single cells through these processes was difficult due to cell motility and matrix degradation. The main conclusions from the implementation of LCI, cell tracking and analysis on the two- and three-dimensional human islet of Langerhans systems are:

i) Two-dimensional derivation of hIPCs is heterogeneous, in terms of the contribution of islets to the hIPC process. Furthermore, the two sub-populations of cells have unique proliferative profiles during the first passage of culture and may to exist in a dynamic equilibrium, as both cell types give rise to progeny of the other cell type.

ii) LCI of three-dimensional derivation of DLSs is hindered by cell morphological dynamics that occur at a time scale similar to the imaging frequency, confounding cell tracking. Furthermore, the formation process also disrupts the collagen matrix and likely does not allow for the onset of cell proliferation.

Chapter five detailed the implementation of monolayer LCI with cell and lineage tracking to characterize the *in vitro* behavior of hESCs and their niche. As opposed to chapter four, where there was no proliferation, and therefore growth, here hESCs proliferated consistently. Results from chapter three were used to consider how transport limitations would affect colony growth, and colonies that were analyzed were imaged and tracked well below the threshold of colony radius that was determined. Significantly, colonies that did grow to a radius of near 200 μm began to develop holes in the centre of the colony, as cells became less adhesive and some began to die. This supports the conclusion from chapter three, which calculated that the maximum islet radius would be about 150 μm. These values are likely different because the intra-colony diffusivities of the two systems due to differing cell density, extracellular matrix composition and nutrient consumption rates.

Cell tracking and scoring of the hESC colonies produced a database consisting of 15 tracked colonies, more than 7000 tracked cells, and lineages of up to 12 generations. The cells were scored for morphology, fate and immunocytochemistry and colonies were scored depending on their proximity to co-transferred hdFs. The main objective of these experiments was to characterize the hESC-niche relationship and detail how hESCs differentiate to create their own niche cells. The main conclusions drawn from chapter five were as follows:

i) hESC colonies are heterogeneous, in that there exists a sub-population of cells that possess a higher potential for niche differentiation

ii) The two sub-populations exist in a dynamic state, as there is an interconvertibility between phenotypes across generations

iii) Niche differentiation-competent cells arise due to a lack of local hdF paracrine signaling

iv) Lack of local hdFs leads to significant cell death and resultant clonal selection of the expanding hESC population

The identification of a previously unappreciated level of heterogeneity with hESC cultures, based on cell morphology, cell cycle, immunocytochemistry, and hdF differentiation is an example of how cell-level and lineage analysis can reveal unexpected properties, as hypothesized. While the initial objective was to determine if all hESCs contributed equally to niche differentiation, the specific combination of cell properties that would reveal this to be untrue were only identified through post-tracking discovery. Cell morphology tracking, which was initially implemented to distinguish between hESCs and existing hdFs co-transferred during passage, led to the identification of the edge cell morphology. Displaying morphology on lineage trees showed the interconvertibility between edge and internal hESCs, and that edge cells were more likely to give rise to differentiated hdFs. Spatial analysis of the tracked cells revealed that both the formation of edge cells and the occurrence of cell death were due to an absence of local hdFs. Overall, the combination of cell and lineage tracking with database queries and visualizations revealed unexpected hESC culture heterogeneity and dynamics.

The implications of these results in the field of embryonic stem cell biology are significant. The long-term goal of *in vitro* hESC culture is the expansion and maintenance of cells capable of eventual differentiation to specific cell types for cell therapies. Recent studies have shown that long term expansion of hESCs leads to cell line transformation and reduced differentiation potential. Heterogeneity in hESCs – such that subpopulations are primed for self-renewal, while others are primed for differentiation – highlights that there is a dynamic balance required to maintain the dual properties of hESCs. Sub-optimal self-renewal conditions, such as those experienced post-passage when there is insufficient co-transferred hdFs, pushes the population towards niche differentiation, thereby depleting the pool of hESCs. The results of chapter five show that hESC sub-populations are

primed not only for differentiation into committed mature cell types, but also for differentiation into supportive niche.

LCI is a growing utility in the biological sciences, and will likely continue to grow as interest in developmental and stem cell biology expands. The dynamic nature of development, differentiation and transdifferentiation requires the acquisition of lineage-structured data over a number of generations for accurate analysis. LCI and cell tracking provide an ideal method for obtaining this data precisely, generally without inference. LCI also provides the opportunity to extract observable cell- and colony-level information, properties and behaviors. This level of information represents emergent properties arising from numerous complex molecular-level events that may not be measurable or predictable. Therefore, the combination of a small number of cell-level measurements is, in fact, a descriptor of a large number of molecular-level interactions, and therefore may be a more suitable discriminator between cell types than the combination of molecular markers, as in FACS, for example. In this respect, LCI, cell tracking and lineage analysis can be used to study specific cell types with specific questions, as presented here. While a comprehensive understanding of the molecular-level regulation of cell properties and events is an ultimate goal in biology, the use of cell-level measures may aid in developing generalized models of cell behavior. Therefore, this system can also be a valuable tool in the emerging field of systems biology, which aims to use the perspective of holism, as opposed to the classical approach of reductionism, to establish a systemic view of the cell. The concept of observing and characterizing cell-level properties fits into a systems biology view, and may be incorporated with other levels of information, for example the metabolome, transcriptome, and proteome, to develop more comprehensive models of cellular function.

The system may also be a useful tool in cell manufacturing strategies, as it may offer a non-destructive method of product characterization and quality control. Because clinical cell therapies will no doubt require stringent quality assurance of input cells, it may be possible that every single cell be interrogated before use. While existing tools exist for single cell sorting, the identification of possibly deleterious cells through existing molecular screen may not be feasible, or provide enough accuracy. It is likely that modification of cells, genetic or otherwise, to be used for therapeutic reasons would not be acceptable due to possible aberrant affects on the normal functions of the cell. An LCI approach to cell screening would enable the observation of individual cell properties and behaviors with no other intervention or physiological disruption. The implementation of such a system would require significant scale-up considerations, as the number of cells required for cell

therapy may approach 10^9. Therefore a continuous system that interrogates large numbers of cells through imaging and selects those appropriate for therapy through automated tracking and classification would be required. While significant advances in automated image analysis, cell tracking and classification are still required, it is likely that increases in both computational power and hard drives will provide the capabilities to handle the requirements of real-time imaging and analysis. The scale-up of culture systems for very wide field imaging may also be challenging. However, as such a system is developed it could undoubtedly be used as a screen to produce a small population of highly purified cells for further expansion in conventional bioreactor configurations.

While the current LCI, cell tracking and analysis package discussed herein was implemented successfully, a number of future improvements may enhance its abilities. While not discussed in this thesis, incorporation of live-cell fluorescence imaging would allow real-time quantification of cellular processes and gene expression. While here immunocytochemistry was only able to reveal expression patterns of cells that existed at the end of imaging, real-time fluorescence would allow for trends in expression to be observed over a number of generations, enhancing the power of the lineage data structure. Because of phototoxicity concerns, the combination of DIC or phase LCI with intermittent fluorescence LCI would enable long term imaging experiments. Such capabilities are indeed currently being implemented. Culture systems should be developed and implemented for the specific cell type and experimental objective. Here, improvement of three-dimensional islet embedding and the imaging chamber dimensions is required to allow long-term imaging of islet of Langerhans transformation without matrix disruption, while still enabling single cell identification. For future hESC imaging studies, protocols may be required to control the spatial distribution and concentration of surrounding hdFs to further evaluate their role in niche regulation. The confined nature of the imaging chamber would likely rule out single cell manipulation through micropipettes, and therefore other strategies for precise cell placement may need to be explored. Regardless of future developments, the key requirements that must be met remain the long term viability and functionality of the cell culture and the ability to observe, identify and track individual cells and divisions.

Incorporation of new tools for analyzing tracked LCI data could be done relatively easily, as the software was designed in-house and is modular in nature. The utility of new and existing visualizations and plots depends on the particular system being explored. Regardless, incorporation of new techniques with the existing data structure, so as to enable active gating and visualization, would likely be a useful addition to the analysis package. While visualizations are valuable as a

means of interpreting data, the ability to convert these to numerical data forms for further analysis would likely be useful, for example, by exporting all cell properties contained with individual gates in a visualization to a spreadsheet. In this thesis, this was done only to count the number of cells that exist in each gate or combination of gates. The identification of new requirements for analysis will likely arise during the cell tracking and analysis process, so the flexibility and adaptability of the software is paramount. Incorporation of lineage descriptors and measures, newly introduced in the literature, would indeed also add another level of information to the system. The standardization of some of these measures would certainly benefit the growth of the emerging field of live cell imaging and lineage analysis.

References

Absher PM, Absher RG, Barnes WD. 1975. Time-lapse cinemicrophotographic studies of cell division patterns of human diploid fibroblasts (WI-38) during their in vitro lifespan. Adv Exp Med Biol 53:91-105.

Abud HE, Young HM, Newgreen DF. 2008. Analysing tissue and gene function in intestinal organ culture. Methods Mol Biol 468:275-86.

Al-Kofahi O, Radke RJ, Goderie SK, Shen Q, Temple S, Roysam B. 2006. Automated cell lineage construction: a rapid method to analyze clonal development established with murine neural progenitor cells. Cell Cycle 5(3):327-35.

Amit M, Carpenter MK, Inokuma MS, Chiu CP, Harris CP, Waknitz MA, Itskovitz-Eldor J, Thomson JA. 2000. Clonally derived human embryonic stem cell lines maintain pluripotency and proliferative potential for prolonged periods of culture. Dev Biol 227(2):271-8.

Apelqvist A, Li H, Sommer L, Beatus P, Anderson DJ, Honjo T, Hrabe de Angelis M, Lendahl U, Edlund H. 1999. Notch signalling controls pancreatic cell differentiation. Nature 400(6747):877-81.

Atouf F, Park CH, Pechhold K, Ta M, Choi Y, Lumelsky NL. 2007. No evidence for mouse pancreatic beta-cell epithelial-mesenchymal transition in vitro. Diabetes 56(3):699-702.

Baeyens L, De Breuck S, Lardon J, Mfopou JK, Rooman I, Bouwens L. 2005. In vitro generation of insulin-producing beta cells from adult exocrine pancreatic cells. Diabetologia 48(1):49-57.

Banerjee M, Bhonde RR. 2003. Islet generation from intra islet precursor cells of diabetic pancreas: in vitro studies depicting in vivo differentiation. JOP 4(4):137-45.

Bao Z, Murray JI, Boyle T, Ooi SL, Sandel MJ, Waterston RH. 2006. Automated cell lineage tracing in Caenorhabditis elegans. Proc Natl Acad Sci U S A 103(8):2707-12.

Bar Y, Russ HA, Knoller S, Ouziel-Yahalom L, Efrat S. 2008. HES-1 is involved in adaptation of adult human beta-cells to proliferation in vitro. Diabetes 57(9):2413-20.

Barbosa H, Bordin S, Stoppiglia L, Silva K, Borelli M, Del Zotto H, Gagliardino J, Boschero A. 2006. Islet Neogenesis Associated Protein (INGAP) modulates gene expression in cultured neonatal rat islets. Regul Pept 136(1-3):78-84.

Beattie GM, Cirulli V, Lopez AD, Hayek A. 1997. Ex vivo expansion of human pancreatic endocrine cells. J Clin Endocrinol Metab 82(6):1852-6.

Becker KA, Ghule PN, Therrien JA, Lian JB, Stein JL, van Wijnen AJ, Stein GS. 2006. Self-renewal

of human embryonic stem cells is supported by a shortened G1 cell cycle phase. J Cell Physiol 209(3):883-93.

Bendall SC, Hughes C, Campbell JL, Stewart MH, Pittock P, Liu S, Bonneil E, Thibault P, Bhatia M, Lajoie GA. 2009. An enhanced mass spectrometry approach reveals human embryonic stem cell growth factors in culture. Mol Cell Proteomics 8(3):421-32.

Bendall SC, Stewart MH, Bhatia M. 2008. Human embryonic stem cells: lessons from stem cell niches in vivo. Regen Med 3(3):365-76.

Bendall SC, Stewart MH, Menendez P, George D, Vijayaragavan K, Werbowetski-Ogilvie T, Ramos-Mejia V, Rouleau A, Yang J, Bosse M and others. 2007. IGF and FGF cooperatively establish the regulatory stem cell niche of pluripotent human cells in vitro. Nature 448(7157):1015-21.

Bernard C, Berthault MF, Saulnier C, Ktorza A. 1999. Neogenesis vs. apoptosis As main components of pancreatic beta cell ass changes in glucose-infused normal and mildly diabetic adult rats. FASEB J 13(10):1195-205.

Bertram R, Pernarowski M. 1998. Glucose diffusion in pancreatic islets of Langerhans. Biophys J 74(4):1722-31.

Bianco P, Riminucci M, Gronthos S, Robey PG. 2001. Bone marrow stromal stem cells: nature, biology, and potential applications. Stem Cells 19(3):180-92.

Blanpain C, Horsley V, Fuchs E. 2007. Epithelial stem cells: turning over new leaves. Cell 128(3):445-58.

Bodnar CA, Sen A, Kallos MS, Behie LA, Petropavlovskaia M, Rosenberg L. 2006. Characterization of human islet-like structures generated from pancreatic precursor cells in culture. Biotechnol Bioeng 93(5):980-8.

Boffa DJ, Waka J, Thomas D, Suh S, Curran K, Sharma VK, Besada M, Muthukumar T, Yang H, Suthanthiran M and others. 2005. Measurement of apoptosis of intact human islets by confocal optical sectioning and stereologic analysis of YO-PRO-1-stained islets. Transplantation 79(7):842-5.

Bolander FF. 2004. Molecular endocrinology. Amsterdam ; Boston: Elsevier Academic Press. viii, 632 p. p.

Bonner-Weir S. 1988. Morphological evidence for pancreatic polarity of beta-cell within islets of Langerhans. Diabetes 37(5):616-21.

Bonner-Weir S, Baxter LA, Schuppin GT, Smith FE. 1993. A second pathway for regeneration of adult exocrine and endocrine pancreas. A possible recapitulation of embryonic development.

Diabetes 42(12):1715-20.

Bonner-Weir S, Deery D, Leahy JL, Weir GC. 1989. Compensatory growth of pancreatic beta-cells in adult rats after short-term glucose infusion. Diabetes 38(1):49-53.

Bonner-Weir S, Taneja M, Weir GC, Tatarkiewicz K, Song KH, Sharma A, O'Neil JJ. 2000. In vitro cultivation of human islets from expanded ductal tissue. Proc Natl Acad Sci U S A 97(14):7999-8004.

Bouwens L. 1998. Transdifferentiation versus stem cell hypothesis for the regeneration of islet beta-cells in the pancreas. Microsc Res Tech 43(4):332-6.

Bouwens L, Lu WG, De Krijger R. 1997. Proliferation and differentiation in the human fetal endocrine pancreas. Diabetologia 40(4):398-404.

Bouwens L, Pipeleers DG. 1998. Extra-insular beta cells associated with ductules are frequent in adult human pancreas. Diabetologia 41(6):629-33.

Bouwens L, Rooman I. 2005. Regulation of pancreatic beta-cell mass. Physiol Rev 85(4):1255-70.

Boyle TJ, Bao Z, Murray JI, Araya CL, Waterston RH. 2006. AceTree: a tool for visual analysis of Caenorhabditis elegans embryogenesis. BMC Bioinformatics 7:275.

Braun V, Azevedo RB, Gumbel M, Agapow PM, Leroi AM, Meinzer HP. 2003. ALES: cell lineage analysis and mapping of developmental events. Bioinformatics 19(7):851-8.

Brink C. 2003. Promoter elements in endocrine pancreas development and hormone regulation. Cell Mol Life Sci 60(6):1033-48.

Brissova M, Fowler MJ, Nicholson WE, Chu A, Hirshberg B, Harlan DM, Powers AC. 2005. Assessment of human pancreatic islet architecture and composition by laser scanning confocal microscopy. J Histochem Cytochem 53(9):1087-97.

Cano DA, Rulifson IC, Heiser PW, Swigart LB, Pelengaris S, German M, Evan GI, Bluestone JA, Hebrok M. 2008. Regulated beta-cell regeneration in the adult mouse pancreas. Diabetes 57(4):958-66.

Cantenys D, Portha B, Dutrillaux MC, Hollande E, Roze C, Picon L. 1981. Histogenesis of the endocrine pancreas in newborn rats after destruction by streptozotocin. An immunocytochemical study. Virchows Arch B Cell Pathol Incl Mol Pathol 35(2):109-22.

Chadwick K, Wang L, Li L, Menendez P, Murdoch B, Rouleau A, Bhatia M. 2003. Cytokines and BMP-4 promote hematopoietic differentiation of human embryonic stem cells. Blood 102(3):906-15.

Chalfie M, Tu Y, Euskirchen G, Ward WW, Prasher DC. 1994. Green fluorescent protein as a marker for gene expression. Science 263(5148):802-5.

Chambers I, Silva J, Colby D, Nichols J, Nijmeijer B, Robertson M, Vrana J, Jones K, Grotewold L, Smith A. 2007. Nanog safeguards pluripotency and mediates germline development. Nature 450(7173):1230-4.

Chase LG, Ulloa-Montoya F, Kidder BL, Verfaillie CM. 2007. Islet-derived fibroblast-like cells are not derived via epithelial-mesenchymal transition from Pdx-1 or insulin-positive cells. Diabetes 56(1):3-7.

Christiansen GS, Danes B, Allen L, Leinfelder PJ. 1953. A culture chamber for the continuous biochemical and morphological study of living cells in tissue culture. Experimental Cell Research 5(1):10-15.

Comandon J. 1917. Phagocytose in vitro des hematozoaires du calfat (enregistrement cinematographique). Compt. Rend. Soc. Biol. (Paris). 80:314-316.

Crittenden SL, Bernstein DS, Bachorik JL, Thompson BE, Gallegos M, Petcherski AG, Moulder G, Barstead R, Wickens M, Kimble J. 2002. A conserved RNA-binding protein controls germline stem cells in Caenorhabditis elegans. Nature 417(6889):660-3.

Davani B, Ikonomou L, Raaka BM, Geras-Raaka E, Morton RA, Marcus-Samuels B, Gershengorn MC. 2007. Human islet-derived precursor cells are mesenchymal stromal cells that differentiate and mature to hormone-expressing cells in vivo. Stem Cells 25(12):3215-22.

Deltour L, Leduque P, Paldi A, Ripoche MA, Dubois P, Jami J. 1991. Polyclonal origin of pancreatic islets in aggregation mouse chimaeras. Development 112(4):1115-21.

Demou ZN, McIntire LV. 2002. Fully automated three-dimensional tracking of cancer cells in collagen gels: determination of motility phenotypes at the cellular level. Cancer Res 62(18):5301-7.

Dickson LM, Rhodes CJ. 2004. Pancreatic beta-cell growth and survival in the onset of type 2 diabetes: a role for protein kinase B in the Akt? Am J Physiol Endocrinol Metab 287(2):E192-8.

DiMilla PA, Stone JA, Quinn JA, Albelda SM, Lauffenburger DA. 1993. Maximal migration of human smooth muscle cells on fibronectin and type IV collagen occurs at an intermediate attachment strength. J Cell Biol 122(3):729-37.

Dionne KE, Colton CK, Yarmush ML. 1989. Effect of oxygen on isolated pancreatic tissue. ASAIO Trans 35(3):739-41.

Donaldson DJ, Mahan JT. 1984. Epidermal cell migration on laminin-coated substrates. Comparison with other extracellular matrix and non-matrix proteins. Cell Tissue Res 235(2):221-4.

Dor Y, Brown J, Martinez OI, Melton DA. 2004. Adult pancreatic beta-cells are formed by self-

duplication rather than stem-cell differentiation. Nature 429(6987):41-6.

Draper JS, Moore HD, Ruban LN, Gokhale PJ, Andrews PW. 2004. Culture and characterization of human embryonic stem cells. Stem Cells Dev 13(4):325-36.

Dvorak P, Dvorakova D, Koskova S, Vodinska M, Najvirtova M, Krekac D, Hampl A. 2005. Expression and potential role of fibroblast growth factor 2 and its receptors in human embryonic stem cells. Stem Cells 23(8):1200-11.

Dykstra B, Ramunas J, Kent D, McCaffrey L, Szumsky E, Kelly L, Farn K, Blaylock A, Eaves C, Jervis E. 2006. High-resolution video monitoring of hematopoietic stem cells cultured in single-cell arrays identifies new features of self-renewal. Proc Natl Acad Sci U S A 103(21):8185-90.

Efrat S. 2008. In vitro expansion of human beta cells. Diabetologia 51(7):1338-9.

Eiselein L, Schwartz HJ, Rutledge JC. 2004. The challenge of type 1 diabetes mellitus. ILAR J 45(3):231-6.

Eldor R, Stern E, Milicevic Z, Raz I. 2005. Early use of insulin in type 2 diabetes. Diabetes Res Clin Pract 68 Suppl1:S30-5.

Elfwing A, LeMarc Y, Baranyi J, Ballagi A. 2004. Observing growth and division of large numbers of individual bacteria by image analysis. Appl Environ Microbiol 70(2):675-8.

Enver T, Soneji S, Joshi C, Brown J, Iborra F, Orntoft T, Thykjaer T, Maltby E, Smith K, Dawud RA and others. 2005. Cellular differentiation hierarchies in normal and culture-adapted human embryonic stem cells. Hum Mol Genet 14(21):3129-40.

Fanti Z, De-Miguel FF, Martinez-Perez ME. 2008. A method for semiautomatic tracing and morphological measuring of neurite outgrowth from DIC sequences. Conf Proc IEEE Eng Med Biol Soc 2008:1196-9.

Fernandes A, King LC, Guz Y, Stein R, Wright CV, Teitelman G. 1997. Differentiation of new insulin-producing cells is induced by injury in adult pancreatic islets. Endocrinology 138(4):1750-62.

Filipczyk AA, Laslett AL, Mummery C, Pera MF. 2007. Differentiation is coupled to changes in the cell cycle regulatory apparatus of human embryonic stem cells. Stem Cell Res 1(1):45-60.

Francis K, Palsson BO. 1997. Effective intercellular communication distances are determined by the relative time constants for cyto/chemokine secretion and diffusion. Proc Natl Acad Sci U S A 94(23):12258-62.

Friedl P, Brocker EB. 2004. Reconstructing leukocyte migration in 3D extracellular matrix by time-lapse videomicroscopy and computer-assisted tracking. Methods Mol Biol 239:77-90.

Frigault MM, Lacoste J, Swift JL, Brown CM. 2009. Live-cell microscopy - tips and tools. J Cell Sci 122(Pt 6):753-67.

Froese G. 1964. The Distribution and Interdependence of Generation Times of Hela Cells. Exp Cell Res 35:415-9.

Gage FH. 2000. Mammalian neural stem cells. Science 287(5457):1433-8.

Gallo R, Gambelli F, Gava B, Sasdelli F, Tellone V, Masini M, Marchetti P, Dotta F, Sorrentino V. 2007. Generation and expansion of multipotent mesenchymal progenitor cells from cultured human pancreatic islets. Cell Death Differ 14(11):1860-71.

Gao R, Ustinov J, Korsgren O, Otonkoski T. 2005. In vitro neogenesis of human islets reflects the plasticity of differentiated human pancreatic cells. Diabetologia 48(11):2296-304.

Geng W, Cosman P, Berry CC, Feng Z, Schafer WR. 2004. Automatic tracking, feature extraction and classification of C elegans phenotypes. IEEE Trans Biomed Eng 51(10):1811-20.

Gerdes HH, Kaether C. 1996. Green fluorescent protein: applications in cell biology. FEBS Lett 389(1):44-7.

Gershengorn MC, Hardikar AA, Wei C, Geras-Raaka E, Marcus-Samuels B, Raaka BM. 2004. Epithelial-to-mesenchymal transition generates proliferative human islet precursor cells. Science 306(5705):2261-4.

Giuliano KA, Post PL, Hahn KM, Taylor DL. 1995. Fluorescent protein biosensors: measurement of molecular dynamics in living cells. Annu Rev Biophys Biomol Struct 24:405-34.

Glauche I, Lorenz R, Hasenclever D, Roeder I. 2009. A novel view on stem cell development: analysing the shape of cellular genealogies. Cell Prolif 42(2):248-63.

Go VLW. 1993. The Pancreas : biology, pathobiology, and disease. New York: Raven Press. xvii, 1176 p. p.

Greber B, Lehrach H, Adjaye J. 2007. Fibroblast growth factor 2 modulates transforming growth factor beta signaling in mouse embryonic fibroblasts and human ESCs (hESCs) to support hESC self-renewal. Stem Cells 25(2):455-64.

Grompe M. 2003. Pancreatic-hepatic switches in vivo. Mech Dev 120(1):99-106.

Gu G, Dubauskaite J, Melton DA. 2002. Direct evidence for the pancreatic lineage: NGN3+ cells are islet progenitors and are distinct from duct progenitors. Development 129(10):2447-57.

Guz Y, Nasir I, Teitelman G. 2001. Regeneration of pancreatic beta cells from intra-islet precursor cells in an experimental model of diabetes. Endocrinology 142(11):4956-68.

Hadjantonakis AK, Papaioannou VE. 2004. Dynamic in vivo imaging and cell tracking using a histone fluorescent protein fusion in mice. BMC Biotechnol 4:33.

Hamahashi S, Onami S, Kitano H. 2005. Detection of nuclei in 4D Nomarski DIC microscope images of early Caenorhabditis elegans embryos using local image entropy and object tracking. BMC Bioinformatics 6:125.

Hand AJ, Sun T, Barber DC, Hose DR, MacNeil S. 2009. Automated tracking of migrating cells in phase-contrast video microscopy sequences using image registration. J Microsc 234(1):62-79.

Hanley SC, Pilotte A, Massie B, Rosenberg L. 2008. Cellular origins of adult human islet in vitro dedifferentiation. Lab Invest 88(7):761-72.

Haraguchi T. 2002. Live cell imaging: approaches for studying protein dynamics in living cells. Cell Struct Funct 27(5):333-4.

Hayashi K, Lopes SM, Tang F, Surani MA. 2008. Dynamic equilibrium and heterogeneity of mouse pluripotent stem cells with distinct functional and epigenetic states. Cell Stem Cell 3(4):391-401.

Hazelwood RL. 1989. The endocrine pancreas. Englewood Cliffs, N.J.: Prentice Hall. xiii, 258 p., [2] p. of plates p.

Hebrok M, Kim SK, Melton DA. 1998. Notochord repression of endodermal Sonic hedgehog permits pancreas development. Genes Dev 12(11):1705-13.

Heid PJ, Voss E, Soll DR. 2002. 3D-DIASemb: a computer-assisted system for reconstructing and motion analyzing in 4D every cell and nucleus in a developing embryo. Dev Biol 245(2):329-47.

Hermann M, Pirkebner D, Draxl A, Margreiter R, Hengster P. 2005. "Real-time" assessment of human islet preparations with confocal live cell imaging. Transplant Proc 37(8):3409-11.

Hess D, Li L, Martin M, Sakano S, Hill D, Strutt B, Thyssen S, Gray DA, Bhatia M. 2003. Bone marrow-derived stem cells initiate pancreatic regeneration. Nat Biotechnol 21(7):763-70.

Holmes S. 2003. Statistics for phylogenetic trees. Theor Popul Biol 63(1):17-32.

Hoorens A, Van de Casteele M, Kloppel G, Pipeleers D. 1996. Glucose promotes survival of rat pancreatic beta cells by activating synthesis of proteins which suppress a constitutive apoptotic program. J Clin Invest 98(7):1568-74.

Hsu TC. 1960. Generation time of HeLa cells determined from cine records. Tex Rep Biol Med 18:31-3.

Jaenisch R, Young R. 2008. Stem cells, the molecular circuitry of pluripotency and nuclear reprogramming. Cell 132(4):567-82.

Jamal AM, Lipsett M, Hazrati A, Paraskevas S, Agapitos D, Maysinger D, Rosenberg L. 2003. Signals for death and differentiation: a two-step mechanism for in vitro transformation of

adult islets of Langerhans to duct epithelial structures. Cell Death Differ 10(9):987-96.

Jamal AM, Lipsett M, Sladek R, Laganiere S, Hanley S, Rosenberg L. 2005. Morphogenetic plasticity of adult human pancreatic islets of Langerhans. Cell Death Differ 12(7):702-12.

Jiang J, Au M, Lu K, Eshpeter A, Korbutt G, Fisk G, Majumdar AS. 2007. Generation of insulin-producing islet-like clusters from human embryonic stem cells. Stem Cells 25(8):1940-53.

Johnson JH, Newgard CB, Milburn JL, Lodish HF, Thorens B. 1990. The high Km glucose transporter of islets of Langerhans is functionally similar to the low affinity transporter of liver and has an identical primary sequence. J Biol Chem 265(12):6548-51.

Jones DL, Wagers AJ. 2008. No place like home: anatomy and function of the stem cell niche. Nat Rev Mol Cell Biol 9(1):11-21.

Kaestner KH, Katz J, Liu Y, Drucker DJ, Schutz G. 1999. Inactivation of the winged helix transcription factor HNF3alpha affects glucose homeostasis and islet glucagon gene expression in vivo. Genes Dev 13(4):495-504.

Kanaan A, Douglas RM, Alper SL, Boron WF, Haddad GG. 2007. Effect of chronic elevated carbon dioxide on the expression of acid-base transporters in the neonatal and adult mouse. Am J Physiol Regul Integr Comp Physiol 293(3):R1294-302.

Kanda T, Sullivan KF, Wahl GM. 1998. Histone-GFP fusion protein enables sensitive analysis of chromosome dynamics in living mammalian cells. Curr Biol 8(7):377-85.

Kantengwa S, Baetens D, Sadoul K, Buck CA, Halban PA, Rouiller DG. 1997. Identification and characterization of alpha 3 beta 1 integrin on primary and transformed rat islet cells. Exp Cell Res 237(2):394-402.

Karpowicz P, Morshead C, Kam A, Jervis E, Ramunas J, Cheng V, van der Kooy D. 2005. Support for the immortal strand hypothesis: neural stem cells partition DNA asymmetrically in vitro. J Cell Biol 170(5):721-32.

Kayali AG, Flores LE, Lopez AD, Kutlu B, Baetge E, Kitamura R, Hao E, Beattie GM, Hayek A. 2007. Limited capacity of human adult islets expanded in vitro to redifferentiate into insulin-producing beta-cells. Diabetes 56(3):703-8.

Keller PJ, Fiordalisi JJ, Berzat AC, Cox AD. 2005. Visual monitoring of post-translational lipid modifications using EGFP-GTPase probes in live cells. Methods 37(2):131-37.

Keller PJ, Schmidt AD, Wittbrodt J, Stelzer EH. 2008. Reconstruction of zebrafish early embryonic development by scanned light sheet microscopy. Science 322(5904):1065-9.

Kemp DM, Thomas MK, Habener JF. 2003. Developmental aspects of the endocrine pancreas. Rev Endocr Metab Disord 4(1):5-17.

Khademhosseini A, Langer R, Borenstein J, Vacanti JP. 2006. Microscale technologies for tissue engineering and biology. Proc Natl Acad Sci U S A 103(8):2480-7.

Killander D, Zetterberg A. 1965a. A quantitative cytochemical investigation of the relationship between cell mass and initiation of DNA synthesis in mouse fibroblasts in vitro. Exp Cell Res 40(1):12-20.

Killander D, Zetterberg A. 1965b. Quantitative Cytochemical Studies on Interphase Growth. I. Determination of DNA, Rna and Mass Content of Age Determined Mouse Fibroblasts in Vitro and of Intercellular Variation in Generation Time. Exp Cell Res 38:272-84.

Kim SK, Hebrok M. 2001. Intercellular signals regulating pancreas development and function. Genes Dev 15(2):111-27.

Kirchhausen T, Boll W, van Oijen A, Ehrlich M. 2005. Single-molecule live-cell imaging of clathrin-based endocytosis. Biochem Soc Symp(72):71-6.

Kobayashi N, Okitsu T, Lakey JR, Tanaka N. 2004. The current situation in human pancreatic islet transplantation: problems and prospects. J Artif Organs 7(1):1-8.

Krapp A, Knofler M, Ledermann B, Burki K, Berney C, Zoerkler N, Hagenbuchle O, Wellauer PK. 1998. The bHLH protein PTF1-p48 is essential for the formation of the exocrine and the correct spatial organization of the endocrine pancreas. Genes Dev 12(23):3752-63.

Kriat M, Fantini J, Vion-Dury J, Confort-Gouny S, Galons JP, Cozzone PJ. 1992. Energetic metabolism of glucose, mannose and galactose in glucose-starved rat insulinoma cells anchored on microcarrier beads. A phosphorus-31 NMR study. Biochimie 74(9-10):949-55.

Kriete A. 2005. Cytomics in the realm of systems biology. Cytometry A 68(1):19-20.

Kriete A. 2006. Bridging biological scales by state-space analysis and modeling using molecular, tissue cytometric and physiological data. Cytometry A 69(3):113-6.

Kritzik MR, Krahl T, Good A, Krakowski M, St-Onge L, Gruss P, Wright C, Sarvetnick N. 2000. Transcription factor expression during pancreatic islet regeneration. Mol Cell Endocrinol 164(1-2):99-107.

Larsen JL. 2004. Pancreas Transplantation: Indications and Consequences. Endocr Rev 25(6):919-946.

Laursen SB, Mollgard K, Olesen C, Oliveri RS, Brochner CB, Byskov AG, Andersen AN, Hoyer PE, Tommerup N, Yding Andersen C. 2007. Regional differences in expression of specific markers for human embryonic stem cells. Reprod Biomed Online 15(1):89-98.

Lechner A, Nolan AL, Blacken RA, Habener JF. 2005. Redifferentiation of insulin-secreting cells after in vitro expansion of adult human pancreatic islet tissue. Biochem Biophys Res

Commun 327(2):581-8.

Lee JC, Smith SB, Watada H, Lin J, Scheel D, Wang J, Mirmira RG, German MS. 2001. Regulation of the pancreatic pro-endocrine gene neurogenin3. Diabetes 50(5):928-36.

Lehmann R, Zuellig RA, Kugelmeier P, Baenninger PB, Moritz W, Perren A, Clavien PA, Weber M, Spinas GA. 2007. Superiority of small islets in human islet transplantation. Diabetes 56(3):594-603.

Leung YM, Ahmed I, Sheu L, Gao X, Hara M, Tsushima RG, Diamant NE, Gaisano HY. 2006. Insulin regulates islet alpha-cell function by reducing KATP channel sensitivity to adenosine 5'-triphosphate inhibition. Endocrinology 147(5):2155-62.

Li K, Chen M, Kanade T. 2007. Cell population tracking and lineage construction with spatiotemporal context. Med Image Comput Comput Assist Interv Int Conf Med Image Comput Comput Assist Interv 10(Pt 2):295-302.

Li L, Xie T. 2005. Stem cell niche: structure and function. Annu Rev Cell Dev Biol 21:605-31.

Li WC, Yu WY, Quinlan JM, Burke ZD, Tosh D. 2005. The molecular basis of transdifferentiation. J Cell Mol Med 9(3):569-82.

Liew CG, Shah NN, Briston SJ, Shepherd RM, Khoo CP, Dunne MJ, Moore HD, Cosgrove KE, Andrews PW. 2008. PAX4 enhances beta-cell differentiation of human embryonic stem cells. PLoS ONE 3(3):e1783.

Lipsett M, Hanley S, Castellarin M, Austin E, Suarez-Pinzon WL, Rabinovitch A, Rosenberg L. 2007. The role of islet neogenesis-associated protein (INGAP) in islet neogenesis. Cell Biochem Biophys 48(2-3):127-37.

Liu YQ, Jetton TL, Leahy JL. 2002. beta-Cell adaptation to insulin resistance. Increased pyruvate carboxylase and malate-pyruvate shuttle activity in islets of nondiabetic Zucker fatty rats. J Biol Chem 277(42):39163-8.

Long A, Mitchell S, Kashanin D, Williams V, Prina Mello A, Shvets I, Kelleher D, Volkov Y. 2004. A multidisciplinary approach to the study of T cell migration. Ann N Y Acad Sci 1028:313-9.

Lu J, Gu YP, Xu X, Liu ML, Xie P, Song HP. 2005. Adult islets cultured in collagen gel transdifferentiate into duct-like cells. World J Gastroenterol 11(22):3426-30.

Madsen OD, Jensen J, Blume N, Petersen HV, Lund K, Karlsen C, Andersen FG, Jensen PB, Larsson LI, Serup P. 1996. Pancreatic development and maturation of the islet B cell. Studies of pluripotent islet cultures. Eur J Biochem 242(3):435-45.

Mantel C, Guo Y, Lee MR, Kim MK, Han MK, Shibayama H, Fukuda S, Yoder MC, Pelus LM, Kim KS and others. 2007. Checkpoint-apoptosis uncoupling in human and mouse embryonic stem

cells: a source of karyotpic instability. Blood 109(10):4518-27.

Marin G, Bender MA. 1966. Radiation-induced mammalian cell death: lapse-time cinemicrographic observations. Exp Cell Res 43(2):413-23.

Martin BC, Warram JH, Krolewski AS, Bergman RN, Soeldner JS, Kahn CR. 1992. Role of glucose and insulin resistance in development of type 2 diabetes mellitus: results of a 25-year follow-up study. Lancet 340(8825):925-9.

Martz E, Steinberg MS. 1972. The role of cell-cell contact in "contact" inhibition of cell division: a review and new evidence. J Cell Physiol 79(2):189-210.

Mashanov GI, Nenasheva TA, Peckham M, Molloy JE. 2006. Cell biochemistry studied by single-molecule imaging. Biochem Soc Trans 34(Pt 5):983-8.

Mazurier F, Gan OI, McKenzie JL, Doedens M, Dick JE. 2004. Lentivector-mediated clonal tracking reveals intrinsic heterogeneity in the human hematopoietic stem cell compartment and culture-induced stem cell impairment. Blood 103(2):545-52.

Metallo CM, Azarin SM, Ji L, de Pablo JJ, Palecek SP. 2008. Engineering tissue from human embryonic stem cells. J Cell Mol Med 12(3):709-29.

Miralles F, Czernichow P, Scharfmann R. 1998. Follistatin regulates the relative proportions of endocrine versus exocrine tissue during pancreatic development. Development 125(6):1017-24.

Miyawaki A, Nagai T, Mizuno H. 2005. Engineering fluorescent proteins. Adv Biochem Eng Biotechnol 95:1-15.

Moogk D, Hanley S, Ramunas J, Blaylock A, Skorepova J, Rosenberg L, Jervis E. 2007. Design and analysis of a long-term live-cell imaging chamber for tracking cellular dynamics within cultured human islets of Langerhans. Biotechnol Bioeng 97(5):1138-47.

Morton RA, Geras-Raaka E, Wilson LM, Raaka BM, Gershengorn MC. 2007. Endocrine precursor cells from mouse islets are not generated by epithelial-to-mesenchymal transition of mature beta cells. Mol Cell Endocrinol 270(1-2):87-93.

Murtaugh LC, Melton DA. 2003. Genes, signals, and lineages in pancreas development. Annu Rev Cell Dev Biol 19:71-89.

Narkilahti S, Rajala K, Pihlajamaki H, Suuronen R, Hovatta O, Skottman H. 2007. Monitoring and analysis of dynamic growth of human embryonic stem cells: comparison of automated instrumentation and conventional culturing methods. Biomed Eng Online 6:11.

Nei M. 1996. Phylogenetic analysis in molecular evolutionary genetics. Annu Rev Genet 30:371-403.

Newgreen DF, Gibbins IL, Sauter J, Wallenfels B, Wutz R. 1982. Ultrastructural and tissue-culture

studies on the role of fibronectin, collagen and glycosaminoglycans in the migration of neural crest cells in the fowl embryo. Cell Tissue Res 221(3):521-49.

Nie Y, Bergendahl V, Hei DJ, Jones JM, Palecek SP. 2009. Scalable culture and cryopreservation of human embryonic stem cells on microcarriers. Biotechnol Prog 25(1):20-31.

Niggemann B, Drell TLt, Joseph J, Weidt C, Lang K, Zaenker KS, Entschladen F. 2004. Tumor cell locomotion: differential dynamics of spontaneous and induced migration in a 3D collagen matrix. Exp Cell Res 298(1):178-87.

Niggemann B, Maaser K, Lu H, Kroczek R, Zanker KS, Friedl P. 1997. Locomotory phenotypes of human tumor cell lines and T lymphocytes in a three-dimensional collagen lattice. Cancer Lett 118(2):173-80.

Nunomura K, Nagano K, Itagaki C, Taoka M, Okamura N, Yamauchi Y, Sugano S, Takahashi N, Izumi T, Isobe T. 2005. Cell surface labeling and mass spectrometry reveal diversity of cell surface markers and signaling molecules expressed in undifferentiated mouse embryonic stem cells. Mol Cell Proteomics 4(12):1968-76.

Oh SK, Choo AB. 2006. Human embryonic stem cell technology: large scale cell amplification and differentiation. Cytotechnology 50(1-3):181-90.

Orkin SH. 2000. Diversification of haematopoietic stem cells to specific lineages. Nat Rev Genet 1(1):57-64.

Otto FJ. 1994. High-resolution analysis of nuclear DNA employing the fluorochrome DAPI. Methods Cell Biol 41:211-7.

Paredes RM, Etzler JC, Watts LT, Zheng W, Lechleiter JD. 2008. Chemical calcium indicators. Methods 46(3):143-51.

Park HW, Shin JS, Kim CW. 2007. Proteome of mesenchymal stem cells. Proteomics 7(16):2881-94.

Parvin B, Qing Y, Fontenay G, Barcellos-Hoff MH. 2002. BioSig: an imaging bioinformatic system for studying phenomics. Computer 35(7):65-71.

Pattison DI, Davies MJ. 2006. Actions of ultraviolet light on cellular structures. EXS(96):131-57.

Peerani R, Rao BM, Bauwens C, Yin T, Wood GA, Nagy A, Kumacheva E, Zandstra PW. 2007. Niche-mediated control of human embryonic stem cell self-renewal and differentiation. Embo J.

Petropavlovskaia M, Bodnar CA, Behie LA, Rosenberg L. 2007. Pancreatic small cells: analysis of quiescence, long-term maintenance and insulin expression in vitro. Exp Cell Res 313(5):931-42.

Petropavlovskaia M, Rosenberg L. 2002. Identification and characterization of small cells in the adult

pancreas: potential progenitor cells? Cell Tissue Res 310(1):51-8.

Prasher DC, Eckenrode VK, Ward WW, Prendergast FG, Cormier MJ. 1992. Primary structure of the Aequorea victoria green-fluorescent protein. Gene 111(2):229-33.

Qian X, Goderie SK, Shen Q, Stern JH, Temple S. 1998. Intrinsic programs of patterned cell lineages in isolated vertebrate CNS ventricular zone cells. Development 125(16):3143-52.

Rabut G, Ellenberg J. 2004. Automatic real-time three-dimensional cell tracking by fluorescence microscopy. J Microsc 216(Pt 2):131-7.

Rafaeloff R, Pittenger GL, Barlow SW, Qin XF, Yan B, Rosenberg L, Duguid WP, Vinik AI. 1997. Cloning and sequencing of the pancreatic islet neogenesis associated protein (INGAP) gene and its expression in islet neogenesis in hamsters. J Clin Invest 99(9):2100-9.

Ramiya VK, Maraist M, Arfors KE, Schatz DA, Peck AB, Cornelius JG. 2000. Reversal of insulin-dependent diabetes using islets generated in vitro from pancreatic stem cells. Nat Med 6(3):278-82.

Ramunas J, Illman M, Kam A, Farn K, Kelly L, Morshead CM, Jervis EJ. 2006. True monolayer cell culture in a confined 3D microenvironment enables lineage informatics. Cytometry A 69(12):1202-11.

Ramunas J, Montgomery HJ, Kelly L, Sukonnik T, Ellis J, Jervis EJ. 2007. Real-time fluorescence tracking of dynamic transgene variegation in stem cells. Mol Ther 15(4):810-7.

Reynaud EG, Krzic U, Greger K, Stelzer EH. 2008. Light sheet-based fluorescence microscopy: more dimensions, more photons, and less photodamage. HFSP J 2(5):266-75.

Rieder CL, Cole RW. 1998. Perfusion chambers for high-resolution video light microscopic studies of vertebrate cell monolayers: some considerations and a design. Methods Cell Biol 56:253-75.

Rink TJ. 1988. Measurement of cytosolic calcium: fluorescent calcium indicators. Miner Electrolyte Metab 14(1):7-14.

Rosenberg L, Brown RA, Duguid WP. 1983a. A new approach to the induction of duct epithelial hyperplasia and nesidioblastosis by cellophane wrapping of the hamster pancreas. J Surg Res 35(1):63-72.

Rosenberg L, Brown RA, Duguid WP. 1983b. A New Approach to the Induction of Duct Epithelial Hyperplasia and Nesidioblastosis by Cellophane Wrapping of the Hamster Pancreas. Journal of Surgical Research 35(1):63-72.

Russ HA, Bar Y, Ravassard P, Efrat S. 2008. In vitro proliferation of cells derived from adult human beta-cells revealed by cell-lineage tracing. Diabetes 57(6):1575-83.

Russ HA, Ravassard P, Kerr-Conte J, Pattou F, Efrat S. 2009. Epithelial-mesenchymal transition in cells expanded in vitro from lineage-traced adult human pancreatic beta cells. PLoS ONE 4(7):e6417.

Ryan EA, Paty BW, Senior PA, Bigam D, Alfadhli E, Kneteman NM, Lakey JR, Shapiro AM. 2005. Five-year follow-up after clinical islet transplantation. Diabetes 54(7):2060-9.

Scadden DT. 2006. The stem-cell niche as an entity of action. Nature 441(7097):1075-9.

Scaglia L, Smith FE, Bonner-Weir S. 1995. Apoptosis contributes to the involution of beta cell mass in the post partum rat pancreas. Endocrinology 136(12):5461-8.

Schinner S, Scherbaum WA, Bornstein SR, Barthel A. 2005. Molecular mechanisms of insulin resistance. Diabet Med 22(6):674-82.

Schmied BM, Ulrich A, Matsuzaki H, Ding X, Ricordi C, Weide L, Moyer MP, Batra SK, Adrian TE, Pour PM. 2001. Transdifferentiation of human islet cells in a long-term culture. Pancreas 23(2):157-71.

Schofield R. 1978. The relationship between the spleen colony-forming cell and the haemopoietic stem cell. Blood Cells 4(1-2):7-25.

Schrattenholz A, Soskic V. 2008. What does systems biology mean for drug development? Curr Med Chem 15(15):1520-8.

Schroeder T. 2005. Tracking hematopoiesis at the single cell level. Ann N Y Acad Sci 1044:201-9.

Schroeder T. 2008. Imaging stem-cell-driven regeneration in mammals. Nature 453(7193):345-51.

Schuit FC, Huypens P, Heimberg H, Pipeleers DG. 2001. Glucose sensing in pancreatic beta-cells: a model for the study of other glucose-regulated cells in gut, pancreas, and hypothalamus. Diabetes 50(1):1-11.

Seaberg RM, Smukler SR, Kieffer TJ, Enikolopov G, Asghar Z, Wheeler MB, Korbutt G, van der Kooy D. 2004. Clonal identification of multipotent precursors from adult mouse pancreas that generate neural and pancreatic lineages. Nat Biotechnol 22(9):1115-24.

Seeberger KL, Dufour JM, Shapiro AM, Lakey JR, Rajotte RV, Korbutt GS. 2006. Expansion of mesenchymal stem cells from human pancreatic ductal epithelium. Lab Invest 86(2):141-53.

Seeberger KL, Eshpeter A, Rajotte RV, Korbutt GS. 2009. Epithelial cells within the human pancreas do not coexpress mesenchymal antigens: epithelial-mesenchymal transition is an artifact of cell culture. Lab Invest 89(2):110-21.

Shapiro AM, Lakey JR, Ryan EA, Korbutt GS, Toth E, Warnock GL, Kneteman NM, Rajotte RV. 2000. Islet transplantation in seven patients with type 1 diabetes mellitus using a glucocorticoid-free immunosuppressive regimen. N Engl J Med 343(4):230-8.

Shapiro AM, Nanji SA, Lakey JR. 2003. Clinical islet transplant: current and future directions towards tolerance. Immunol Rev 196:219-36.

Shen F, Hodgson L, Hahn K. 2006a. Digital autofocus methods for automated microscopy. Methods Enzymol 414:620-32.

Shen Q, Wang Y, Dimos JT, Fasano CA, Phoenix TN, Lemischka IR, Ivanova NB, Stifani S, Morrisey EE, Temple S. 2006b. The timing of cortical neurogenesis is encoded within lineages of individual progenitor cells. Nat Neurosci 9(6):743-51.

Shen W, Scearce LM, Brestelli JE, Sund NJ, Kaestner KH. 2001. Foxa3 (hepatocyte nuclear factor 3gamma) is required for the regulation of hepatic GLUT2 expression and the maintenance of glucose homeostasis during a prolonged fast. J Biol Chem 276(46):42812-7.

Shim JH, Kim SE, Woo DH, Kim SK, Oh CH, McKay R, Kim JH. 2007. Directed differentiation of human embryonic stem cells towards a pancreatic cell fate. Diabetologia 50(6):1228-38.

Singh AM, Hamazaki T, Hankowski KE, Terada N. 2007. A heterogeneous expression pattern for Nanog in embryonic stem cells. Stem Cells 25(10):2534-42.

Skottman H, Narkilahti S, Hovatta O. 2007. Challenges and approaches to the culture of pluripotent human embryonic stem cells. Regen Med 2(3):265-73.

Slack JM. 1995. Developmental biology of the pancreas. Development 121(6):1569-80.

Song KH, Ko SH, Ahn YB, Yoo SJ, Chin HM, Kaneto H, Yoon KH, Cha BY, Lee KW, Son HY. 2004. In vitro transdifferentiation of adult pancreatic acinar cells into insulin-expressing cells. Biochem Biophys Res Commun 316(4):1094-100.

Stephens DJ, Allan VJ. 2003. Light microscopy techniques for live cell imaging. Science 300(5616):82-6.

Stewart MH, Bosse M, Chadwick K, Menendez P, Bendall SC, Bhatia M. 2006. Clonal isolation of hESCs reveals heterogeneity within the pluripotent stem cell compartment. Nat Methods 3(10):807-815.

Stojkovic P, Lako M, Stewart R, Przyborski S, Armstrong L, Evans J, Murdoch A, Strachan T, Stojkovic M. 2005. An autogeneic feeder cell system that efficiently supports growth of undifferentiated human embryonic stem cells. Stem Cells 23(3):306-14.

Sugden JK. 2004. Photochemistry of dyes and fluorochromes used in biology and medicine: some physicochemical background and current applications. Biotech Histochem 79(2):71-90.

Sund NJ, Vatamaniuk MZ, Casey M, Ang SL, Magnuson MA, Stoffers DA, Matschinsky FM, Kaestner KH. 2001. Tissue-specific deletion of Foxa2 in pancreatic beta cells results in hyperinsulinemic hypoglycemia. Genes Dev 15(13):1706-15.

Sweet IR, Khalil G, Wallen AR, Steedman M, Schenkman KA, Reems JA, Kahn SE, Callis JB. 2002. Continuous measurement of oxygen consumption by pancreatic islets. Diabetes Technol Ther 4(5):661-72.

Tassy O, Daian F, Hudson C, Bertrand V, Lemaire P. 2006. A quantitative approach to the study of cell shapes and interactions during early chordate embryogenesis. Curr Biol 16(4):345-58.

Terryn C, Bonnomet A, Cutrona J, Coraux C, Tournier JM, Nawrocki-Raby B, Polette M, Birembaut P, Zahm JM. 2009. Video-microscopic imaging of cell spatio-temporal dispersion and migration. Crit Rev Oncol Hematol 69(2):144-52.

Teta M, Rankin MM, Long SY, Stein GM, Kushner JA. 2007. Growth and regeneration of adult beta cells does not involve specialized progenitors. Dev Cell 12(5):817-26.

Thompson DM, King KR, Wieder KJ, Toner M, Yarmush ML, Jayaraman A. 2004. Dynamic gene expression profiling using a microfabricated living cell array. Anal Chem 76(14):4098-103.

Thomson JA, Itskovitz-Eldor J, Shapiro SS, Waknitz MA, Swiergiel JJ, Marshall VS, Jones JM. 1998. Embryonic stem cell lines derived from human blastocysts. Science 282(5391):1145-7.

Wang RN, Kloppel G, Bouwens L. 1995. Duct- to islet-cell differentiation and islet growth in the pancreas of duct-ligated adult rats. Diabetologia 38(12):1405-11.

Wang RN, Rosenberg L. 1999. Maintenance of beta-cell function and survival following islet isolation requires re-establishment of the islet-matrix relationship. J Endocrinol 163(2):181-90.

Watanabe K, Ueno M, Kamiya D, Nishiyama A, Matsumura M, Wataya T, Takahashi JB, Nishikawa S, Muguruma K, Sasai Y. 2007. A ROCK inhibitor permits survival of dissociated human embryonic stem cells. Nat Biotechnol 25(6):681-6.

Weinberg N, Ouziel-Yahalom L, Knoller S, Efrat S, Dor Y. 2007. Lineage tracing evidence for in vitro dedifferentiation but rare proliferation of mouse pancreatic beta-cells. Diabetes 56(5):1299-304.

Weir GC, Bonner-Weir S. 2004. Five stages of evolving beta-cell dysfunction during progression to diabetes. Diabetes 53 Suppl 3:S16-21.

Wells JM. 2003. Genes expressed in the developing endocrine pancreas and their importance for stem cell and diabetes research. Diabetes Metab Res Rev 19(3):191-201.

Wells JM, Melton DA. 2000. Early mouse endoderm is patterned by soluble factors from adjacent germ layers. Development 127(8):1563-72.

Welsh S, Kay SA. 1997. Reporter gene expression for monitoring gene transfer. Curr Opin Biotechnol 8(5):617-22.

Werbowetski-Ogilvie T, Bosse M, Stewart M, Schnerch A, Ramos-Mejia V, Rouleau A, Wynder T, Smith M, Dingwall S, Carter T and others. 2008. Characterization of human embryonic stem cells with features of neoplastic progression. Nature Biotechnology published online January 4, 2009.

Wessels D, Voss E, Von Bergen N, Burns R, Stites J, Soll DR. 1998. A computer-assisted system for reconstructing and interpreting the dynamic three-dimensional relationships of the outer surface, nucleus and pseudopods of crawling cells. Cell Motil Cytoskeleton 41(3):225-46.

White J, Dalton S. 2005. Cell cycle control of embryonic stem cells. Stem Cell Rev 1(2):131-8.

Whitesell RR, Powers AC, Regen DM, Abumrad NA. 1991. Transport and metabolism of glucose in an insulin-secreting cell line, beta TC-1. Biochemistry 30(49):11560-6.

Wilson ME, Scheel D, German MS. 2003. Gene expression cascades in pancreatic development. Mech Dev 120(1):65-80.

Wu DQ, Zhang GL, Shen C, Zhao Q, Li H, Meng Q. 2005. Evaluation of diffusion in gel entrapment cell culture within hollow fibers. World J Gastroenterol 11(11):1599-604.

Wu P, Brand L. 1994. Resonance energy transfer: methods and applications. Anal Biochem 218(1):1-13.

Xie T, Spradling AC. 2000. A niche maintaining germ line stem cells in the Drosophila ovary. Science 290(5490):328-30.

Xu C, Inokuma MS, Denham J, Golds K, Kundu P, Gold JD, Carpenter MK. 2001. Feeder-free growth of undifferentiated human embryonic stem cells. Nat Biotechnol 19(10):971-4.

Yu ZT, Kamei K, Takahashi H, Shu CJ, Wang X, He GW, Silverman R, Radu CG, Witte ON, Lee KB and others. 2009. Integrated microfluidic devices for combinatorial cell-based assays. Biomed Microdevices 11(3):547-55.

Yuan S, Rosenberg L, Paraskevas S, Agapitos D, Duguid WP. 1996. Transdifferentiation of human islets to pancreatic ductal cells in collagen matrix culture. Differentiation 61(1):67-75.

Zhou Q, Brown J, Kanarek A, Rajagopal J, Melton DA. 2008. In vivo reprogramming of adult pancreatic exocrine cells to beta-cells. Nature 455(7213):627-32.

Zulewski H, Abraham EJ, Gerlach MJ, Daniel PB, Moritz W, Muller B, Vallejo M, Thomas MK, Habener JF. 2001. Multipotential nestin-positive stem cells isolated from adult pancreatic islets differentiate ex vivo into pancreatic endocrine, exocrine, and hepatic phenotypes. Diabetes 50(3):521-33.

Appendix A - Fundamentals of Microscopy

Light microscopy has been at the center of biological investigation for centuries. Along the way, steady advances in microscopic components and techniques have allowed scientists to examine biological specimens with increasingly greater detail. Such advances included improved contrast techniques, incorporation of new configurations that led to the inverted compound microscope, digital image acquisition tools such as the CCD array, and the ability to image sub-cellular components through the incorporation of dyes and fluorescent molecules. These advances have made light microscopy an invaluable tool for studying living cell systems.

A.1 Electromagnetic radiation phenomena

The basis of microscopic investigation is the interaction of electromagnetic radiation with matter and the subsequent detection of this interaction. It is the combination of the properties of the electromagnetic radiation, the type of interaction with the specimen, and the method of detecting their interaction that forms the basis of the different typse of microscopy. Other microscopic techniques, such as fluorescence and electron microscopy, have contributed to advances in microscopy, enabling single molecule resolution. Herein, references to microscope specimens will generally mean cells, either living or fixed, attached to the surface of a cover slip, unless otherwise mentioned. The interactions of electromagnetic waves with matter, including reflection, refraction, diffraction, interference and polarization are utilized for microscopy. It is these phenomena that allow for the detection and visualization of the molecules, structures, cell and organisms that we wish to characterize.

A.1.1 Reflection and refraction

Electromagnetic waves traveling through a medium that encounter the surface of another medium undergo both reflection and refraction. The fraction of which will occur depends on properties of both the incident radiation and media, including the angle of incidence and the smoothness of the surface. In microscopy applications, scattered reflection and refraction are highly undesirable, as it will not enable images to be formed from these surfaces.

A.1.2 Diffraction

Electromagnetic waves interact with edges of media through diffraction. When electromagnetic waves pass through a circular aperture or lens, as in microscopy, a circular diffraction pattern arises, called the Airy pattern (Figure A-1).

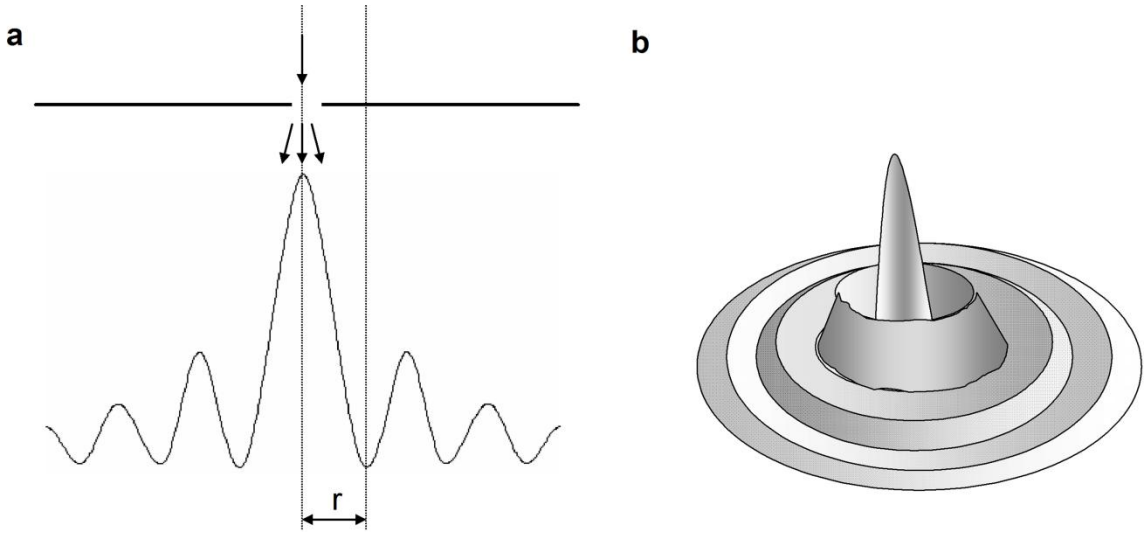

Figure A-1. Diffraction patterns (a) 2-dimensional diffraction pattern (b) 3-dimensional (Airy) diffraction pattern.

The diffraction angles at which maxima occur are calculated by:

$$\sin \theta = n\lambda/d \qquad \text{(a-1)}$$

Where θ is the angle of diffraction, n is an integer, d is the width of the specimen that is causing the diffraction.

A.1.3 Interference

Interference is the superposition of two waves, or the sum of the waves, with consideration of their phases. Waves that are in phase will interfere constructively, to produce a wave with greater magnitude than the originals, whereas waves that are out of phase with interfere destructively, resulting in decreased wave intensity.

A.1.4 Polarization

Electromagnetic waves are polarized when their oscillations, perpendicular to the direction of propagation, are oriented. Unoriented, non-polarized light can be polarized by using a polarizing filter, which allows only radiation with a specific orientation to pass through and all remaining orientations of radiation are absorbed by the filter. The use of polarized light in microscopy is useful as it can be used to reveal structures that are aligned along a certain axis, either by allowing or blocking the transmittance of the polarized light, depending on its orientation. This phenomenon is referred to as birefringence.

A.2 Basic elements of microscopy and image formation

A.2.1 Numerical aperture

The numerical aperture is a dimensionless number characterizing the range of angle that an optical system (e.g. an objective lens) can accept light, also known as the acceptance angle.

$$NA = n \sin\theta$$

Where NA is the numerical aperture, n is the index of refraction of the medium, and θ is the acceptance angle, which is half of the angle of the maximum cone of light that can be accepted. Practical issues, such as how large the diameter of the lens can be and how close it can get to the

specimen, limit the acceptance angle. As well, at large angles light may undergo internal reflection at the cover slip.

A.2.2 Resolution

Resolution is the diffraction-based limit on detail that an image can attain. If the Airy patterns of two image points are too close together, they will merge to give the appearance of only one image point. The ability to distinguish the central maxima of two Airy patterns is possible if the Raleigh criterion is met, which states that the maxima of one pattern must fall at least at the first minimum of the second pattern. This distance is calculated by:

$$r = 1.22\lambda / 2\sin\theta \qquad \text{(a-2)}$$

Where r is the radial distance to the first minima of an Airy pattern, and θ is the acceptance angle. The resolution of an image, r, is therefore:

$$r = 0.61\lambda / n \sin\theta \qquad \text{(a-3)}$$

Low values of resolution are referred to as 'high resolution' and vice versa. Therefore, in order to achieve as high resolution as possible, the acceptance angle and refractive index of the immersion medium should be maximized and as short a wavelength as possible should be used.

A.2.3 Diffraction and interference as the basis for image formation

Provided that a particle being imaged is large enough to interact with the wavelength of light being utilized, edges of the particle will diffract light, and these diffracted rays can recombine to form a diffraction pattern through constructive and destructive interference (Figure A-2).

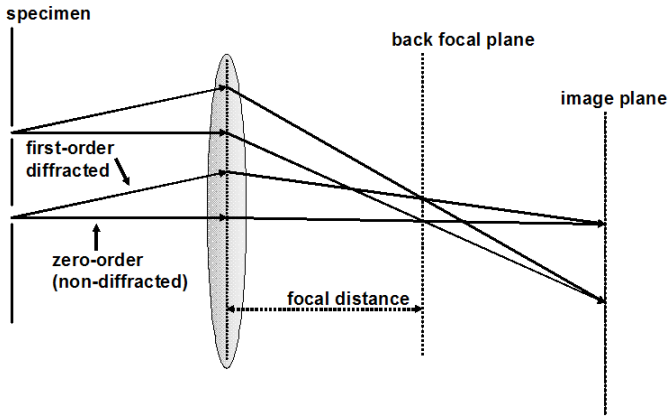

Figure A-2. Diffraction as the basis of image formation in microscopy.

The diameter of the particle is therefore the distance between two diffracting surfaces, and must be large enough that at least the zero order and first order diffracted waves can be recombined to form an image. As the diameter of the particle decreases, the diffraction angles increase, and the first order diffracted waves move further to the periphery of the lens, and at some point will not be gathered by the lens due to the acceptance angle. The formation of an image is therefore dependent on both diffraction and interference.

A.3 Fluorescence

Fluorescence is the process by which the absorption of a photon by a molecule triggers the emission of a second photon of longer wavelength, generally on a time scale of nanoseconds. A molecule that has this ability is referred to as a fluorophore, and results from having highly delocalized electrons, typically in the form of an aromatic ring structure. Fluorescence occurs when molecule is excited from its ground state by a photon with specific energy, followed by relaxation to its ground state, resulting in the emission of the energy as a photon (Figure A-3). The photon is of longer wavelength, and therefore lower energy, because some of the energy is lost as heat or transferred to a secondary molecule by fluorescence resonance energy transfer. Other pathways of de-excitation are possible, such as chemical reaction with oxygen (photobleaching) or phosphorescence. Due to environmental differences, such as temperature fluctuation and stretching and rotation of bonds, the specific energy required to excite a given molecule will vary, resulting in a probability distribution of excitation

wavelengths. The same applies for the resulting emission wavelengths. The difference between the peak of the excitation and emission distributions is referred to as the Stokes shift (Figure 3).

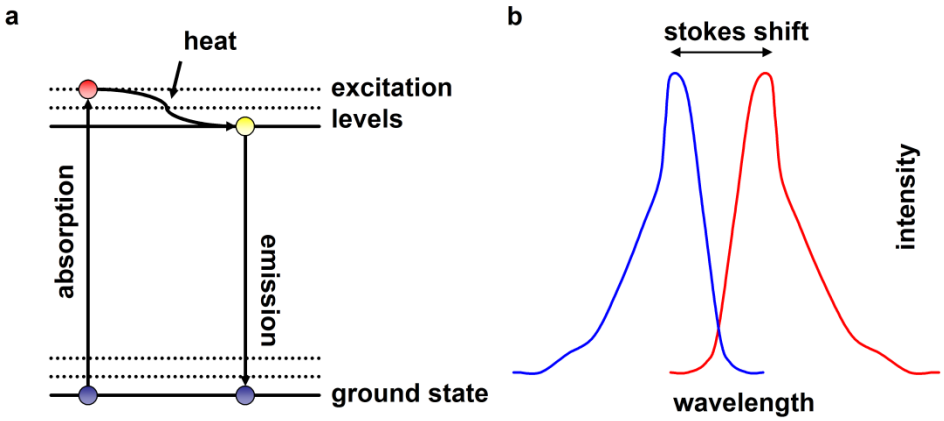

Figure A-3. a - Jablonski diagram illustrating the excitation of an electron through absorption of an incident photon and subsequent emission of a photon of longer wavelength due to relaxation of the electron back to its ground state. b - The difference in the wavelength of photon absorbed by a molecule and emitted during fluorescence it called the Stokes shift

Appendix B - Fundamentals of Islet of Langerhans Development

B.1 Early pancreatic development

Knowledge of the factors involved in the stages of pancreatic development is useful for the study of islet regeneration, as many of the same factors and mechanisms have been implicated in the regeneration process. For a general review of pancreas development see (Murtaugh and Melton 2003). The early embryo subdivides, through the process of gastrulation, into three distinct groups of cells: the skin and central nervous system-forming ectoderm, the blood, bone and muscle-forming mesoderm, and the respiratory and digestive tract-forming endoderm (Wells 2003). The earliest signs of pancreatic development occur as two evaginations, dorsal and ventral, of the primitive foregut, which itself arises from the endoderm. The pre-pancreatic endoderm cells receive signals from the ectodermal and mesodermal layers, which make it competent to respond to subsequent permissive signals (Wells and Melton 2000). Table B-1 summarizes the roles of some of the important factors during this stage of pancreatic development.

Table B-1. Factors involved in early specification of the pancreas during embryogenesis

Factor	Role	References
Shh	Inhibition of pancreatic cell formation from endoderm	(Kim and Hebrok 2001)
Activin-Bβ, TGF-β, FGF2, notch	Induction of pancreatic gene expression from endoderm by repression of Shh	(Hebrok et al. 1998; Wells 2003)
Pdx-1	Specification of all pancreatic cell types during embyrogenesis	(Wilson et al. 2003)
HB9	Pancreas specification	(Wells 2003)
Ptf1a	Specification of ventral pancreas	(Bouwens and Rooman 2005)
Hlxb9	Specification of dorsal pancreas	(Bouwens and Rooman 2005)

B.2 Endocrine and exocrine pancreas specification

Following stimulation by mesenchymal signals, the dorsal and ventral pancreatic buds proliferate, branch and eventually fuse together, forming an apparently uniform pool of pancreatic progenitor cells expressing Pdx-1 and HB9 (Wilson et al. 2003). Signals from the adjacent mesenchyme are responsible for directing these cells towards an endocrine or exocrine fate and also for achieving the appropriate ratio of the two cells types; however the secretion of follistatin results in preferential exocrine differentiation (Miralles et al. 1998). Neurogenin3 (ngn3) expressing cells function as endocrine progenitor cells (Gu et al. 2002), and therefore its expression, initiated by several transcription factors such as HNF1α, HNF3β, HNF6 and Foxa (Kemp et al. 2003; Lee et al. 2001), is necessary for endocrine differentiation. Table B-2 lists the known roles of some of the factors

involved in endocrine and exocrine commitment of pancreatic precursors during development, as well as genes known to be downstream from each factor.

Table B-2. Factors involved in endocrine and exocrine determination during embryonic development of the pancreas

Factor	Role	Downstream genes	References
Hnf6	Endocrine comittment	Foxa2, Hnf4, Ngn3	(Brink 2003)
Hes-1	Restriction of pancreatic cell fate by inhibition of Ngn3		(Apelqvist et al. 1999)
Hnf1α, Hnf3β	Initiation of Ngn3 expression		(Kemp et al. 2003)
Ngn3	Endocrine progenitor marker	NeuroD1, Pax4	(Gu et al. 2002; Lee et al. 2001)
NeuroD1	Proendocrine gene	Insulin	(Kemp et al. 2003)
P48	Proexocrine gene	Exocrine enzyme genes	(Krapp et al. 1998)

B.3 Differentiation of endocrine progenitors into specific subtypes

Cells expressing ngn3 are destined to become one of the several endocrine cell types. Factors co-expressed with ngn3 within endocrine progenitors, such as pax4, nkx2.2 and nkx6.1, deemed early factors, as well as so called late factors, such as pax6, isl1, brn4, HB9 and Pdx-1, which are found in more mature cells, are all thought to play a role in determining endocrine subtype fate (Wilson et al. 2003). However, none of these factors has been shown to be necessary or sufficient in determining cell fate, which has led to the belief that complex pathways involving multiple factors are likely responsible for determining endocrine subtype fate. Table B-3 lists some of the factors involved and known functions thereof.

Table B-3. Factors involved in specification and function of endocrine cell sub-types

Factor	Role	References
Pax4	B and D-cell development	(Wilson et al. 2003)
Pax6	Pdx-1 promoter, upstream of insulin, glucagon and somatostatin	(Wilson et al. 2003)
Pdx-1	B and A-cell expression, upstream of insulin, Glut2 and glucokinase	(Brink 2003)
Foxa1	A-cell function, regulation of glucagon promoter	(Kaestner et al. 1999)
Foxa2	B-cell function, interaction with Pdx-1 promoter	(Sund et al. 2001)
Foxa3	Regulation of Glut2 expression	(Shen et al. 2001)

Several models of endocrine progenitor differentiation to specific islet cell types have been postulated, yet much is still unknown about this stage of islet development. A strictly linear pathway of differentiation and divergence from neuroD1 expressing cells to specific islet cell phenotypes, as depicted in Figure B-2, is likely an oversimplification of a much more dynamic and plastic process (Kemp et al. 2003). Numerous transcription factors involved in driving the cell pathways towards terminal differentiation have been identified, including those mentioned above. However, the role of these factors has only been inferred from gene knock-out models in mice. It is likely that the complete ensemble sequencing and differential expression of many factors in the context of the developing tissue, together with complex and interrelated pathways, directs terminal differentiation.

Mature Islet Formation

The exact mechanism by which mature islets form is unknown, but it has been established that individual islets are not clonally derived during embyrogenesis (Deltour et al. 1991). Before

differentiating into mature islet cells, endocrine precursors migrate through the basal membrane into the mesenchyme (Kim and Hebrok 2001). Islet cell aggregation and sorting is likely coordinated through cell-ECM and cell-cell interactions (Kim and Hebrok 2001). It is thought that islet cell integrins, transmembrane receptors that bind to ECM proteins, affect islet cell organization (Kantengwa et al. 1997), and may also play a role in endocrine progenitor differentiation into mature islet cells (Kim and Hebrok 2001). Similarly, cell-cell interaction mediated by cell adhesion molecules and cadherin molecules also play a role in establishing mature islet architecture (Kim and Hebrok 2001).

Appendix C - Imaging Chamber Transport Model Reports

Oxygen Model

Application modes and modules used in this model:

Geom1 (3D)

Diffusion (Chemical Engineering Module)

Constants

Name	Expression
D	2*10^-9
p	0.3
Deff	D*p
vf	0.02

Mesh

Number of degrees of freedom	3735
Number of mesh points	660
Number of elements	1761
Tetrahedral	1761
Prism	0
Hexahedral	0
Number of boundary elements	1326
Triangular	1326
Quadrilateral	0
Number of edge elements	188
Number of vertex elements	16
Minimum element quality	0.19
Element volume ratio	0.078

Application Mode

Diffusion (chdi)

Application mode type: Diffusion (Chemical Engineering Module)

Application mode name: chdi

Application Mode Properties

Property	**Value**
Default element type	Lagrange - Quadratic
Analysis type	Stationary
Equilibrium assumption	Off
Frame	Frame (ref)
Weak constraints	Off
Constraint type	Ideal

Variables

Dependent variables: c

Shape functions: shlag(2,'c')

Interior boundaries active

Boundary Settings

Boundary		1, 3-4, 8-9, 12	2, 5	6-7, 10-11
Type		Insulation/Symmetry	Concentration	Continuity
Concentration (c0)	mol/m^3	0	0.218	0

Subdomain Settings

Subdomain		1	2
Diffusion coefficient (D)	m^2/s	D	Deff
Reaction rate (R	$mol/(m^3 \cdot s)$	0	-0.00591

Subdomain initial value		1	2
Concentration, c (c)	mol/m^3	0.218	0.218

Solver Settings

Analysis type	Stationary
Auto select solver	On
Solver	Time dependent
Solution form	Automatic
Symmetric	On
Adaptive mesh refinement	Off
Optimization/Sensitivity	Off
Plot while solving	Off

Conjugate gradients

Solver type: Linear system solver

Parameter	**Value**
Relative tolerance	1.0E-6
Factor in error estimate	400.0
Maximum number of iterations	10000
Preconditioning	Left

Solver type: Preconditioner

Parameter	**Value**
Number of iterations	2
Multigrid cycle	V-cycle
Maximum number of levels	6
Max DOFs at coarsest level	5000
Quality of multigrid hierarchy	3

Solver type: Presmoother

Parameter	**Value**
Number of iterations	2
Relaxation factor (omega)	1.0
Blocked version	On

Solver type: Postsmoother

Parameter	Value
Number of iterations	2
Relaxation factor (omega)	1.0
Blocked version	On

Solver type: Coarse solver

Parameter	Value
Drop tolerance	0.0
Pivot threshold	0.1
Memory allocation factor	0.7

Time Stepping

Parameter	Value
Times	range(0,100,10000)
Relative tolerance	0.01
Absolute tolerance	0.0010
Times to store in output	Specified times
Time steps taken by solver	Free
Maximum BDF order	5
Singular mass matrix	Maybe
Consistent initialization of DAE systems	Backward Euler
Error estimation strategy	Include algebraic
Allow complex numbers	Off

Advanced

Parameter	Value
Constraint handling method	Elimination
Null-space function	Automatic
Automatic assembly block size	On
Assembly block size	5000
Use Hermitian transpose of constraint matrix and in symmetry detection	Off
Use complex functions with real input	Off
Stop if error due to undefined operation	On
Store solution on file	Off
Type of scaling	Automatic
Manual scaling	
Row equilibration	On
Manual control of reassembly	Off
Load constant	On
Constraint constant	On
Mass constant	On
Damping (mass) constant	On
Jacobian constant	On
Constraint Jacobian constant	On

Variables

Boundary

Name	Description	Unit	Expression
ndflux_c_chdi	Normal diffusive flux, c	mol/(m^2*s)	nx_chdi * dflux_c_x_chdi+ny_chdi * dflux_c_y_chdi+nz_chdi * dflux_c_z_chdi

Subdomain

Name	Description	Unit	Expression
grad_c_x_chdi	Concentration gradient, c, x component	mol/m^4	cx
dflux_c_x_chdi	Diffusive flux, c, x component	mol/(m^2*s)	-Dxx_c_chdi * cx-Dxy_c_chdi * cy-Dxz_c_chdi * cz
grad_c_y_chdi	Concentration gradient, c, y component	mol/m^4	cy
dflux_c_y_chdi	Diffusive flux, c, y component	mol/(m^2*s)	-Dyx_c_chdi * cx-Dyy_c_chdi * cy-Dyz_c_chdi * cz
grad_c_z_chdi	Concentration gradient, c, z component	mol/m^4	cz
dflux_c_z_chdi	Diffusive flux, c, z component	mol/(m^2*s)	-Dzx_c_chdi * cx-Dzy_c_chdi * cy-Dzz_c_chdi * cz
grad_c_chdi	Concentration gradient, c	mol/m^4	sqrt(grad_c_x_chdi^2+grad_c_y_chdi^2+grad_c_z_chdi^2)
dflux_c_chdi	Diffusive flux, c	mol/(m^2*s)	sqrt(dflux_c_x_chdi^2+dflux_c_y_chdi^2+dflux_c_z_chdi^2)

Glucose Model

Application modes and modules used in this model:

Geom1 (3D)

Diffusion (Chemical Engineering Module)

Constants

Name	Expression
D	1.44*10^-10
p	0.03
Deff	D*p
Di	D/100
Km	17
Vmax	0.53
vf	0.02

Mesh

Number of degrees of freedom	1768
Number of mesh points	165
Number of elements	393
Tetrahedral	393
Prism	0
Hexahedral	0
Number of boundary elements	332
Triangular	332
Quadrilateral	0
Number of edge elements	84
Number of vertex elements	16
Minimum element quality	0.162
Element volume ratio	0.078

Application Mode

Diffusion (chdi)

Application mode type: Diffusion (Chemical Engineering Module)

Application mode name: chdi

Application Mode Properties

Property	**Value**
Default element type	Lagrange - Quadratic
Analysis type	Stationary
Equilibrium assumption	Off
Frame	Frame (ref)
Weak constraints	Off
Constraint type	Ideal

Variables

Dependent variables: c, ci

Shape functions: shlag(2,'c'), shlag(2,'ci')

Interior boundaries active

Boundary Settings

Boundary		1, 3-4, 8-9, 12	2, 5	6-7, 10-11
Type		Insulation/Symmetry	Concentration	Continuity
Concentration (c0)	mol/m^3	{0;0}	**{5.2;0}**	{0;0}

Subdomain Settings

Subdomain		1	2
Diffusion coefficient (D)	m^2/s	{Deff;0}	{Deff;Di}
Reaction rate (R)	$mol/(m^3 \cdot s)$	{0;0}	{-(1/vf)*Vmax*Km*(c-ci)/((Km+c)*(Km+ci));(1/vf)*Vmax*Km*(c-ci)/((Km+c)*(Km+ci))}

Subdomain initial value		1	2
Concentration, c (c)	mol/m^3	0.2	5.2
Concentration, ci (ci)	mol/m^3	0	4.16

Solver Settings

Analysis type	Stationary
Auto select solver	On
Solver	Time dependent
Solution form	Automatic
Symmetric	On
Adaptive mesh refinement	Off
Optimization/Sensitivity	Off
Plot while solving	Off

Conjugate gradients

Solver type: Linear system solver

Parameter	**Value**
Relative tolerance	1.0E-6
Factor in error estimate	400.0
Maximum number of iterations	10000
Preconditioning	Left

Solver type: Preconditioner

Parameter	**Value**
Number of iterations	2
Multigrid cycle	V-cycle
Maximum number of levels	6
Max DOFs at coarsest level	5000
Quality of multigrid hierarchy	3

Solver type: Presmoother

Parameter	**Value**
Number of iterations	2
Relaxation factor (omega)	1.0
Blocked version	On

Solver type: Postsmoother

Parameter	Value
Number of iterations	2
Relaxation factor (omega)	1.0
Blocked version	On

Solver type: Coarse solver

Parameter	Value
Drop tolerance	0.0
Pivot threshold	0.1
Memory allocation factor	0.7

Time Stepping

Parameter	Value
Times	range(0,100,100000)
Relative tolerance	0.01
Absolute tolerance	0.0010
Times to store in output	Specified times
Time steps taken by solver	Free
Maximum BDF order	5
Singular mass matrix	Maybe
Consistent initialization of DAE systems	Backward Euler
Error estimation strategy	Include algebraic
Allow complex numbers	Off

Advanced

Parameter	Value
Constraint handling method	Elimination
Null-space function	Automatic
Automatic assembly block size	On
Assembly block size	5000
Use Hermitian transpose of constraint matrix and in symmetry detection	Off
Use complex functions with real input	Off
Stop if error due to undefined operation	On
Store solution on file	Off
Type of scaling	Automatic
Manual scaling	
Row equilibration	On
Manual control of reassembly	Off
Load constant	On
Constraint constant	On
Mass constant	On
Damping (mass) constant	On
Jacobian constant	On
Constraint Jacobian constant	On

Variables

Boundary

Name	Description	Unit	Expression
ndflux_c_chdi	Normal diffusive flux, c	mol/(m^2*s)	nx_chdi * dflux_c_x_chdi+ny_chdi * dflux_c_y_chdi+nz_chdi * dflux_c_z_chdi
ndflux_ci_chdi	Normal diffusive flux, ci	mol/(m^2*s)	nx_chdi * dflux_ci_x_chdi+ny_chdi * dflux_ci_y_chdi+nz_chdi * dflux_ci_z_chdi

Subdomain

Name	Description	Unit	Expression
grad_c_x_chdi	Concentration gradient, c, x component	mol/m^4	cx
dflux_c_x_chdi	Diffusive flux, c, x component	mol/(m^2*s)	-Dxx_c_chdi * cx-Dxy_c_chdi * cy-Dxz_c_chdi * cz
grad_c_y_chdi	Concentration gradient, c, y component	mol/m^4	cy
dflux_c_y_chdi	Diffusive flux, c, y component	mol/(m^2*s)	-Dyx_c_chdi * cx-Dyy_c_chdi * cy-Dyz_c_chdi * cz
grad_c_z_chdi	Concentration gradient, c, z component	mol/m^4	cz
dflux_c_z_chdi	Diffusive flux, c, z component	mol/(m^2*s)	-Dzx_c_chdi * cx-Dzy_c_chdi * cy-Dzz_c_chdi * cz
grad_c_chdi	Concentration gradient, c	mol/m^4	sqrt(grad_c_x_chdi^2+grad_c_y_chdi^2+grad_c_z_chdi^2)
dflux_c_chdi	Diffusive flux, c	mol/(m^2*s)	sqrt(dflux_c_x_chdi^2+dflux_c_y_chdi^2+dflux_c_z_chdi^2)
grad_ci_x_chdi	Concentration gradient, ci, x component	mol/m^4	cix
dflux_ci_x_chdi	Diffusive flux, ci, x component	mol/(m^2*s)	-Dxx_ci_chdi * cix-Dxy_ci_chdi * ciy-Dxz_ci_chdi * ciz
grad_ci_y_chdi	Concentration gradient, ci, y component	mol/m^4	ciy
dflux_ci_y_chdi	Diffusive flux, ci, y component	mol/(m^2*s)	-Dyx_ci_chdi * cix-Dyy_ci_chdi * ciy-Dyz_ci_chdi * ciz

grad_ci_z_chdi	Concentration gradient, ci, z component	mol/m^4	ciz
dflux_ci_z_chdi	Diffusive flux, ci, z component	mol/(m^2*s)	-Dzx_ci_chdi * cix-Dzy_ci_chdi * ciy-Dzz_ci_chdi * ciz
grad_ci_chdi	Concentration gradient, ci	mol/m^4	sqrt(grad_ci_x_chdi^2+grad_ci_y_chdi^2+grad_ci_z_chdi^2)
dflux_ci_chdi	Diffusive flux, ci	mol/(m^2*s)	sqrt(dflux_ci_x_chdi^2+dflux_ci_y_chdi^2+dflux_ci_z_chdi^2)

Appendix D – Supplementary Movie 1

This appendix is a video file of a live cell imaging experiment of human islet of Langerhans cultured under maintenance conditions.

The file name of this sound file is “Movie 1 Islet maintained in 25 µm gap chamber for 5 days.wmv”.

Appendix E – Supplementary Movie 2

This appendix is a video file of a live cell imaging experiment of human islet of Langerhans cultured under cholera toxin-induced DEC-transformation conditions.

The file name of this sound file is “Movie 2 Islet phenotype transformation in a 25 μm gap chamber for 5 days.wmv”.

Appendix F – Supplementary Movie 3

This appendix is a video file of a live cell imaging experiment of human embryonic stem cells with cell tracking information overlaid. The red markers represent tracked hESC colony cells, while the green markers represent tracked hdF cells.

The file name of this sound file is “Movie 3 hESC colony cells (red) and hdF cells (green) in 4.7um imaging chamber.wmv”.